UNIVERSITÉ DE LORRAINE | BIBLIOTHÈQUES UNIVERSITAIRES

AVERTISSEMENT
DROIT D'AUTEUR

Ce document est le fruit d'un long travail approuvé par le jury de soutenance et mis à disposition de l'ensemble de la communauté universitaire élargie.

Il est soumis à la propriété intellectuelle de l'auteur. Ceci implique une obligation de citation et de référencement lors de l'utilisation de ce document. Toute contrefaçon, plagiat ou reproduction illicite encourt une poursuite pénale.

Contact bibliothèque : ddoc-theses-contact@univ-lorraine.fr
(Cette adresse ne permet pas de contacter les auteurs)

Code de la Propriété Intellectuelle. articles L 122. 4
Code de la Propriété Intellectuelle. articles L 335.2- L 335.10

UNIVERSITÉ DE LORRAINE
34 COURS LÉOPOLD — CS 25233
54052 NANCY CEDEX
TÉL : 03 54 50 54 00
CONTACT@UNIV-LORRAINE.FR
WWW.UNIV-LORRAINE.FR

Development of new advanced estimation algorithms for improving the resilience of the autonomous and connected vehicle

PhD Thesis

Presented and publicly defended on 05 May 2026 for obtaining the title of

by

Quang Huy NGUYEN

Under the supervision of

Ali ZEMOUCHE
Hugues RAFARALAHY
Madjid HADDAD

Jury Composition

Reviewer	**Naïma Aït Oufroukh Mammar**	Associate Professor - HDR, University of Paris Saclay
Reviewer	**Angelo Alessandri**	Professor, University of Genoa
Examiner	**Madiha Nadri-Wolf**	Associate Professor, University of Lyon
Examiner	**Vicenç Puig**	Professor, Polytechnic University of Catalonia
Jury Chair	**Taous Meriem Laleg Kirati**	Research Director, Inria
PhD Director	**Ali Zemouche**	Professor, Université de Lorraine
Co-supervisor	**Hugues Rafaralahy**	Associate Professor, Université de Lorraine
Industrial Supervisor	**Madjid Haddad**	Research Director, SEGULA Technologies

Acknowledgements

I would like to express my sincere gratitude to the many individuals who have supported me throughout my doctoral journey.

First and foremost, I extend my deepest appreciation to my supervisors, Prof. Ali Zemouche, Dr. Hugues Rafaralahy, and Dr. Madjid Haddad, for granting me the opportunity to pursue this research. I am profoundly grateful for their continuous guidance, encouragement, and trust. Their insightful advice, valuable discussions, and unwavering support both scientific and personal have been essential to the completion of this dissertation. Without their mentorship, this work would not have reached its present form.

I am also extremely grateful to my colleagues Hasni, Shengya, Echrak, Hichem, Oussama, Sesabil, Tansuh, Siyu, Viet, Melissa and Li Qi for their cooperation, constructive feedback, and camaraderie throughout my PhD studies. As the saying goes, "If you want to go fast, go alone; if you want to go far, go together." From my first day in the laboratory to my first scientific publication, they were always willing to offer help. I particularly appreciate their patience and understanding when I took on my first leadership role during a team project. Despite my limited experience, they supported me with tolerance and encouragement rather than faulting my mistakes, allowing me to grow both professionally and personally.

Similarly, during my first teaching experiences, I faced significant challenges overcoming shyness. The continuous support of my colleagues played a crucial role in helping me surmount these obstacles and build my confidence.

Last but not least, I express my heartfelt gratitude to my family, my parents, and my girlfriend for their unconditional love, patience, and support. I am especially thankful to my uncle and aunt, who have provided unwavering financial and spiritual support throughout my entire academic journey. Their encouragement and sacrifices have been a constant source of motivation, contributing significantly to my pursuit of higher academic achievements.

Résumé

La fiabilité et la sécurité des véhicules connectés et autonomes (VCA) dépendent de manière critique de la disponibilité en temps réel d'informations précises sur l'état dynamique. Cependant, les contraintes économiques limitent souvent l'utilisation de capteurs haut de gamme. De plus, les VCA sont vulnérables aux défauts de capteurs et aux cyberattaques ciblant les communications inter-véhicules (V2V/V2I). Pour relever ces défis, cette thèse propose un cadre de « capteur logiciel » résilient basé sur la redondance analytique.

Cette recherche développe une méthodologie de modélisation hybride intégrant des équations physiques et des réseaux de neurones neuro-adaptatifs. Cette approche permet une représentation précise des paramètres complexes et variables dans le temps ainsi que des dynamiques non modélisées. S'appuyant sur ces modèles, des algorithmes d'estimation non linéaires avancés observateurs à entrées inconnues (UIO) et observateurs neuro-adaptatifs sont développés pour garantir la résilience du système.

L'efficacité des stratégies proposées est démontrée à travers trois axes principaux :

- **CACC Cyber-sécurisé :** Des architectures d'observateurs sont conçues pour détecter et atténuer une large gamme de cybermenaces, incluant l'injection de fausses données (FDI), le déni de service (DoS), ainsi que les retards et pertes de paquets. Ces observateurs permettent la reconstruction des signaux d'attaque, assurant un contrôle longitudinal robuste.

- **Peloton et Suivi de Véhicules :** Un cadre d'estimation distribué est proposé pour gérer des modèles dynamiques non linéaires. Couplé à un mécanisme de gestion de la confiance, il permet de filtrer les données non fiables et d'assurer la cohésion du peloton lors de manœuvres complexes.

- **Estimation des Forces et Dynamique du Véhicule :** L'application des observateurs hybrides neuronaux est étendue à l'estimation de forces inconnues et de dynamiques complexes, adressant des problèmes critiques tels que le risque de renversement, où la connaissance précise des forces externes est essentielle pour la sécurité.

Enfin, un prototype de carte électronique embarquée est développé pour faciliter le déploiement futur des algorithmes proposés sur des véhicules réels, démontrant une solution rentable et évolutive pour améliorer l'autonomie et la sécurité des véhicules de nouvelle génération.

Mots clés : Estimation distribuée, observateur neuronal, Cyberattaque, Carte electronique embarquée V2V

Résumé étendu en français

Contexte général et motivations

Les véhicules autonomes et connectés occupent aujourd'hui une place centrale dans l'évolution des systèmes de transport intelligents. Leur promesse est double : améliorer la sécurité routière en réduisant la dépendance aux décisions humaines, et augmenter l'efficacité du trafic grâce à la coopération entre véhicules, infrastructures et systèmes embarqués. Cette évolution repose cependant sur une condition essentielle : le véhicule doit disposer, à chaque instant, d'une information fiable sur son propre état dynamique et sur l'état de son environnement proche. Les grandeurs telles que la position, la vitesse, l'accélération, la distance inter-véhicules, les forces de contact pneu-chaussée ou les états transmis par les véhicules voisins ne sont pas toujours directement mesurables avec la précision, la fréquence et la robustesse nécessaires. Elles doivent donc être reconstruites à partir de capteurs imparfaits, de modèles physiques et de données échangées par communication.

Dans ce contexte, l'estimation d'état constitue un élément fondamental de la chaîne de décision et de contrôle. Un observateur bien conçu permet de reconstruire des variables non mesurées, de filtrer le bruit, de détecter des incohérences et d'alimenter les lois de commande avec des informations plus régulières que les mesures brutes. Cette fonction devient critique dans les architectures de conduite automatisée, où les décisions de freinage, d'accélération ou de maintien de trajectoire dépendent directement de la qualité des estimations. Une erreur d'estimation peut se propager jusqu'au contrôle longitudinal ou latéral, provoquer une mauvaise évaluation de la distance de sécurité ou masquer l'apparition d'un défaut. La problématique n'est donc pas seulement académique : elle est directement liée à la sûreté de fonctionnement et à l'acceptabilité industrielle des véhicules autonomes.

Les véhicules connectés ajoutent une difficulté supplémentaire. Les fonctions coopératives telles que l'Adaptive Cruise Control (ACC), le Cooperative Adaptive Cruise Control (CACC) ou le peloton de véhicules utilisent les informations reçues par communication véhicule-à-véhicule (V2V). Ces informations peuvent enrichir la perception locale, réduire les temps de réaction et améliorer la fluidité du trafic. En revanche, elles introduisent aussi une surface d'attaque et de défaillance. Les messages peuvent être retardés, perdus, corrompus ou falsifiés. Une attaque par injection de fausses données peut, par exemple, modifier l'accélération transmise par un véhicule leader et perturber la réponse de ses suiveurs. De même, une interruption de communication ou un défaut capteur peut rendre une donnée partagée inutilisable. Les mécanismes d'estimation doivent donc être capables de distinguer les informations fiables des informations douteuses, de reconstruire les perturbations inconnues et de limiter leur effet sur

la commande.

Cette thèse s'inscrit dans cette problématique générale de résilience. Le terme résilience désigne ici la capacité d'un système d'estimation et de contrôle à maintenir un comportement acceptable malgré les incertitudes de modèle, les défauts, les attaques et les limitations de communication. La thèse ne se limite pas à détecter qu'une anomalie est présente. Elle cherche à reconstruire son effet, à réduire son influence dans la boucle de contrôle et à fournir une estimation exploitable pour les fonctions de conduite. Cette orientation explique le choix d'un cadre fondé sur les observateurs à entrées inconnues, les observateurs hybrides intégrant l'apprentissage, et les mécanismes distribués de confiance.

Objectifs scientifiques de la thèse

L'objectif principal de la thèse est de développer de nouveaux algorithmes d'estimation avancée pour améliorer la résilience des véhicules autonomes et connectés. Trois axes scientifiques structurent le manuscrit. Le premier concerne la reconstruction d'attaques ou de perturbations modélisées comme des entrées inconnues dans un système CACC. Le deuxième traite des incertitudes non linéaires et variables dans le temps à l'aide d'une architecture hybride, combinant un observateur fondé sur le modèle et un observateur neuronal adaptatif. Le troisième étend l'estimation au cadre distribué des pelotons de véhicules, où les informations reçues des voisins doivent être pondérées selon leur niveau de confiance.

Le premier objectif consiste à concevoir un observateur capable d'estimer simultanément l'état d'un véhicule et les signaux malveillants affectant les communications. Les observateurs à entrées inconnues sont particulièrement adaptés à cette tâche, car ils permettent de traiter une perturbation non mesurée comme une variable à reconstruire. Toutefois, les conditions classiques d'existence de ces observateurs, notamment les conditions de rang et de couplage entre entrées inconnues et sorties mesurées, ne sont pas toujours satisfaites par les modèles réalistes de véhicules. La thèse cherche donc à proposer des formulations discrètes et des transformations adaptées pour rendre cette reconstruction possible dans des cas pratiques.

Le deuxième objectif est lié aux limites des modèles physiques. Un modèle de véhicule utilisé pour la conception d'un observateur doit rester suffisamment simple pour être exploitable en temps réel, mais suffisamment riche pour représenter les phénomènes dominants. Or les forces pneu-chaussée, les variations d'adhérence, les effets aérodynamiques ou les dynamiques d'actionneurs peuvent être difficiles à décrire avec précision. Les méthodes purement apprenantes peuvent approximer ces effets, mais elles sont souvent difficiles à certifier et à intégrer dans une architecture sûre. La thèse adopte donc une position intermédiaire : utiliser l'apprentissage pour approximer les dynamiques résiduelles, tout en conservant une structure d'observateur qui fournit des garanties de stabilité et de bornitude.

Le troisième objectif porte sur la coopération. Dans un peloton, chaque véhicule peut utiliser ses mesures locales et les messages reçus de ses voisins. Cette redondance peut améliorer l'observabilité et la robustesse, mais elle devient dangereuse si certains voisins transmettent des données compromises. La thèse propose alors une architecture d'observateur distribué couplée à un mécanisme de confiance. Les poids attribués aux informations reçues ne sont pas fixés une fois pour toutes : ils évoluent en fonction de critères de cohérence portant sur la vitesse, la distance, l'accélération et les estimations globales. L'objectif est de réduire automatiquement l'influence des données non fiables sans rompre la coopération

entre véhicules sains.

Cadre méthodologique

La méthodologie générale repose sur la redondance analytique. Au lieu de dépendre uniquement de capteurs physiques coûteux ou de messages V2V supposés parfaits, la thèse exploite les relations dynamiques entre les variables du système. Les modèles de véhicule, les équations d'espacement, les sorties mesurées et les lois de commande fournissent des contraintes qui permettent de vérifier la cohérence des données et de reconstruire les grandeurs manquantes. Cette redondance analytique est utilisée comme un capteur logiciel : elle produit des estimations d'état et d'attaques à partir des mesures disponibles.

Le manuscrit combine plusieurs niveaux de modélisation. Le niveau local décrit la dynamique d'un véhicule, ses états longitudinaux ou latéraux, ses entrées de commande et ses sorties mesurées. Le niveau coopératif décrit les interactions entre véhicules, notamment les distances relatives, les vitesses échangées et les informations transmises par communication. Le niveau cyber-physique introduit des attaques ou des défauts sous forme d'entrées inconnues, de délais, de pertes de paquets ou de données incohérentes. Ce choix permet d'étudier la résilience non seulement comme une propriété de robustesse au bruit, mais comme une réponse structurée à des dégradations physiques et informationnelles.

Sur le plan algorithmique, la thèse utilise des observateurs à entrées inconnues, des conditions de synthèse sous forme d'inégalités matricielles linéaires, des transformations de systèmes et des mécanismes d'adaptation neuronale. Les inégalités matricielles linéaires permettent de formuler la stabilité et l'atténuation des perturbations sous une forme calculable numériquement. Les transformations de modèles permettent de contourner certaines restrictions classiques de rang. Les réseaux neuronaux sont utilisés non pas comme un remplacement complet du modèle physique, mais comme un module d'approximation des résidus. Enfin, les scores de confiance servent à adapter les poids d'un observateur distribué en fonction de la qualité estimée des informations reçues.

La validation est menée à plusieurs niveaux. Des simulations MATLAB/Simulink permettent d'évaluer précisément les erreurs d'estimation, la reconstruction d'attaques et la réponse des observateurs dans des scénarios contrôlés. Des environnements plus proches de l'expérimentation, comme CARLA et Quanser QLabs, introduisent des contraintes supplémentaires : dynamique plus réaliste, bruit, trajectoires complexes, communication simulée et architecture logicielle modulaire. Le dernier chapitre prépare le passage vers l'embarqué en décrivant une plateforme matérielle dédiée à l'acquisition, à la communication et à l'exécution future des algorithmes proposés.

Estimation résiliente et reconstruction d'attaques pour le CACC

La première contribution majeure concerne l'estimation résiliente dans un système CACC soumis à des cyberattaques. Dans une architecture CACC, un véhicule suiveur utilise non seulement ses propres mesures, mais aussi les informations envoyées par le véhicule leader ou par les véhicules voisins. Cette coopération permet d'améliorer la réponse longitudinale, de réduire les distances de sécurité et de limiter les oscillations dans le peloton. Toutefois, si une information transmise est falsifiée, le contrôleur peut agir sur une base erronée. Une fausse accélération communiquée peut ainsi provoquer un freinage ou une

accélération inadaptée, dégrader la stabilité de chaîne et créer un risque de collision.

La thèse modélise ces signaux corrompus comme des entrées inconnues affectant le modèle discret du système. L'enjeu est de reconstruire ces entrées en même temps que les états du véhicule. Une approche de simple détection fournirait un indicateur d'anomalie, mais ne donnerait pas nécessairement la valeur du signal à compenser. La reconstruction permet au contraire d'estimer l'amplitude et l'évolution temporelle de l'attaque. Cette information peut ensuite être utilisée dans une stratégie de défense, par exemple en soustrayant l'effet estimé de l'attaque ou en adaptant la donnée transmise avant son utilisation par le contrôleur.

Le chapitre développe une structure d'observateur à entrées inconnues en temps discret. La formulation tient compte du fait que les données de contrôle et de communication sont échantillonnées. Cette caractéristique est importante pour l'implémentation automobile, car les calculateurs embarqués fonctionnent avec des périodes d'échantillonnage fixes. Une attention particulière est portée à la reconstruction avec délai borné : l'estimation de l'attaque ne doit pas arriver trop tard, car une compensation tardive pourrait être inutile pour la sécurité. La thèse propose également une approche de discrétisation exacte afin de limiter les erreurs dues au passage du modèle continu au modèle discret.

Les résultats de simulation montrent que l'observateur proposé est capable de reconstruire des attaques variables dans le temps et de maintenir une estimation fiable des états longitudinaux. Les scénarios étudiés incluent des attaques par injection de fausses données et des perturbations de communication. Les comparaisons avec des approches plus classiques mettent en évidence l'intérêt de la formulation proposée, en particulier lorsque la dynamique de l'attaque évolue rapidement. La stratégie de défense améliore la capacité du véhicule à suivre la trajectoire ou l'espacement désiré malgré la présence de données compromises.

Cette contribution établit le socle cyber-résilient de la thèse. Elle montre que l'attaque ne doit pas seulement être considérée comme une anomalie externe, mais comme une variable dynamique à estimer. Elle fournit aussi une première illustration de la redondance analytique : les relations entre les états, les entrées et les sorties permettent de reconstruire une information qui n'est pas directement mesurée.

Observateurs hybrides et apprentissage de dynamiques non modélisées

La deuxième contribution traite le cas des dynamiques non linéaires et mal connues. Les véhicules réels présentent des comportements difficiles à modéliser exactement. Les forces latérales, les forces longitudinales, l'adhérence, les effets de charge ou les variations de route introduisent des termes non linéaires qui peuvent changer au cours du temps. Un observateur conçu sur un modèle simplifié peut donc produire une estimation biaisée si ces effets ne sont pas correctement pris en compte.

Pour répondre à cette difficulté, la thèse développe une architecture d'apprentissage fondée sur un observateur à entrées inconnues généralisé et un observateur neuronal adaptatif. L'idée principale est de séparer deux fonctions complémentaires. Le premier niveau, fondé sur le modèle, fournit une estimation robuste et bornée des états ou des résidus. Le second niveau apprend les composantes non modélisées à partir de ces informations. Cette stratégie évite de confier toute l'estimation à un réseau neuronal isolé. Le réseau apprend dans un cadre structuré, supervisé par un observateur qui exploite les équations physiques du système.

Le chapitre commence par analyser les limitations des observateurs à entrées inconnues classiques lorsque la condition de rang n'est pas satisfaite. Une formulation utilisant les dérivées de sortie et une régularisation est ensuite introduite pour construire un modèle généralisé. Cette transformation rend possible l'estimation dans des situations où les méthodes standard seraient trop restrictives. La synthèse de l'observateur est formulée au moyen de conditions matricielles assurant la stabilité de l'erreur d'estimation et un niveau de robustesse vis-à-vis des perturbations.

Le module neuronal est ensuite intégré pour approximer les dynamiques résiduelles. Les paramètres d'apprentissage sont ajustés à partir d'une fonction de perte liée aux erreurs ou aux résidus observés. Une discrétisation de l'observateur neuronal et un calcul de gradients par analyse de sensibilité sont proposés pour rendre la méthode exploitable numériquement. La stratégie de learning continu vise à mettre à jour l'approximation au fil du fonctionnement, tout en évitant une adaptation non contrôlée qui pourrait dégrader la stabilité.

L'application à un modèle de véhicule met en évidence l'intérêt de cette architecture hybride. L'observateur généralisé traite les difficultés structurelles liées aux entrées inconnues, tandis que le module neuronal améliore l'estimation des termes complexes, comme les résidus associés aux forces pneu-chaussée. Les simulations montrent une amélioration de la qualité d'estimation par rapport à une approche purement modèle lorsque les dynamiques non modélisées deviennent significatives. Elles confirment également que l'apprentissage peut être introduit dans un cadre compatible avec les exigences de stabilité et de robustesse.

Cette contribution répond à un enjeu important pour l'industrialisation des méthodes d'estimation. Les modèles analytiques sont interprétables et certifiables, mais parfois incomplets. Les modèles appris sont flexibles, mais difficiles à garantir. L'approche proposée cherche à combiner les avantages des deux familles : l'observateur fournit la structure et la stabilité, tandis que l'apprentissage apporte l'adaptabilité nécessaire face aux incertitudes complexes.

Estimation distribuée et gestion de la confiance dans les pelotons

La troisième contribution porte sur les pelotons de véhicules connectés. Dans un peloton, chaque véhicule peut améliorer son estimation en utilisant les informations issues de ses voisins. Cette coopération est utile lorsque certaines grandeurs ne sont pas observables localement ou lorsque les mesures locales sont bruitées. Néanmoins, elle crée une dépendance vis-à-vis de la qualité des messages reçus. Si un voisin transmet une information compromise, son influence peut se propager dans l'observateur distribué et contaminer l'estimation de plusieurs véhicules.

La thèse propose une architecture d'observateur distribué dans laquelle les poids attribués aux voisins sont modulés par un score de confiance. Ce score n'est pas seulement une valeur abstraite. Il est construit à partir d'indicateurs de cohérence entre les données reçues, les mesures locales, les estimations globales et les contraintes physiques du peloton. Les critères incluent notamment la cohérence de vitesse, la cohérence de distance et la cohérence d'accélération. Lorsqu'une donnée reçue devient incompatible avec les informations disponibles localement ou avec la dynamique attendue, son niveau de confiance diminue.

Le mécanisme de confiance est conçu à plusieurs niveaux. La confiance locale évalue la cohérence

immédiate des messages reçus. La confiance distribuée tient compte des estimations partagées et de la cohérence avec l'état global reconstruit. Une mémoire temporelle permet de ne pas réagir uniquement à un écart instantané, qui pourrait provenir d'un bruit ou d'un transitoire normal, mais d'accumuler l'historique de fiabilité. Cette mémoire est importante pour distinguer une perturbation ponctuelle d'un comportement durablement suspect. Les scores obtenus sont ensuite normalisés et transformés en poids utilisés par l'observateur.

La conception des poids vise à préserver deux propriétés contradictoires. D'une part, il faut réduire l'influence des véhicules non fiables pour éviter la propagation des attaques. D'autre part, il faut conserver suffisamment de connectivité pour que l'observateur distribué reste utile. Une coupure trop brutale de toutes les communications pourrait dégrader l'estimation, surtout si certaines grandeurs dépendent de l'information coopérative. Le compromis proposé consiste à adapter progressivement les poids en fonction de la confiance, avec des bornes et des règles de normalisation.

Les simulations de peloton montrent que cette approche améliore la résilience face à différents scénarios d'attaque. Lorsqu'un véhicule envoie des données incohérentes, son influence diminue dans les estimations des autres véhicules. Le peloton conserve ainsi une meilleure cohérence d'état et une meilleure capacité de contrôle. Les résultats soulignent également que la confiance doit être liée à des critères physiques et non uniquement à des statistiques de communication. Un message peut être reçu correctement sur le plan réseau tout en étant physiquement faux ; l'observateur doit donc vérifier sa compatibilité avec le comportement dynamique attendu.

Cette contribution élargit la thèse du véhicule isolé vers le système multi-agent. Elle montre que la résilience ne dépend pas seulement de l'observateur local, mais aussi de la manière dont les informations sont partagées, évaluées et pondérées. Elle ouvre ainsi la voie à des architectures de coopération plus sûres pour les véhicules connectés.

Validation expérimentale simulée et préparation à l'embarqué

La dernière partie du manuscrit s'intéresse au passage des algorithmes vers des environnements plus proches de l'expérimentation. Les validations purement numériques sont indispensables pour analyser les erreurs et comparer les méthodes, mais elles ne suffisent pas à évaluer les contraintes d'intégration. Un système embarqué doit gérer des fréquences d'échantillonnage, des délais, des pertes de communication, des capteurs hétérogènes et une architecture logicielle modulaire. C'est pourquoi la thèse introduit des plateformes de simulation et de prototypage telles que Quanser QCar2/QLabs et une carte électronique embarquée dédiée.

L'environnement QLabs permet de mettre en place des scénarios de conduite avec véhicules virtuels, capteurs simulés, communication V2V et injection d'attaques. Il sert de banc de validation intermédiaire entre MATLAB/Simulink et les essais réels. Les fonctions de perception, de communication, de contrôle longitudinal et de contrôle latéral peuvent y être testées dans un cadre plus intégré. Cette étape est importante pour vérifier que les observateurs développés ne restent pas isolés, mais peuvent s'insérer dans une chaîne complète comprenant acquisition, estimation, décision et commande.

Le chapitre décrit également une architecture de contrôle combinant le suivi longitudinal, le maintien de trajectoire et des mécanismes coopératifs. L'objectif est de préparer l'utilisation des estimations dans

une boucle de conduite réelle. Les données produites par les observateurs et les indicateurs de confiance doivent pouvoir être transmises aux modules de commande, mais aussi enregistrées pour analyse. Cette logique de journalisation facilite la comparaison entre simulation, essais virtuels et futurs essais physiques.

La carte électronique embarquée proposée constitue une base matérielle pour l'implémentation future des observateurs. Elle est pensée comme un noeud d'estimation et de communication capable d'acquérir des données locales, de recevoir des messages V2V, de synchroniser les informations et d'exécuter des traitements de confiance ou d'estimation. La conception prend en compte les contraintes d'un environnement embarqué : alimentation, interfaces capteurs, communication sans fil, routage de circuit imprimé, compatibilité électromagnétique et modularité logicielle. Même si l'intégration complète des algorithmes sur cette carte reste une perspective, sa conception montre que la thèse anticipe le transfert vers des plateformes réelles.

Cette partie expérimentale et matérielle complète les contributions théoriques. Elle met en évidence les contraintes qui devront être traitées pour passer d'un observateur validé en simulation à un module embarqué utilisable. Elle rappelle aussi que la résilience ne se limite pas à une preuve mathématique : elle dépend de la qualité des capteurs, de la synchronisation temporelle, du logiciel embarqué, de la communication et de la capacité à diagnostiquer le système en fonctionnement.

Apports principaux

Les apports de la thèse peuvent être résumés autour de quatre points. Premièrement, elle propose une approche de reconstruction d'attaques dans les systèmes CACC en modélisant les données corrompues comme des entrées inconnues. Cette approche permet d'aller au-delà de la détection et de fournir une information directement utile pour la compensation. Deuxièmement, elle développe un observateur généralisé capable de traiter des situations où les conditions classiques des observateurs à entrées inconnues ne sont pas satisfaites. Troisièmement, elle introduit une architecture hybride où l'apprentissage neuronal approxime les dynamiques résiduelles sans abandonner la structure de stabilité fournie par l'observateur. Quatrièmement, elle étend la résilience au cadre distribué grâce à un mécanisme de confiance qui adapte les poids de coopération dans un peloton.

Ces apports sont complémentaires. La reconstruction d'attaque traite la menace cyber-physique dans une chaîne CACC. L'observateur hybride traite l'incertitude de modèle et les dynamiques non linéaires. La confiance distribuée traite la fiabilité des informations coopératives. L'ensemble forme un cadre cohérent pour l'estimation résiliente dans les véhicules autonomes et connectés. Ce cadre repose sur une idée commune : exploiter les modèles, les mesures et les relations de cohérence pour produire des estimations fiables malgré des données imparfaites.

La thèse contribue également à rapprocher les méthodes de contrôle avancé des préoccupations industrielles. Les algorithmes sont formulés dans des structures compatibles avec le temps discret, les contraintes d'échantillonnage et les validations par simulation réaliste. Les perspectives d'implémentation embarquée sont explicitement abordées, ce qui facilite le passage vers des prototypes matériels. Cette orientation est importante car les solutions destinées aux véhicules autonomes doivent être non seulement performantes, mais aussi explicables, vérifiables et intégrables dans des architectures sûres.

Limites et perspectives

Malgré les résultats obtenus, plusieurs limites restent ouvertes. Les validations expérimentales doivent être poursuivies sur des plateformes physiques, d'abord à échelle réduite puis, à terme, sur des véhicules réels. Les effets combinés de bruit capteur, délais variables, pertes de paquets, limitations de calcul et incertitudes de synchronisation devront être évalués de manière plus systématique. Le passage à l'embarqué nécessitera aussi une analyse fine de la charge de calcul, de la mémoire, de la robustesse numérique et de la tolérance aux défauts logiciels.

Une deuxième perspective concerne l'extension vers la perception coopérative. Les véhicules futurs n'échangeront pas seulement des états cinématiques, mais aussi des objets détectés, des nuages de points, des images ou des cartes locales. L'évaluation de la confiance devra donc s'étendre à des données plus riches et plus hétérogènes. Les principes développés dans cette thèse, fondés sur la cohérence physique et temporelle, pourront servir de base à ces extensions, mais de nouveaux critères seront nécessaires.

Une troisième perspective concerne l'intégration plus étroite entre estimation, contrôle et décision. Dans cette thèse, l'accent est mis sur l'estimation et sur son effet sur les fonctions de contrôle. Des travaux futurs pourraient utiliser explicitement les niveaux de confiance et les incertitudes estimées pour adapter les décisions de haut niveau : changement de mode de conduite, augmentation de la distance de sécurité, isolement d'un voisin, ou passage à une stratégie dégradée. Une telle intégration renforcerait le rôle de l'observateur comme module central de diagnostic et de décision.

Enfin, l'apprentissage dans les observateurs mérite d'être approfondi. Les réseaux neuronaux peuvent améliorer l'estimation des dynamiques complexes, mais leur utilisation dans un système critique exige des garanties supplémentaires. Les perspectives incluent l'apprentissage avec quantification d'incertitude, les architectures physiquement informées, la mise à jour sûre des paramètres et la certification de performances dans des domaines de fonctionnement bornés. Ces développements permettront de mieux concilier adaptabilité et sûreté.

Conclusion du résumé étendu

Cette thèse propose un ensemble d'outils pour améliorer la résilience des véhicules autonomes et connectés par l'estimation d'état. Elle traite simultanément les cyberattaques sur les communications, les incertitudes non linéaires des modèles de véhicules et la fiabilité variable des données coopératives. Les méthodes développées reposent sur des observateurs à entrées inconnues, des architectures hybrides avec apprentissage et des mécanismes distribués de confiance. Les validations montrent que ces approches permettent de reconstruire des signaux d'attaque, d'améliorer l'estimation en présence de dynamiques non modélisées et de limiter l'influence de voisins compromis dans un peloton.

Au-delà des résultats spécifiques, le manuscrit défend une vision intégrée de l'estimation résiliente. Dans les véhicules connectés, la sûreté ne peut pas dépendre d'une seule source d'information supposée parfaite. Elle doit émerger de la comparaison entre mesures, modèles, communications et historiques de confiance. Les contributions de la thèse s'inscrivent dans cette direction et constituent une base pour le développement de capteurs logiciels embarqués capables de soutenir les futures fonctions de conduite coopérative, sûre et autonome.

Abstract

The reliability and safety of Connected and Autonomous Vehicles (CAVs) critically depend on the real-time availability of precise dynamic state information. However, economic constraints often limit the use of high-end sensors. Furthermore, CAVs are vulnerable to sensor faults and cyber-attacks targeting inter-vehicle communications (V2V/V2I). To address these challenges, this thesis proposes a resilient "soft sensor" framework based on analytical redundancy.

This research develops a hybrid modeling methodology integrating physical equations with neuro-adaptive neural networks. This approach enables the accurate representation of complex, time-varying parameters and unmodeled dynamics. Building on these models, advanced nonlinear estimation algorithms: Unknown Input Observers (UIO) and neuro-adaptive observers are developed to ensure system resilience.

The effectiveness of the proposed strategies is demonstrated through three main axes:

- **Cyber-Secure CACC:** Observer architectures are designed to detect and mitigate a wide range of cyber-threats, including False Data Injection (FDI), Denial of Service (DoS), as well as delays and packet losses. These observers enable the reconstruction of attack signals, ensuring robust longitudinal control.

- **Platooning and Vehicle Tracking:** A distributed estimation framework is proposed to handle nonlinear dynamic models. Coupled with a trust management mechanism, it allows filtering out unreliable data and ensuring platoon cohesion during complex maneuvers.

- **Vehicle Dynamics and Force Estimation:** The application of hybrid neural observers is extended to the estimation of unknown forces and complex dynamics, addressing critical issues such as rollover risk, where precise knowledge of external forces is essential for safety.

Finally, a prototype embedded electronic board is developed to facilitate future deployment of the proposed algorithms on real vehicles, demonstrating a cost-effective and scalable solution for enhancing the autonomy and security of next-generation vehicles.

Keywords : State Estimation, Neural Observer, Cyber-attack, Electronic Board V2V

Table of Contents

Acknowledgements i

Résumé ii

Résumé étendu en français iii

Abstract xi

Table of Contents xi

List of Figures xvi

List of Tables xviii

1 General Introduction 1
- 1 Historical Background of Estimation Theory and Observer Design . . . 2
- 2 Recent Advances in Hybrid and Resilient Estimation . . . 2
- 3 Literature Review Summary . . . 4
- 4 Positioning and challenges . . . 7
- 5 Main contributions . . . 8
- 6 Organization of the manuscript . . . 8

2 Resilient State Estimation and Cyber-Attack Reconstruction 10
- 1 Introduction . . . 11
- 2 Problem Formulation . . . 11
  - 2.1 General description of the CACC system . . . 11
  - 2.2 CACC modeling subject to cyberattack . . . 12
  - 2.3 Problem formulation and objectives . . . 14
- 3 Discrete-Time Model-Based UIO design for CACC system . . . 16
  - 3.1 UIO structure for the shifted system . . . 16
  - 3.2 LMI-Baed ISS design method . . . 17
  - 3.3 Defense strategy . . . 18
- 4 Simulation results by Using Matlab and Carla Platform . . . 19
  - 4.1 Simulation result using Matlab . . . 20
- 5 Exact Discretization Approach . . . 21
  - 5.1 Simulation Results and Comparison . . . 23
- 6 Conclusion . . . 26

3 Learning with Unknown Input Observers for Robust Nonlinear Estimation 28

1 Introduction . . . 30
2 Problem Formulation and Motivation . . . 31
3 LMI-Based $\mathcal{H}^1$ UIO Design . . . 33
3.1 System transformation . . . 33
3.2 UIO structure and error dynamics . . . 34
3.3 New LMI-based UIO design conditions . . . 36
4 Output Derivative-Based Generalized UIO . . . 39
4.1 Output derivative-based generalized model . . . 39
4.2 Regularization of the generalized model . . . 39
4.3 Generalized UIO . . . 40
4.4 Specific cases and discussion . . . 41
4.4.1 Case $\mathrm{rank}(CB) = \mathrm{rank}(B)$ . . . 41
4.4.2 Case $C_\chi = 0$ . . . 42
4.4.3 Case $\mathrm{rank}(CB) < \mathrm{rank}(B)$ . . . 42
4.4.4 On the use of $\dot{y}$ . . . 42
5 UIO-Based Neural Online Approximation of Unmodeled Nonlinearity . . . 43
5.1 Fully UIO-based Learning Architecture . . . 43
5.1.1 Design of the Neural Adaptive Observer . . . 44
5.1.2 Optimization of the Learning Parameter θ . . . 45
5.2 Minimization of the Loss Function . . . 45
5.2.1 Discretization of the Neural Adaptive Observer . . . 46
5.2.2 Gradient Computation via Sensitivity Analysis . . . 46
6 Continuous Learning Strategy . . . 47
7 Simulation Results . . . 48
7.1 Nonlinear Vehicle Plant . . . 48
7.1.1 QCar Simulation Setup and Residual Injection . . . 49
7.2 LPV Model Used by the Observers . . . 50
7.2.1 Rank Condition Check (Why a Generalized/Regularized UIO Is Needed) 50
7.2.2 LPV Scheduling and Polytopic Embedding . . . 51
7.2.3 Step-by-Step Application of the Generalized UIO to the Vehicle Model 51
7.2.4 Neural Adaptive Observer (NAO) — Application of Theorem 3 . . . 55
7.2.5 Gradient Computation Using the Vehicle LPV Model . . . 55
7.3 Results and Discussion . . . 55
7.3.1 Trajectory Tracking and Control Inputs . . . 56
7.3.2 State Estimation . . . 56
7.3.3 Tire-Force Residual Estimation . . . 57
8 Open Problems and Future Directions . . . 59
9 Conclusion . . . 60

4 Resilient Trust–Aware Distributed Observer Design for Connected Vehicle Platoons 61
1 Introduction . . . 63
1.1 General introduction . . . 63
1.2 Graph theory . . . 64
1.3 Vehicle mathematical model . . . 64
2 Distributed State Observer Architecture . . . 65
2.1 General structure of the observer . . . 65
2.2 On the structure of the observer (4.5) . . . 66
2.3 Introduction of a virtual communication graph . . . 67
2.4 Main objectives . . . 67

3 Trust Score Framework . . . 67
3.1 Data validity indicator . . . 68
3.2 Local trust . . . 68
3.2.1 Velocity consistency: . . . 68
3.2.2 Distance consistency: . . . 70
3.2.3 Acceleration consistency: . . . 70
3.2.4 Fusion and update rule: . . . 71
3.3 Distributed trust . . . 71
3.3.1 Consistency with host's global estimate: . . . 71
3.3.2 Consistency with host's local measurement: . . . 72
3.3.3 Self-consistency with host's local measurement: . . . 73
3.4 Target trust and temporal evolution . . . 73
3.4.1 Discretization into trust quality: . . . 73
3.4.2 Accumulated trust history: . . . 74
3.4.3 Normalized trust distribution: . . . 74
3.4.4 Expected trust level: . . . 74
3.5 Generalized trust vector . . . 74
4 Weight Design for observer based on the trust . . . 77
4.1 Weight based on the trust . . . 77
4.2 Stability of the error . . . 77
5 Simulation Results . . . 80
5.1 Simulation setup . . . 81
5.2 Attack scenarios . . . 81
5.3 Results . . . 81
5.4 Distributed State Estimation for Platoon Control . . . 83
5.4.1 Notation . . . 83
5.4.2 Inner/Local Controller: Intelligent Driver Model (IDM) . . . 85
5.4.3 Cooperative Controller: Cooperative Adaptive Cruise Control (CACC) 86
5.4.4 Final Controller . . . 87
5.4.5 Expected Distance (Spacing) . . . 87
6 Conclusion and Future Work . . . 89
6.1 Open Problems and Future Directions . . . 89

5 Vehicle experiments and Board electronic 91
1 Vehicle Experiments . . . 92
1.1 Experimental methodology: from virtual validation to real trials . . . 92
2 Quanser QCar2/QLabs experimental platform . . . 93
2.1 Virtual environment and scenario definition . . . 93
2.2 Measurements and perception pipeline . . . 94
2.3 V2V communication and modular software architecture and Attack design . . . 95
2.3.1 Design of V2V communication . . . 95
2.3.2 Attack injection mechanism . . . 96
3 Control architecture . . . 97
3.1 Longitudinal control: cooperative cruise control . . . 97
3.2 Lateral control: extended look-ahead to reduce corner cutting . . . 98
3.3 MPC for following path . . . 98
4 Custom embedded electronic board for future onboard deployment . . . 98
4.1 Motivation and design objectives . . . 98
4.2 Architectural Alignment with State-of-the-Art . . . 99

4.3 Architecture and PCB design . . . 100
4.4 Firmware structure and first validation tests . . . 102
4.5 Integration roadmap with thesis algorithms . . . 105
5 Conclusion . . . 106

Conclusion and Perspectives **107**
1 General Conclusion . . . 107
2 Outlook and Perspectives . . . 108

List of Publications **110**

Bibliography **111**

List of Figures

1.1 CACC under cyber-attack scenario. . . . 5
1.2 Hybrid resilient estimation framework for connected vehicles. . . . 7
1.3 Organization of the thesis. . . . 9

2.1 Illustration of CACC working on a vehicle platoon. . . . 12
2.2 Discrete-time model-based UIO. . . . 15
2.3 Resilient control for CACC system. . . . 19
2.4 State estimation case 1. . . . 20
2.5 Attack estimation using UIO case 1. . . . 21
2.6 Attack estimation and the errors case 2. . . . 21
2.7 Discrete-time model-based UIO 22
2.8 Carla Simulator platform (GitHub repository). . . . 23
2.9 Vehicle trajectories of preceding-following vehicle. . . . 24
2.10 Control input of preceding-following vehicle. . . . 24
2.11 State estimation error of 2 discretization method. . . . 25
2.12 Comparison of cyberattack estimation and error. . . . 26

3.1 Diagram of the proposed hybrid estimation strategy. . . . 44
3.2 Schematic of the continuous learning with forgetting mechanism. . . . 48
3.3 Vehicle trajectory in the XY-plane with near-zero position tracking error (inset), and the corresponding steering and throttle control inputs computed using the Layer 2 (NAO) state estimates as feedback. . . . 56
3.4 State estimation results: all estimated states closely follow the true signals, including the unmeasured lateral velocity v_y. . . . 57
3.5 Tire-force residual and slip angle estimation: Layer 2 (NAO) achieves faster convergence and higher precision compared to Layer 1 (UIO), while both estimates remain bounded. . . 58

4.1 Schematic diagram of the estimation method. . . . 66
4.2 Trust framework. . . . 68
4.3 Weight based distance for $\mathcal{O}_{i,j}^{\text{dis}}$. . . . 76
4.4 Heatmap of normalized impact scores for all vehicles and attack cases. . . . 83
4.5 Trust score evolution during DoS attack (***Case 6***). . . . 84
4.6 State-estimation errors for all vehicles. . . . 84
4.7 State trajectories of the four-vehicle platoon (vehicle 4 is the tail vehicle). . . . 85
4.8 Acceleration command (controller output) for vehicles 2. . . . 88
4.9 Acceleration command (controller output) for vehicles 3. . . . 88
4.10 Relative distance to the predecessor in the platoon. . . . 89

5.1 Modular Experimental Phases. 92
5.2 Experimental workflow for the virtual validation on QLabs/QCar2 and preparation of real trials. 93
5.3 QLabs map and example of selected waypoints for the vehicle. 94
5.4 Layered architecture of the V2V communication stack used in the QLabs experiments. . 96
5.5 Attack injection mechanism integrated into the V2V communication layer. 97
5.6 Effect of extended look-ahead on corner cutting in curves. 98
5.7 Block architecture. 103
5.8 Embedded board design: KiCad PCB implementation. 103
5.9 Prototype validation and manufactured embedded board. 104

List of Tables

2.1 Parameters of CACC system and the controller gains. 19
2.2 Control input metrics u_{sync} for Euler and exact (ZOH) discretization (CARLA simulation). 25
2.3 State estimation error metrics for Euler and exact discretization (CARLA simulation). . . 25

3.1 Summary of specific cases: assumptions, design choices, and convergence properties. . . 42

4.1 Summary of observer notation, trust variables, and index meaning. 69
4.2 Main simulation parameters. 81
4.3 Six attack cases in the scenario. 81

5.1 Summary of measurements and metadata available on QCar2/QLabs used for control, estimation, and trust evaluation. 95
5.2 Examples of COTS V2X products relevant to this thesis motivation. 100
5.3 Embedded board design targets for thesis-to-vehicle transfer (high-level, implementation-dependent). 102

Chapter 1

General Introduction

Objectives

This chapter lays the foundation for the thesis by outlining the research context, challenges, and objectives in resilient state estimation for connected autonomous vehicles. It motivates the need for hybrid and cooperative observer designs, summarizes the main contributions, and presents the organization of the manuscript.

Contents

1 Historical Background of Estimation Theory and Observer Design **2**
2 Recent Advances in Hybrid and Resilient Estimation **2**
3 Literature Review Summary **4**
4 Positioning and challenges **7**
5 Main contributions **8**
6 Organization of the manuscript **8**

1 Historical Background of Estimation Theory and Observer Design

State observers have been a cornerstone of control theory since the 1960s. The classical Luenberger observer, introduced by Luenberger (1964/1966), uses available inputs and outputs to reconstruct the internal state of a plant and asymptotically drive the estimate toward the true state. In parallel, Kalman's work on the Kalman filter (1960) established the foundations of stochastic state estimation, widely adopted for navigation and sensor fusion.

As control applications grew in complexity (e.g., aerospace and automotive systems), observer theory expanded to cope with unknown inputs, such as disturbances or unmeasured actuator effects. Unknown Input Observers (UIOs) were developed to estimate states despite these signals, under algebraic design conditions (often expressed as rank/matching constraints), and were applied extensively to fault detection and isolation. Representative contributions include the UIO-based fault-diagnosis frameworks of [1] . In the same period, sliding-mode observers emerged as a robust alternative: by injecting discontinuous corrective terms, they can enforce finite-time error convergence and, in sliding motion, reduce sensitivity to certain matched uncertainties, enabling reconstruction of faults or disturbances via the so-called equivalent input.

Throughout the 1990s and 2000s, a broad family of robust and adaptive designs including H_∞, high-gain, and adaptive observers were proposed to maintain estimation performance under modeling errors, noise, and component faults. In automotive systems, these observers and filters became core building blocks, from early ECUs using Kalman filtering to multi-sensor schemes estimating lateral dynamics (e.g., slip angle or roll angle) [2], wheel slip for anti-lock braking, and difficult-to-measure quantities such as road bank angle or tire forces modeled as disturbances [3]. This historical evolution, from classical linear observers to robust and unknown-input extensions, sets the stage for today's resilient estimation frameworks.

2 Recent Advances in Hybrid and Resilient Estimation

Contemporary estimation research for connected and autonomous vehicles has converged on three directions: resilience to attacks/faults, hybrid model–data observer architectures, and cooperative distributed estimation. Purely model-based observers remain attractive because they provide explicit stability and robustness guarantees, but they can degrade under strong model mismatch or violated matching/observability conditions. Purely data-driven estimators can be accurate yet difficult to certify for safety-critical deployment. As a result, current designs increasingly combine a robust nominal observer with learning-based compensation to preserve guarantees while adapting to unmodeled dynamics.

At the same time, resilience is now treated as a first-class requirement rather than an add-on robustness property. Modern estimators explicitly account for malicious data injection, sensor faults, and communication anomalies, often by modeling attacks as unknown inputs and reconstructing them for mitigation. In parallel, distributed observer frameworks exploit V2V cooperation so that vehicles can recover states or disturbances that are not locally observable.

Another strong trend is the relaxation of restrictive classical UIO conditions through output augmentation, geometric constructions, and optimization-based designs, making unknown-input estimation

feasible for more realistic vehicle models. Detailed evidence from recent papers is synthesized in the Literature Review Summary section below, where each methodological pillar is reviewed in depth.

Industrial relevance and deployment challenges

Bridging these advanced techniques from research to industry is a non-trivial task. Automotive systems are a prime example of cyber-physical systems where estimation algorithms must satisfy real-world constraints beyond theoretical performance. One major consideration is functional safety: industry standards demand that any component affecting vehicle control be robustly verified and fail-safe. This means an estimator must not only perform well nominally, but also handle worst-case scenarios (sensor failures, extreme environmental conditions, communication dropouts) without causing unsafe behavior. Model-based observers have an advantage here – their behavior under faults can often be bounded or analyzed using control theory. For instance, a well-designed H_∞ observer or interval observer can guarantee that estimation errors remain within set bounds for any disturbance within a specified energy or interval limit. In contrast, purely data-driven or black-box learning approaches raise concerns because proving their correctness or stability in all cases is difficult. Industry engineers thus tend to favor algorithms that come with analytic guarantees or at least are interpretable. This conservatism has motivated the hybrid approaches discussed earlier, which allow incorporation of machine learning without sacrificing the rigor of classical observers.

Another challenge is real-time computational constraints. Automotive electronic control units (ECUs) and networks have limited processing power and strict timing deadlines (often on the order of 1–10 ms for low-level control loops). Estimation algorithms with heavy computation (e.g. large neural networks or complex optimization-based observers) might be infeasible to run on current in-vehicle hardware. This drives the need for efficient implementations or hardware acceleration. It is not uncommon for advanced estimation algorithms to be prototyped in MATLAB/Simulink on a PC and then have to be simplified or optimized (e.g. using fixed-point arithmetic or reducing neural network size) for an actual vehicle ECU. The gap between academic prototypes and automotive-qualified software can be significant. Additionally, any algorithm intended for market deployment faces extensive testing: billions of miles of simulations and road tests are needed to validate autonomous vehicle software under diverse conditions. Estimation errors that are negligible on average could prove catastrophic in rare edge cases, so engineers must identify and mitigate these through scenario testing.

Environmental uncertainty presents further difficulties. Autonomous and connected vehicles operate in dynamic, unstructured environments where sensor data can degrade (heavy rain or fog affecting cameras and LiDAR, for example [4]) and where the vehicle's dynamics can change (tire friction changes with road surface, load variations, etc.). Estimation algorithms must be robust to these variations or adaptive enough to track them. This is closely tied to resilience: an estimator should ideally detect when sensors are providing poor data (whether due to faults, attacks, or harsh conditions) and adjust weightings or switch to fallback sensors. Industrial systems often include redundancy (e.g. multiple sensors measuring the same quantity) so that observer-based fault detection can exclude a bad sensor reading and use an alternative. For connected vehicles, redundancy can even be virtual – if a vehicle loses its own sensor, it might use a neighbor's information via V2V communication. However, this introduces the vulnerability of connectivity: as mentioned earlier, V2V signals may arrive delayed, be missing, or be maliciously corrupted. The estimator and the overall control system must be designed to maintain safety despite

these communication issues. For example, cooperative Adaptive Cruise Control (CACC) algorithms typically degrade gracefully to normal ACC if V2V data is lost or untrustworthy, relying only on local radar sensing. This graceful degradation requires observers to quickly detect anomalies in received data (e.g. a sudden improbable drop in a neighbor's reported speed might indicate a spoofed message) and isolate or reject that data.

From an industrial standpoint, resilience against cyber-attacks is increasingly recognized as a necessary feature of autonomous vehicle software. High-profile demonstrations of car hacking have led to efforts in securing communications and ensuring observer-based monitors can promptly detect intrusions. Estimation algorithms that can reconstruct an attack signal (like the false acceleration command in a platoon) in real time are valuable for triggering mitigation strategies (such as switching to a safe mode). In this thesis, for instance, one objective is to estimate false data injection attacks on V2V links as unknown inputs and remove their effect. This kind of capability is likely to be incorporated in future vehicle intrusion detection systems (IDS) and resilient controllers.

Finally, it is important to mention the role of high-fidelity simulation and real-world testing platforms in bridging theory to practice. Researchers and engineers increasingly use platforms like CARLA [5] (an open-source vehicle simulator) and industry tools like dSPACE/Simulink for validation of estimation algorithms in realistic scenarios. For example, in Chapter 2 of this thesis, a resilient observer for a CACC platoon under attack was tested in the CARLA simulator. The scenario involved a lead vehicle broadcasting false acceleration data to its followers; using CARLA allowed the inclusion of realistic vehicle dynamics and sensor noise. Results showed that the proposed observer could still detect and estimate the attack, though with a convergence delay of a few seconds and some noise-induced estimation error. Such studies underscore practical issues (estimator convergence time, noise sensitivity, model discrepancies) that might not be evident in pure theory. By incorporating realistic benchmarks and case studies, the development of observers can be guided to address the gaps between an idealized design and a deployable solution. In summary, while advanced estimation algorithms hold great promise for improving autonomy and safety, their industrial adoption hinges on meeting strict requirements for real-time performance, reliability, and certifiability in the unpredictable conditions of the real world.

3 Literature Review Summary

Before proceeding to the detailed contributions, we summarize the key themes from the recent literature that underpin this thesis. Rather than reiterating the historical background already presented above, this section focuses on the most relevant and up-to-date advances (primarily from 2020 onward) organized around the four pillars of this work. In particular, recent surveys emphasize that modern CAV estimation must be simultaneously *robust*, *attack-resilient*, and increasingly *hybrid* (physics + learning), due to both modeling uncertainty and expanding cyber-attack surfaces in connected driving [6, 7].

Resilient estimation and attack mitigation for CACC. Resilient estimation for connected vehicle platoons has become a distinct research area combining observer design with cybersecurity, and recent surveys highlight observer-based detection, secure fusion, and redundancy as cornerstone techniques for CAV resilience [6, 7]. [8] demonstrated simultaneous cyber-attack detection and radar sensor health

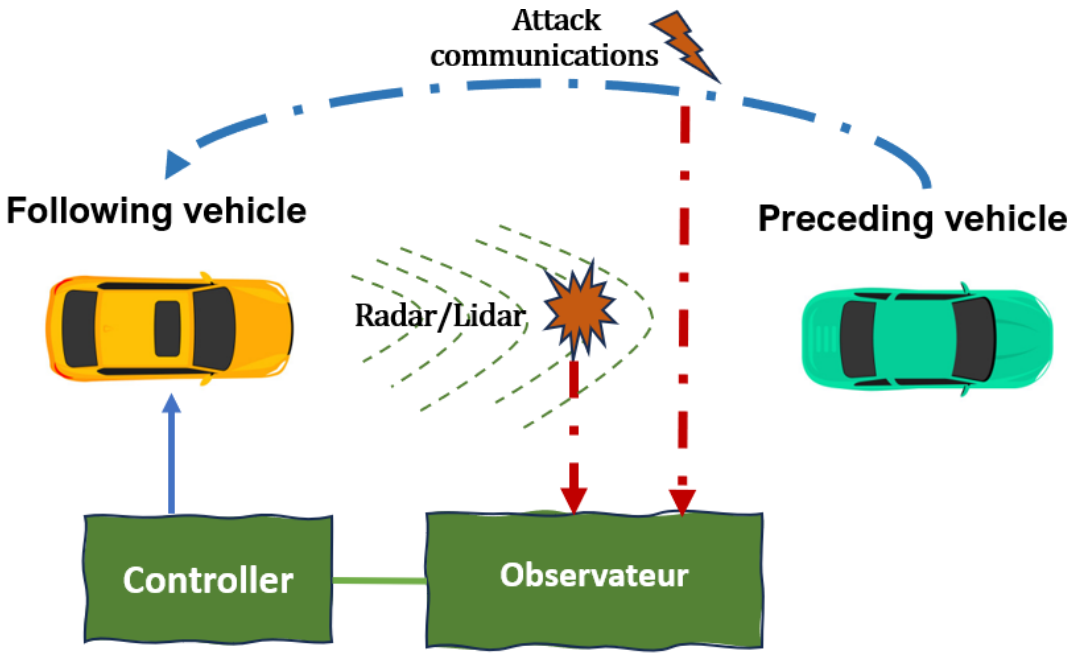

Figure 1.1: CACC under cyber-attack scenario.

monitoring in a connected ACC system using a bank of observers, though limited to constant attack signals. This limitation was addressed in [9], which handles time-varying attacks via a discrete-time UIO with bounded reconstruction delay. For DoS attacks, [10] proposed an observer-based resilient CACC controller that estimates transmission delays induced by denial-of-service scenarios. [11] developed an adaptive UIO with disturbance-aware thresholds for improved attack detection accuracy in intelligent transportation systems. Secure multi-sensor fusion frameworks under sensor attacks provide complementary building blocks to observer-based approaches in connected settings [12]. At the platoon level, the direct impact of false-data injection on string stability has been quantified, reinforcing the need for attack-aware estimation tightly coupled to control objectives [13]. At the fundamental level, [14] established that with $2s$ sensors, exact state recovery is possible under up to s corrupted sensor attacks, providing theoretical limits that guide redundancy-based resilient designs. More recently, [15] formalized resilient synchronization of distributed multi-agent systems under attacks, introducing conditions under which cooperative control can tolerate adversarial agents. These works collectively define the landscape in which the contributions of Chapters 2–4 are situated.

Distributed and trust-aware cooperative estimation. The shift from single-vehicle to network-level estimation has accelerated with the deployment of V2V communication. [16] developed a distributed UIO for vehicle platoons that enforces a joint observability condition across the network, enabling cooperative estimation of unknown inputs that are locally unobservable. A complementary theoretical perspective is provided by [17], which bridges centralized and distributed UIO frameworks and establishes conditions under which distributed designs recover centralized performance. In the fault-tolerance domain, [18] designed sensor fault-tolerant distributed observers using geometric state-estimation methods, ensuring that estimation remains accurate even when individual sensor channels fail. Trust and resilience in multi-agent consensus have been formalized by [19], who characterize the relationship between agents' trust

values and Byzantine resilience in cyberphysical networks. At the application level, [20] proposed a real-time sensor anomaly detection and recovery mechanism for connected automated vehicles, combining statistical consistency checks with onboard sensor redundancy. For platoon-level operation, secure multi-sensor fusion under sensor attacks and the impact of false-data injection on string stability further motivate trust-aware distributed estimation and control co-design [12, 13]. Taken together, these works motivate the trust-aware distributed observer architecture proposed in Chapter 4 of this thesis.

Learning-augmented and hybrid observers. The integration of machine learning within observer frameworks has matured considerably in recent years. [21] developed a neuro-adaptive observer with LMI-based design that guarantees exponential stability of both state and neural-parameter estimation errors, with an H_∞ bound when the neural approximation is imperfect. [8] applied this paradigm to simultaneous state estimation and tire-model learning for autonomous vehicles, demonstrating how a neural network can learn tire-force nonlinearities online while a model-based observer ensures bounded errors. Physics-informed neural network (PINN) observers have also emerged: [22] proposed an adaptive PINN observer for nonlinear systems that embeds physical constraints into the network training loss, improving estimation robustness for partially known dynamics. More broadly, recent work has shown that hybrid physics–data-driven designs can improve vehicle dynamics state estimation while preserving structure and interpretability [23], and that PINN-aided filtering on manifolds can enhance consistency for vehicle state estimation [24]. In addition, robust learning-based ego-state estimation has been proposed for autonomous driving under challenging conditions [25]. In the continuous-discrete setting, [26] designed a sampled-data neural-network observer for vehicle systems, addressing the practical constraint that measurements arrive at discrete instants while dynamics evolve continuously. From a robotics perspective, [27] introduced knowledge-based neural ordinary differential equations for learning-enhanced state estimation. Finally, because tire–road interaction is a dominant uncertainty source, recent reviews and methods have advanced tire-road friction estimation (including data-enforced filtering and intelligent-tire approaches) [28, 29, 30]. These contributions collectively demonstrate that hybrid model-data estimation can achieve both the safety guarantees of control-theoretic observers and the adaptability of machine learning – a paradigm central to Chapter 3 of this thesis. Figure 1.2 provides an overview of the hybrid resilient estimation viewpoint adopted throughout the manuscript.

Unknown input observers under relaxed conditions. Estimating states and disturbances modeled as unknown inputs remains a central challenge when the classical observer matching condition ($\mathrm{rank}(CB) = \mathrm{rank}(B)$) is not met. Recent efforts have explored several avenues to bypass this restriction. [31] demonstrated that auxiliary outputs generated by high-gain approximate differentiators enable sliding-mode observer construction even when the standard rank condition fails. Building on this idea, [32] combined reduced-order and high-order sliding-mode observers for joint state and unknown-input reconstruction in process systems. In the discrete-time domain, [33] proposed an unknown input observer for networked systems corrupted by sparse malicious packet drops, showing that exact discretization preserves the UIO existence conditions under adversarial communication. More recently, [9] developed a discrete-time UIO for CACC systems that reconstructs time-varying cyberattack signals with bounded delay, while [34] introduced an adaptive higher-order sliding-mode differentiator achieving finite-time attack estimation

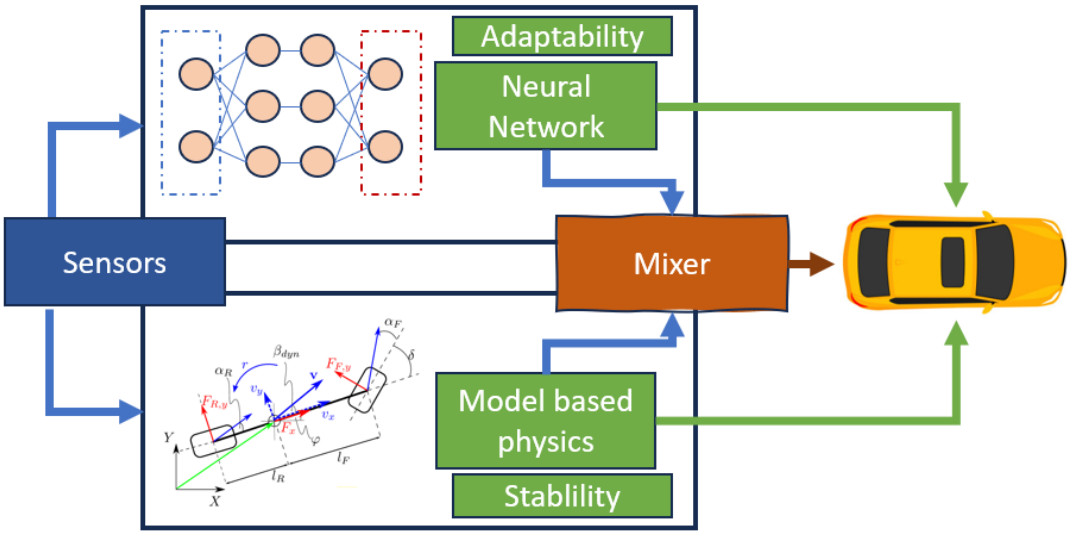

Figure 1.2: Hybrid resilient estimation framework for connected vehicles.

under measurement noise. At the system-theoretic level, [35] proposed unknown-input estimation algorithms for LPV/nonlinear systems and demonstrated them on a wastewater treatment benchmark, and [36] addressed robust UIOs for nonlinear time-delay systems with H_∞ guarantees. These works show that modern UIO designs can handle realistic vehicle models where rank conditions are violated, provided appropriate augmentation or regularization strategies are employed; this is increasingly relevant in CAV settings where unknown-input/attack reconstruction is a key resilience mechanism [7].

In summary, the recent literature exhibits a clear convergence toward *resilient, hybrid, and cooperative* estimation paradigms for connected vehicles. The subsequent chapters build directly on this foundation: Chapter 2 addresses resilient UIO design for CACC under time-varying attacks, Chapter 3 introduces a teacher–student architecture combining a generalized UIO with a neural adaptive observer, and Chapter 4 proposes a trust-aware distributed observer for platoon-level estimation under adversarial conditions.

4 Positioning and challenges

Three methodological challenges motivate the developments in this manuscript.

- **Unknown input reconstruction under realistic assumptions:** estimating attacks/disturbances is not only a detection problem; reconstruction is needed for mitigation and control. Yet, classical unknown input observer (UIO) designs rely on rank/matching conditions that may fail for practical vehicle models.
- **Nonlinear and time-varying uncertainty:** vehicle dynamics include effects that are difficult to capture with fixed parametric models (e.g., aggregated tire/road effects, drag, actuator dynamics variations). Learning can approximate these uncertainties, but must be embedded into a stable observer structure.

- **Distributed estimation with adversarial information:** in platoons, estimation depends on exchanged data. Robustness requires mechanisms to reduce the influence of compromised or unreliable neighbors without destroying convergence.

The remainder of the thesis proposes observer designs addressing these points in a unified resilient estimation viewpoint.

5 Main contributions

The thesis follows a consistent workflow from modeling and observer design to learning/trust augmentation and simulation-based validation.

The main contributions of this thesis can be summarized as follows:

- **Resilient estimation and attack reconstruction for CACC:** an observer-based framework that estimates vehicle states and reconstructs corrupted communicated signals modeled as unknown inputs.
- **Learning with generalized UIOs for nonlinear estimation:** a hybrid teacher–student architecture combining a generalized UIO (robust bounded estimation) with a neural adaptive observer (learning structured uncertainty) under LMI-based stability conditions.
- **Trust-aware distributed state estimation for platoons:** a distributed observer architecture that adapts neighbor influence using a trust/divergence metric to maintain estimation performance under cyber/communication attacks.

Overall, the thesis contributes observer designs that combine robustness, adaptivity, and resilience in connected vehicle applications.

6 Organization of the manuscript

The manuscript is organized as follows. Figure 1.3 summarizes the overall structure and chapter dependencies.

- Chapter 2 studies resilient state estimation and cyber-attack reconstruction for connected autonomous vehicles in a CACC setting.
- Chapter 3 introduces a two-layer, physics-informed learning framework for vehicle state estimation, where a tire-residual teacher observer supervises a neural residual student to compensate remaining modeling errors.
- Chapter 4 proposes a resilient trust-aware distributed observer design for connected vehicle platoons under adversarial conditions.
- The conclusion summarizes the main results and outlines perspectives for future work.

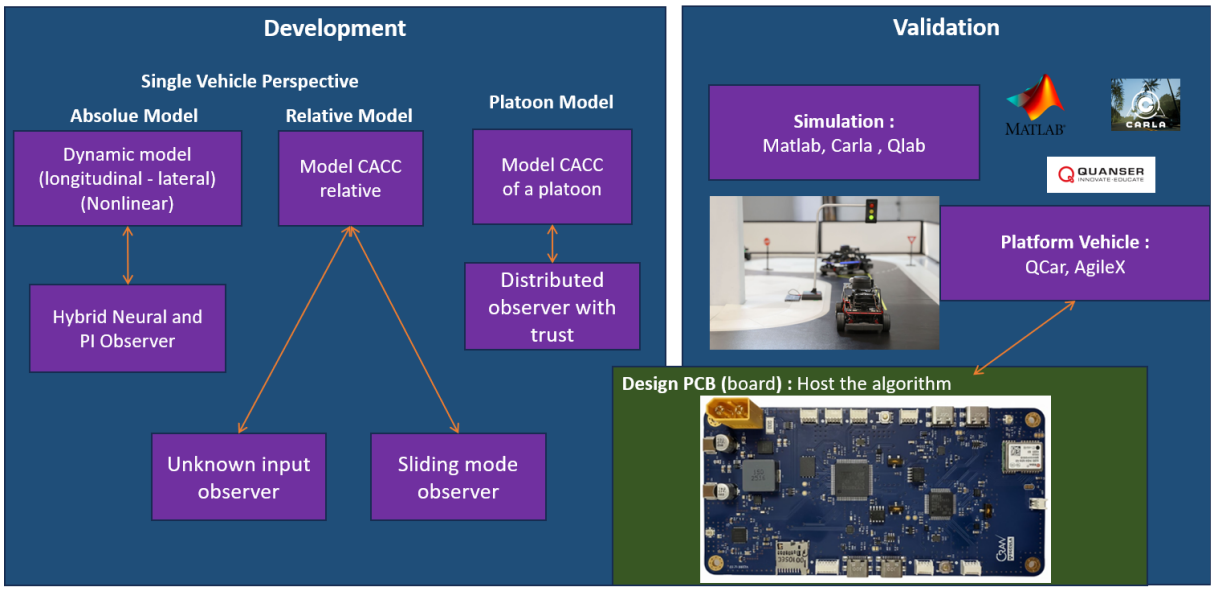

Figure 1.3: Organization of the thesis.

Chapter 2

Resilient State Estimation and Cyber-Attack Reconstruction for Connected Autonomous Vehicles

Objectives

This chapter aims to improve CACC resilience against cyberattacks by designing a discrete-time Unknown Input Observer (UIO) to estimate relative vehicle states and reconstruct false data injection signals, addressing rank-condition issues caused by standard discretization through output delay and exact discretization, and developing observer-based control to compensate attacks in real time while maintaining platoon safety and stability.

Contents

1 Introduction **11**
2 Problem Formulation **11**
2.1 General description of the CACC system 11
2.2 CACC modeling subject to cyberattack 12
2.3 Problem formulation and objectives 14
3 Discrete-Time Model-Based UIO design for CACC system **16**
3.1 UIO structure for the shifted system 16
3.2 LMI-Baed ISS design method 17
3.3 Defense strategy 18
4 Simulation results by Using Matlab and Carla Platform **19**
4.1 Simulation result using Matlab 20
5 Exact Discretization Approach **21**
5.1 Simulation Results and Comparison 23
6 Conclusion **26**

1 Introduction

Connected autonomous vehicles (CAVs) have revolutionized conventional transportation systems through the facilitation of wireless communication and interaction among vehicles [37]. A significant stride in this domain is the emergence of Cooperative Adaptive Cruise Control (CACC), which builds upon the capabilities of Adaptive Cruise Control (ACC). While ACC autonomously adjusts vehicle speeds based on preceding traffic, CACC elevates this functionality by integrating inter-vehicle communication. As wireless communication and data exchange become more prevalent in CAVs, there is a growing concern about cyberattacks. It is essential to detect these attacks to maintain the safety, reliability, and integrity of vehicular communication systems. These attacks can take many forms, such as false data injection, Denial of Service (DoS), eavesdropping, or interference, targeting communication channels or sensor systems. Hence, detecting and mitigating these attacks is crucial for ensuring that CAVs function correctly and road safety is maintained [38, 39, 40, 41].

In prior work, a proportional integral observer was introduced in [42] for state estimation and spoofing attack detection, and in [10] for addressing the DoS attack issue by estimating data transmission delays. Nevertheless, these results are limited to scenarios where the attack evolves slowly. Some other work such as [43] and [11] utilize the concept of unknown input observer (UIO) residual. This residual is used to detect attacks and is enhanced by setting an adaptive threshold that considers the impact of disturbances, thereby improving the accuracy of the attack detector. This UIO-based technique, as utilized also in [8] within the ACC framework, is specifically designed for constant cyberattack signals.

In this paper, we address the challenge of cyberattack detection by utilizing an UIO to estimate attacks and create an observer-based control to mitigate their adverse effects on platoons with CACC. This algorithm can also be used to monitor cyberattack status with different types of control and modifications. A significant difference in our method is that we transmit data using the acceleration of the preceding vehicle rather than the control input. The advantage of this approach is that in a platoon, we cannot have the same control input, and using acceleration data is more suitable. In contrast to the methodology presented in [42, 10, 8], our proposed approach demonstrates the capability to effectively handle time-varying cyberattack. Unlike the framework outlined in [42, 10, 8], which offers adaptability to dynamic cyberattack scenarios.

On each vehicle, the UIO-based estimator computes the relative state between the preceding and following vehicles while examining any potentially erroneous communication signal data. In the event of a cyberattack, a resilience-controlled system is activated, leveraging the state estimated from UIO. Simulation experiments have demonstrated that the proposed mechanism accurately estimates the system state with a 1-step delay and detects attacks with a 2-step delay. This mechanism not only enhances the system stability but also mitigates safety losses induced by cyberattacks.

2 Problem Formulation

2.1 General description of the CACC system

The CACC scenario working on a platoon can be illustrated as in Figure 2.1. The acceleration of preceding vehicle a_{i-1} transmitted through a wireless communication channel to the following vehicle; δ_i denotes

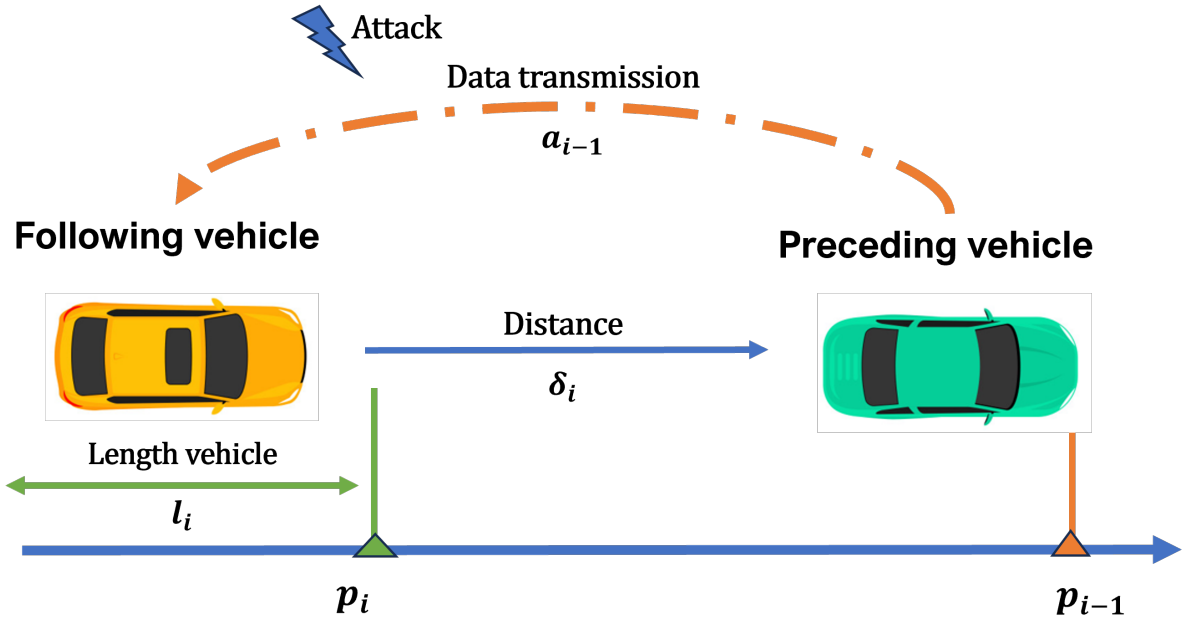

Figure 2.1: Illustration of CACC working on a vehicle platoon.

the distance between the rear of the preceding vehicle and the bumper of the following vehicle; l_i is the length of the following vehicle; p_i and p_{i-1} correspond to the positions of the following and preceding vehicles, respectively.

Following the logic of [44], The CACC control system focuses only on the upper-level controller for acceleration input. It assumes the lower-level execution of throttle and brake control is already functional and optimized

2.2 CACC modeling subject to cyberattack

Basically, the dynamics of ith vehicle are a Position-Velocity-Acceleration third-order linear model given by the following set of equations:

$$\begin{cases} \dot{p}_i(t) = v_i(t) \\ \dot{v}_i(t) = a_i(t) \\ \dot{a}_i(t) = \frac{1}{\tau_i} u_i(t) - \frac{1}{\tau_i} a_i(t) \end{cases} \tag{2.1}$$

where

- $p_i(t), v_i(t)$ and $a_i(t)$ denote the position, velocity and acceleration of the ith vehicle, respectively;
- $u_i(t)$ is the ith vehicle control input representing the desired driving/braking force or acceleration;
- τ is the engine's constant time lag.

The actual spacing between vehicles are $\varepsilon_{i,act} = p_{i-1} - p_i$ and the desired spacing between vehicles in the constant time-gap spacing policy is given by $\varepsilon_{i,des} = L + hv_i$. It follows that the spacing error can be written as:

$$\varepsilon_{i,des} - \varepsilon_{i,act} \triangleq p_i - p_{i-1} + L + hv_i = \varepsilon_i + hv_i, \tag{2.2}$$

where L is the minimum safety distance and h is the time-gap. Then, the controller u_{i} is given by [44]:

$$u_{\mathrm{i}} = -k_1 a_{i-1} + (k_1 + hk_1k_2)a_i - \frac{1}{h}(1 - hk_1k_2)\dot{\varepsilon}_i - \frac{k_2}{h}\varepsilon_i - k_2 v_i \tag{2.3}$$

where a_{i-1} is the acceleration of the preceding vehicle obtained by using inter-vehicle communication. The scalar gains k_1 and k_2 are the controller design parameters to be designed according to the detailed procedure introduced in [44].

The controller u_{i} defined in (2.3) is convenient in perfect situation where the acceleration of the preceding vehicle, a_{i-1}, provided through V2V communication channel is not corrupted by intruders. Unfortunately, in CACC platoons, the V2V communication may provide unreliable acceleration due to potential tampering by attackers. To develop a resilient controller to cyberattacks, we have to consider the attack signal in the design of the controller. To this purpose, we assume that the following vehicle receives the signal $\mu(t)$ corrupted by injected false data in the wireless communication channel:

$$\mu(t) = a_{i-1}(t) + f^c(t) \tag{2.4}$$

where $a_{i-1}(t)$ is the true acceleration and $f^c(t)$ is the additive cyberattack signal. This cyberattack scheme under additive false signals can cover several cyberattack architectures. These may include message falsification attacks, spoofing attacks, and denial of service (DoS) attacks. For instance, in the DoS case, by using the differential mean value theorem, there exists $\theta_t \in [t - \tau(t),\ t]$ such that the delayed signal $a_{i-1}(t - \tau(t))$ can be represented as follows:

$$\begin{aligned}\mu(t) = a_{i-1}(t - \tau(t)) &= a_{i-1}(t) \underbrace{- \frac{\mathrm{d}a_{i-1}}{\mathrm{d}t}(\theta_t)\tau(t)}_{f^c} \\ &= a_{i-1}(t) + f^c.\end{aligned} \tag{2.5}$$

Under a cyberattack, the following vehicle receives μ and will utilize it in its controller. Then, instead of (2.3), the controller u_{i} will be implemented as follows:

$$u_{\mathrm{i}} = -k_1 \mu(t) + (k_1 + hk_1k_2)a_i - \frac{1}{h}(1 - hk_1k_2)\dot{\varepsilon}_i - \frac{k_2}{h}\varepsilon_i - k_2 v_i. \tag{2.6}$$

As shown in Figure 2.1, the radar-measured rear-to-bumper distance is defined as follows:

$$\delta_i = p_{i-1} - p_i - l_{i-1}, \tag{2.7}$$

Then, taking the time derivative of δ_i results in:

$$\dot{\delta}_i = v_{i-1} - v_i, \ddot{\delta}_i = a_{i-1} - a_i, \dddot{\delta}_i = \dot{a}_{i-1} - \dot{a}_i \tag{2.8}$$

where $\dot{\delta}_i$, $\ddot{\delta}_i$, and $\dddot{\delta}_i$ are the relative speed, acceleration, and jerk (rate of acceleration changes) between

two adjacency vehicle. By using (2.7) and (2.8), the controller (2.6) becomes

$$\begin{aligned} u_{\mathrm{i}} = (hk_1k_2)\,\mu - (k_1 + hk_1k_2)\,f^c - k_2 v_i - \frac{k_2}{h}\,(L - l_{i-1}) \\ - (k_1 + hk_1k_2)\,\ddot{\delta}_i + \frac{1}{h}\,(1 - hk_1k_2)\,\dot{\delta}_i + \frac{k_2}{h}\delta_i. \end{aligned} \tag{2.9}$$

We obtain acceleration information of the preceding vehicle directly through wireless communication. Consequently, we introduce the following assumption regarding the jerk of the preceding vehicle.

Assumption 1 (Bounded Jerk). *The jerk of the preceding vehicle is assumed to be negligible over one sampling period, i.e.,*

$$\dot{a}_{i-1} \approx 0. \tag{2.10}$$

This assumption is standard in upper-level CACC design and is justified by the limited bandwidth of vehicle actuators.

Substituting equation (2.9) into (2.1) and using (2.10) and the notation $x = \begin{bmatrix}\delta_i & \dot{\delta}_i & \ddot{\delta}_i\end{bmatrix}^\top$, we obtain the model expressed under the following condensed matrix form:

$$\begin{cases} \dot{x} = Ax + Bv_i + F\mu + \Delta - Wf^c \\ y = Cx \end{cases} \tag{2.11}$$

with

$$A = \begin{bmatrix} 0 & 1 & 0 \\ 0 & 0 & 1 \\ \frac{-k_2}{\tau h} & \frac{-k_3}{\tau h} & \frac{(k_1-k_3)}{\tau} \end{bmatrix}, B = \begin{bmatrix} 0 \\ 0 \\ \frac{k_2}{\tau} \end{bmatrix}, F = \begin{bmatrix} 0 \\ 0 \\ \frac{k_3}{\tau} \end{bmatrix},$$

$$\Delta = \begin{bmatrix} 0 \\ 0 \\ \frac{k_2(L-l_{i-1})}{\tau h} \end{bmatrix}, W = \begin{bmatrix} 0 \\ 0 \\ \frac{k_3-k_1}{\tau} \end{bmatrix}, C = \begin{bmatrix} 1 & 0 & 0 \\ 0 & 1 & 0 \end{bmatrix}$$

where $k_3 \triangleq 1 - hk_1k_2$.

To avoid cumbersome equations, we omit the subscripts i and $i-1$ when representing the interaction between two cars in the CACC scenario. We remove these subscripts from the matrices A, B, F, Δ, W, and C, as well as from the vectors x, y, and f_c. We retain only v_i to avoid confusion with previous equations.

2.3 Problem formulation and objectives

The primary objective in the CACC control problem is to estimate the false data, f^c, and compensate for it within the controller u_{i}. A natural solution involves using the Unknown Input Observer (UIO) technique to simultaneously estimate the state x and the false data f^c.

However, standard UIO design requires a specific rank condition, namely $\mathrm{rank}(CW) = \mathrm{rank}(W)$ [35, 45]. For the CACC system defined in (2.11), we observe that $\mathrm{rank}(CW) = 0$ while $\mathrm{rank}(W) = 1$. Consequently, the standard rank constraint is not satisfied, preventing direct application of the method.

To overcome this limitation, we require additional information, specifically the relative acceleration. One approach is to use a real-time differentiator to estimate the derivative of the relative velocity online.

Since $CB = CF = C\Delta = CW = 0$, we can define the derivative of y as a pseudo-measurement:

$$\bar{y} \triangleq \dot{y} = CAx = \bar{C}x. \tag{2.12}$$

With this new measurement, we verify that $\text{rank}(\bar{C}W) = \text{rank}(W) = 1$, which allows us to construct a UIO to estimate both x and f^c, provided that additional stability conditions are met.

There are numerical differentiators in the literature allowing the online calculation of the derivative of a given signal, such as the famous sliding mode observer [32], and the high-gain observer [46]. However, these numerical differentiators fail in some situations, namely in the presence of sensor noises. An alternative solution to avoid real-time estimation of the derivative of y consists in investigating the problem by using the discrete-time version of the model, as shown in Figure 2.2 which considers additive sensor noise ω.

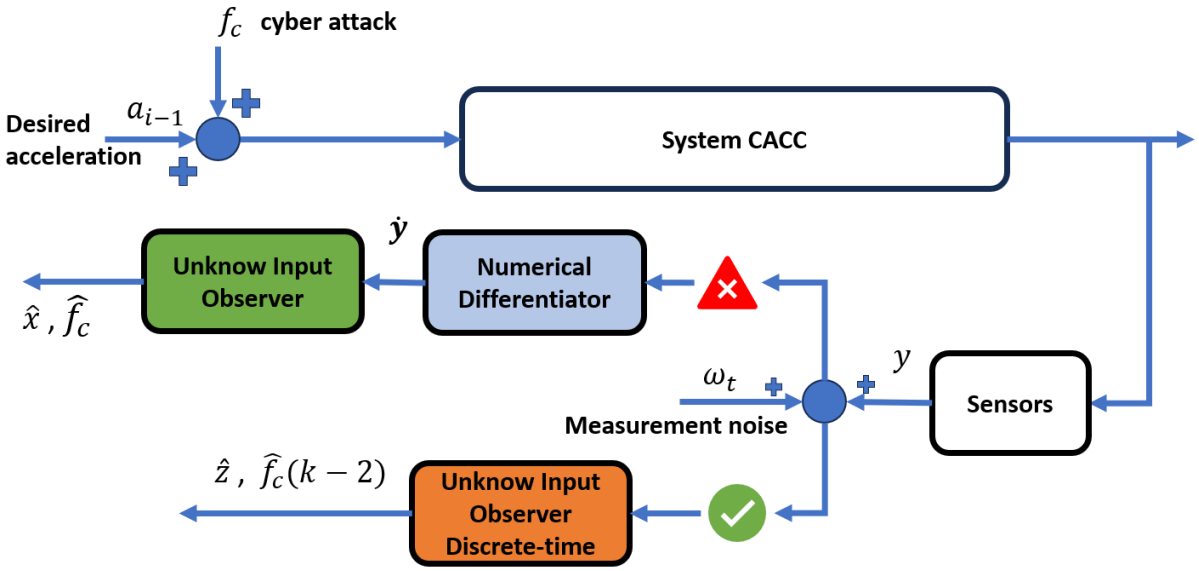

Figure 2.2: Discrete-time model-based UIO.

Indeed, in discrete time, there is no differentiation since the measured signal is a sequence of numbers. The discrete-time version of equation (2.11) is given as follows:

$$\begin{cases} x_{k+1} = \mathcal{A}x_k + \mathcal{B}v_{i,k} + \mathcal{F}\mu_k + \bar{\Delta} - \mathcal{W}f_k^c \\ y_k = Cx_k \end{cases} \tag{2.13}$$

where

$$\mathcal{A} = (\mathbb{I}_3 + TA),\ \mathcal{B} = TB,$$

$$\mathcal{F} = TF,\ \mathcal{W} = TW,\ \bar{\Delta} = T\Delta,$$

and T being the sampling time. In this case, we propose shifting the output equation backward using the discrete-time state equation (2.13). This allows us to express the output y_k as a function of the delayed state $x_{k-\tau}$, where τ is the smallest positive integer that satisfies the necessary rank condition.

In the following section, we adopt this strategy to develop a discrete-time model-based UIO for the

CACC system, enabling the estimation of the cyberattack signal f^c.

3 Discrete-Time Model-Based UIO design for CACC system

This section is devoted to the development of a new unknown input observer based on the discrete-time model (2.13). By introducing the variables

$$z_t \triangleq x_{k-1} \text{ and } \bar{y}_t \triangleq y_{k-1} \tag{2.14}$$

with $t = k - 1$ and considering additive vector noises, ω_t, in both the output measurements and in the process equation, we obtain the following new system

$$\begin{cases} z_{t+1} = \mathcal{A}z_t + \mathcal{B}v_{i,t} + \mathcal{F}\mu_t + \bar{\Delta} - \mathcal{W}f_t^c + E_\omega\omega_t \\ \bar{y}_t = \mathcal{C}z_t + D_\omega\omega_t \end{cases} \tag{2.15}$$

for which the rank condition is satisfied, i.e.:

$$\text{rank}(\mathcal{C}\mathcal{W}) = \text{rank}(\mathcal{W}) = 1. \tag{2.16}$$

3.1 UIO structure for the shifted system

By using an UIO corresponding to the shifted system (2.15), we will estimate simultaneously z_t and f_{t-1}^c. By using the notation

$$\xi_t \triangleq \begin{bmatrix} z_t \\ f_{t-1}^c \end{bmatrix},$$

$$\mathbb{E} = \begin{bmatrix} \mathbb{I}_3 & \mathcal{W} \end{bmatrix}, \; A_\xi = \begin{bmatrix} \mathcal{A} & 0 \end{bmatrix}, \; C_\xi = \begin{bmatrix} \mathcal{C} & 0 \end{bmatrix}$$

the system (2.15) is written under the following descriptor form:

$$\begin{cases} \mathbb{E}\xi_{t+1} = A_\xi\xi_t + \mathcal{B}v_t + \mathcal{F}\mu_t + \Delta + E_\omega\omega_t \\ \bar{y}_t = C_\xi\xi_t + D_\omega\omega_t. \end{cases} \tag{2.17}$$

From (2.16), we have

$$\text{rank}\left(\begin{bmatrix} \mathbb{E} \\ C_\xi \end{bmatrix}\right) = n + \text{rank}(\mathcal{C}\mathcal{W}) = n + 1.$$

Now, let P_z and Q_z be two matrices of appropriate dimensions such that

$$\begin{bmatrix} P_z & Q_z \end{bmatrix} = \left(\begin{bmatrix} \mathbb{E} \\ C_\xi \end{bmatrix}^\top \begin{bmatrix} \mathbb{E} \\ C_\xi \end{bmatrix} \right)^{-1} \begin{bmatrix} \mathbb{E} \\ C_\xi \end{bmatrix}^\top. \tag{2.18}$$

It follows that

$$P_z\mathbb{E} + Q_zC_\xi = \mathbb{I}_p \tag{2.19}$$

where p is the number of output measurements.

By considering the following two-stage observer

$$\begin{cases} \kappa_{t+1} = \Big(P_z A_\xi - K C_\xi\Big)\kappa_t + P_z \mathcal{B} v_{i,t} \\ \qquad\quad + \Big[\Big(P_z A_\xi - K C_\xi\Big) Q_z + K\Big]\,\bar{y}_t \\ \qquad\quad + P_z \mathcal{F}\mu_t + P_z \Delta \\ \hat{\xi}_t = \kappa_t + Q_z \bar{y}_t \end{cases} \tag{2.20}$$

the estimation error $\tilde{\xi}_t = \hat{\xi}_t - \xi_t$ satisfies the equation:

$$\tilde{\xi}_{t+1} = \Big(P_z A_\xi - K C_\xi\Big)\tilde{\xi}_t + \Big[\Big(K D_\omega - P_z E_\omega\Big) \quad Q_z D_\omega\Big]\,\bar{\omega}_t, \tag{2.21}$$

where $\bar{\omega}_t$ is defined as follows:

$$\bar{\omega}_t \triangleq \Big[\omega_t^\top \quad \omega_{t+1}^\top\Big]^\top. \tag{2.22}$$

Remark 1. *The central focus of this paper does not lie in the details of designing controller parameters k_1 and k_2. Rather, our attention is directed towards the development of a novel cyberattack detection algorithm. It is crucial to note that in the proposed methodology, we make an assumption that the control design phase, specifically ensuring the string stability of the controller (2.3), is considered as a distinct and independent process from the estimation design procedure outlined in this paper. As demonstrated in [44], the controller (2.3) achieves string stability under specific conditions. This stability depends on the transfer function $H(s) = \frac{\bar{\varepsilon}_i}{\bar{\varepsilon}_{i-1}}$, where $\bar{\varepsilon}_i$ is defined in (2.2), satisfying the inequality $|H(j\omega)| \leq 1$. Detailed analysis in [44] reveals that such a condition is met when two critical parameters adhere to certain criteria. Specifically, the condition holds when $-k_1 h > \tau$ and $k_2 > 0$, as meticulously explained in the calculations provided in [44, Eqs.(32)-(34)].*

3.2 LMI-Baed ISS design method

The objective consists in determining the observer gain K such that the estimation error $\tilde{\xi}_t$ is exponentially robust with respect to the bounded disturbance ω_t. The next theorem provides sufficient conditions expressed in terms of LMIs ensuring the robust exponential stability of $\tilde{\xi}_t$. For the sake of brevity, we put $\mathcal{A}_z \triangleq P_z A_\xi$, $\mathcal{D}_z \triangleq Q_z D_\omega$, and $\mathcal{E}_z \triangleq P_z E_\omega$.

Theorem 1. *Assume there exist two symmetric and positive definite matrices $\mathcal{P}$ and $\mathcal{S}$, a matrix $\mathcal{Z}$ of appropriate dimension, and a scalar α, with $\alpha \in]0,1[$, such that the following LMI condition holds:*

$$\begin{bmatrix} -\alpha\mathcal{P} & 0 & \mathcal{A}_z^\top \mathcal{P} - C_\xi^\top \mathcal{Z} \\ (\star) & -\mathcal{S} & \begin{bmatrix} D_\omega^\top \mathcal{Z} - \mathcal{E}_z^\top \mathcal{P} \\ \mathcal{D}_z^\top \mathcal{P} \end{bmatrix} \\ (\star) & (\star) & -\mathcal{P} \end{bmatrix} < 0 \tag{2.23}$$

Then the estimation error $\tilde{\xi}_k$, with $K = \mathcal{P}^{-1}\mathcal{Z}^\top$, satisfies the following exponential Input-to-State Stable (ISS) bound:

$$\boxed{\left\|\tilde{\xi}_t\right\| \leq \sqrt{\frac{\lambda_{\max}(\mathcal{P})}{\lambda_{\min}(\mathcal{P})}}\left\|\tilde{\xi}_0\right\| \alpha^{\frac{t}{2}} + \sqrt{\frac{\lambda_{\max}(\mathcal{S})}{(1-\alpha)\lambda_{\min}(\mathcal{P})}} \max_{0\leq k\leq t} \|\bar{\omega}_k\|.} \tag{2.24}$$

Proof. The proof is based on the Lyapunov function $\vartheta_t \triangleq \tilde{\xi}_t^\top \mathcal{P}\tilde{\xi}_t$. By expanding the expression of ϑ_{t+1} along the trajectories of (2.21), we can deduce easily that under the LMI condition (2.23), we have

$$\vartheta_{t+1} - \alpha\vartheta_t \leq \bar{\omega}_t^\top \mathcal{S}\bar{\omega}_t.$$

Hence, by induction technique and backward substitution, we deduce that

$$\vartheta_t \leq \vartheta_0\alpha^t + \frac{\lambda_{\max}(\mathcal{S})}{1-\alpha} \max_{0\leq k\leq t} \|\bar{\omega}_k\|^2.$$

Consequently, we can conclude by using the double inequality

$$\lambda_{\min}(\mathcal{P})\left\|\tilde{\xi}_t\right\|^2 \leq \vartheta_t \leq \lambda_{\max}(\mathcal{P})\left\|\tilde{\xi}_t\right\|^2.$$

□

3.3 Defense strategy

The key idea consists of developing a Resilient, Robust, and Reliable CACC ($3\mathbb{R}-$CACC) controller able to cope with cyberattacks, external disturbances, and data loss. The $3\mathbb{R}-$CACC defense mechanism is as depicted in Figure 2.3. As soon as an attack or a significant external disturbance is detected, the CACC controller (2.3) will switch to the ACC controller to forget the false data in communication data.

$$u_{\mathrm{i}} = -\frac{1}{h}(v_i - v_{i-1} + \lambda\bar{\epsilon}_i) \tag{2.25}$$

with the condition $h > 2\tau$ and $\lambda > 0$ in order to ensure the string stability. After implementing the controller (2.25), the system no longer remains the same as (2.13). Therefore, we need to transform the controller (2.25) in terms of x and rewrite a new system similar to (2.13). This enables the system to detect cyberattacks, which will be treated as unknown inputs.

Remark 2. *The LMI conditions (2.23) correspond to the system without uncertainties, which guarantee certain robustness with respect to the parameter uncertainties in the sense of the exponential ISS criterion (2.24). Indeed, with the proposed method, if we have uncertainties, i.e.: $A + \delta A$ and $C + \delta C$ instead of A and C, for instance, we can add $\delta Ax(t)$ and $\delta Cx(t)$ in the disturbance vector ω and then the LMIs ensure the exponential ISS bound with respect to the new vector of disturbances, ω, containing the parameter uncertainties. However, such a technique does not ensure exponential convergence of the estimation and tracking errors to zero in the free-disturbance case (with the initial vector of disturbances without including the uncertain parameters), and the boundedness of δA and δC does not imply necessarily the boundedness of $\delta Ax(t)$ and $\delta Cx(t)$. To overcome this issue, we need to develop an extended LMI condition that consider both the structure and magnitude of uncertainties.*

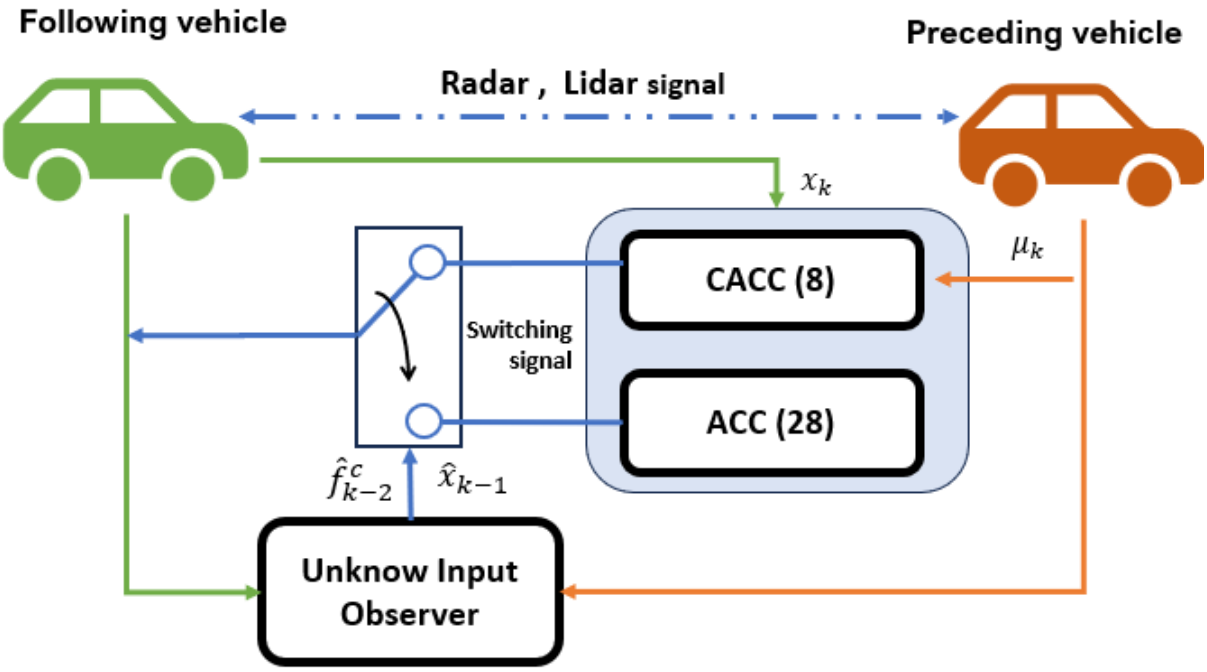

Figure 2.3: Resilient control for CACC system.

4 Simulation results by Using Matlab and Carla Platform

We demonstrate the effectiveness of the proposed observer by conducting MATLAB and CARLA simulations with two cyberattack scenarios. The parameters of the CACC system and its controller are given in Table 2.1.

Parameter	τ	L	l_i	h	k_1	k_2	t_s
Value	0.4	7.3	5	0.5	-0.8	2.5	0.01
Unit	s	m	m	s	-	-	-

Table 2.1: Parameters of CACC system and the controller gains.

It is assumed that two vehicles are driving longitudinally on the road, and each vehicle is equipped with a cruise control system. The preceding vehicle should pursue the following desired trajectory: $a_{i-1}(t) = 3\sin(\frac{2\pi}{10})t$. The two simulation scenarios of cyberattacks explored here are outlined below:

Case 1: *Sparse attack, DoS, packet-loss:*

$$f^c(t) = \begin{cases} X(t) & 6 \leq t < 8 \\ a_{i-1}(t) & 10 \leq t < 15 \\ 0 & \text{otherwise} \end{cases} \tag{2.26}$$

Case 2: *False data injected :*

$$f^c(t) = \begin{cases} -5 & 6 \leq t < 8 \\ 2(t-4) & 10 \leq t < 15 \\ 0 & \text{otherwise} \end{cases} \tag{2.27}$$

where $X(t) \sim U(-5, 5)$ is a random variable following a uniform distribution, with probability $P(X(t)) = 0.2$.

4.1 Simulation result using Matlab

By solving the LMI condition (2.23), we obtain the observer gain K given by:

$$K = \begin{bmatrix} 0.5000 & -0.005 & 0.0498 & -8.9295 \\ -0.005 & 1.000 & -99.9950 & 1427.22 \end{bmatrix}^\top.$$

The proposed observer is designed to estimate the state vector, including relative position, relative velocity, and relative acceleration, as well as provide an accurate estimation of any cyberattacks even in the presence of a Gaussian noise $\omega_t = \mathcal{N}(0.02^2[m])$ for both system and measurement. For both attack scenarios, we set the initial conditions of the actual system as $\xi_0 = \begin{bmatrix} 5 & 10 & 0 & 0 \end{bmatrix}^\top$, while the initial state of the observer is set to $\hat{\xi}_0 = \begin{bmatrix} 0 & 0 & 0 & 0 \end{bmatrix}^\top$.

Simulation results for the first scenario of cyberattack (2.26) are presented in Figure 2.4 and Figure 2.5. In Figure 2.4, we can see the error of the relative position, relative velocity, and relative acceleration along with their estimates. The observer demonstrates similar good performance in accurately reconstructing a random cyberattack and packet-loss, as depicted in Figure 2.5. As we can see, the estimated delay attack is exactly 2 steps.

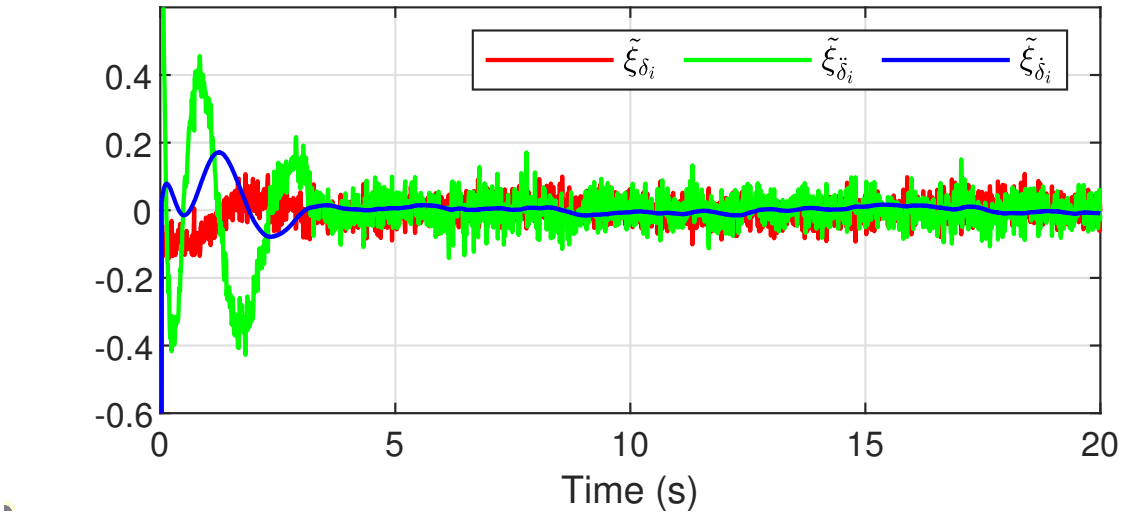

Figure 2.4: State estimation case 1.

For the second case of time-varying and bounded attack signal (2.27), it can be observed from the Figure 2.6 that the cyberattack signal is accurately estimated, and the estimation error is bound.

We can see that the proposed observer can estimate the full state with good accuracy, while the unknown input is reconstructed with a fixed delay of two units based on the available output measurements.

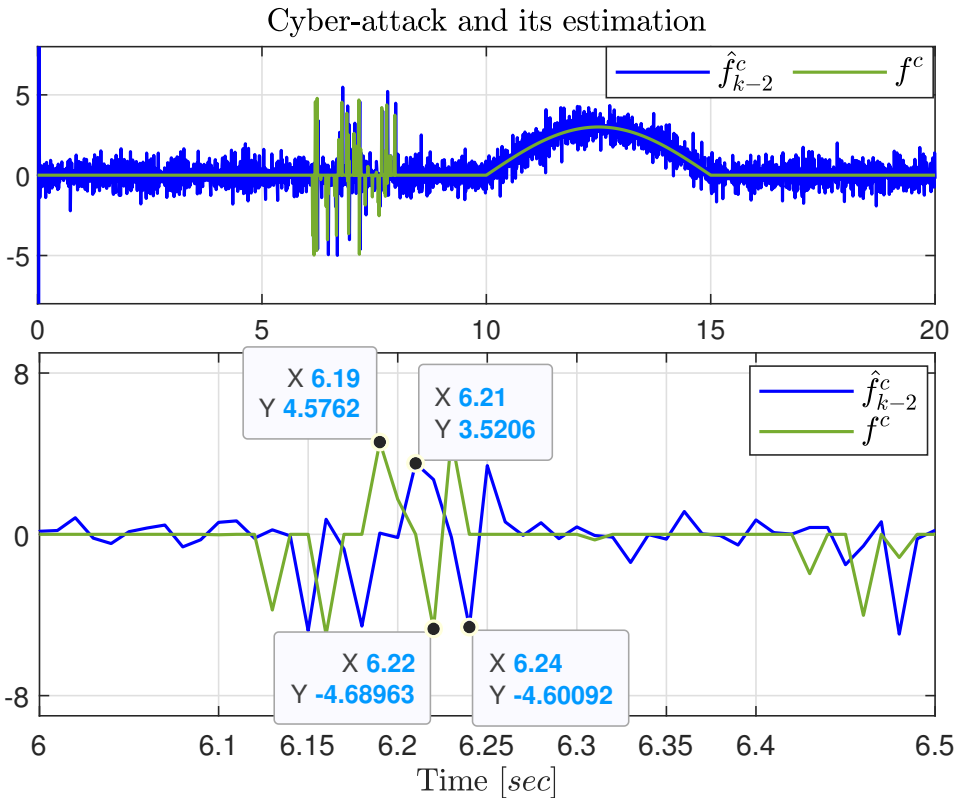

Figure 2.5: Attack estimation using UIO case 1.

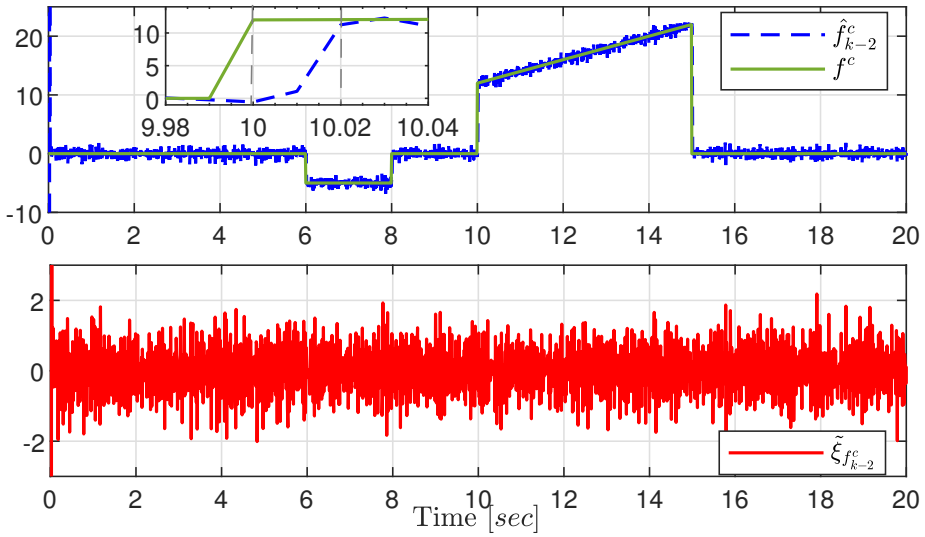

Figure 2.6: Attack estimation and the errors case 2.

5 Exact Discretization Approach

The observer design developed in the previous sections relies on a discrete-time model obtained via forward Euler discretization. This choice is convenient because it preserves the continuous-time structure

and enables the direct use of classical UIO existence and stability results. However, forward Euler may destroy the algebraic coupling between the unknown input and the measured output, which can lead to a violation of the rank condition and, consequently, to the use of delayed outputs. Importantly, this delay is not a physical requirement of the CACC dynamics; it is a numerical artifact induced by the discretization method.

The key intuition is simple: a force (or acceleration) affects the vehicle motion *within* each sampling interval. In particular, acceleration influences velocity and position through higher-order terms (e.g., $\frac{1}{2}aT_s^2$). By contrast, the Euler update $p_{k+1} = p_k + T_s v_k$ neglects this intra-sample coupling, which can sever the direct link needed by the rank condition. To preserve these higher-order effects, we adopt an exact (ZOH) discretization based on the matrix exponential [33]. The resulting discrete-time model captures the full state evolution between samples and restores the structural coupling required for a delay-free UIO.

Figure 2.7 illustrates the observer-based cyberattack estimation framework using the exact discretization model.

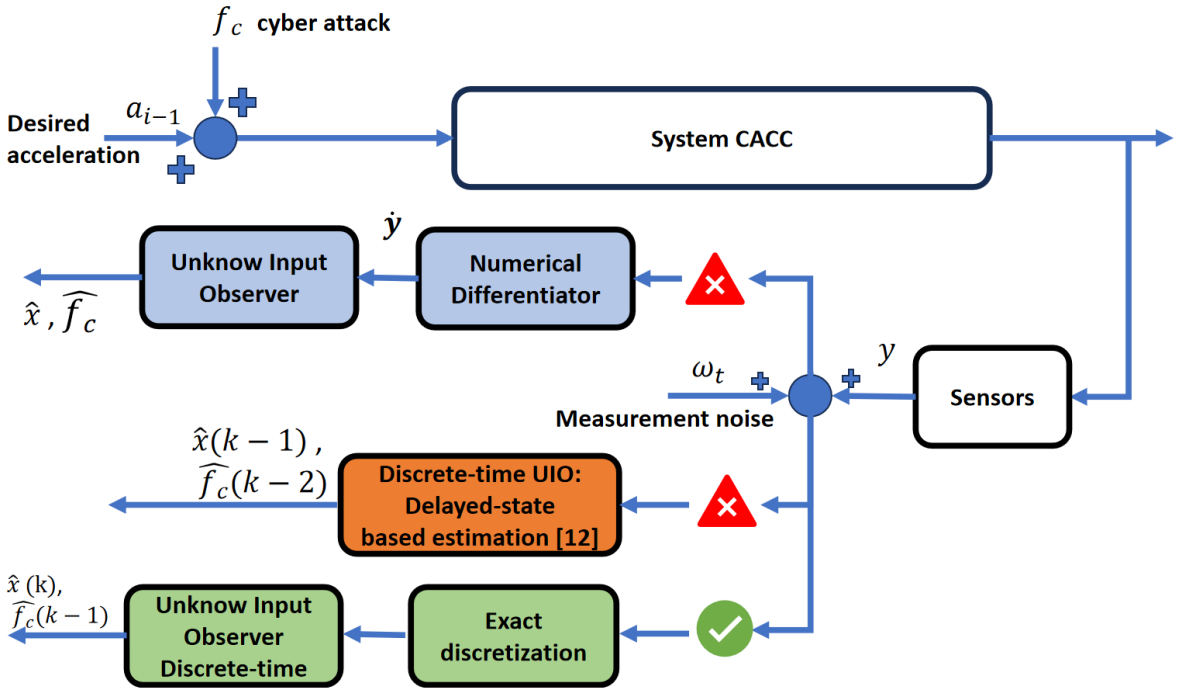

Figure 2.7: Discrete-time model-based UIO

Following the exact discretization method detailed in [33], the discrete-time model of the CACC system is given by:

$$\begin{cases} x_{k+1} = A_d x_k + B_d v_{i,k} + F_d \mu_k + \hat{\Delta} - W_d f_k^c \\ y_k = C_d x_k \end{cases} \tag{2.28}$$

where the system matrices are computed as:

$$A_d = e^{AT_s}, \quad B_d = \int_0^{T_s} e^{A\eta} B d\eta, \quad C_d = C,$$
$$F_d = \int_0^{T_s} e^{A\eta} F d\eta, \quad W_d = \int_0^{T_s} e^{A\eta} W d\eta, \quad \hat{\Delta} = \int_0^{T_s} e^{A\eta} \Delta d\eta,$$

with T_s denoting the sampling period (under a zero-order hold assumption over $[kT_s, (k+1)T_s)$).

We now verify the rank condition for the discretized system (2.28). Using the system parameters given in Table 2.1, we obtain:

$$C_d W_d = \begin{pmatrix} 0.0008 \times 10^{-3} \\ 0.2442 \times 10^{-3} \end{pmatrix} \neq 0.$$

Since $C_d W_d \neq 0$, the rank condition $\mathrm{rank}(C_d W_d) = \mathrm{rank}(W_d) = 1$ is satisfied. This confirms that the unknown input f_k^c can be estimated directly from the output y_k without requiring any delay.

5.1 Simulation Results and Comparison

To evaluate the impact of the discretization method, we compare two discrete-time designs built from the same continuous-time model: (i) the Euler-discretized (delayed-output) observer presented in the previous sections and (ii) the proposed delay-free observer based on exact (ZOH) discretization. We conduct CARLA simulations following the general procedures described in [9].

We solve the LMI conditions for the observer gains using the CVX Toolbox with the exponential stability parameter $\alpha = 0.5$. The resulting gains are:

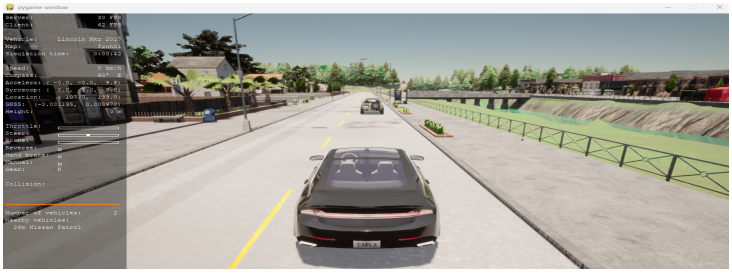

Figure 2.8: Carla Simulator platform (GitHub repository).

$$K_{euler} = \begin{bmatrix} 0.2500 & -0.0025 & 0.2500 & -11.1139 \\ -0.0050 & 1.0000 & -99.9950 & 1851.0714 \end{bmatrix}^\top.$$

$$K_{exact} = \begin{bmatrix} 0.2500 & 0.0012 & -0.3080 & 6.6744 \\ -5.3 \times 10^{-5} & 0.4461 & -46.1776 & 1216.7071 \end{bmatrix}^\top.$$

Figure 2.10 indicates that the discretization method also impacts the control effort. In particular, the exact discretization leads to a less aggressive input. Table 2.2 confirms this trend by showing reductions in both RMS and peak values of u_{sync} after the warm-up period.

Figure 2.11 compares the state estimation errors for position, velocity, and acceleration under Euler and exact discretization. Overall, the exact discretization approach yields a faster transient response

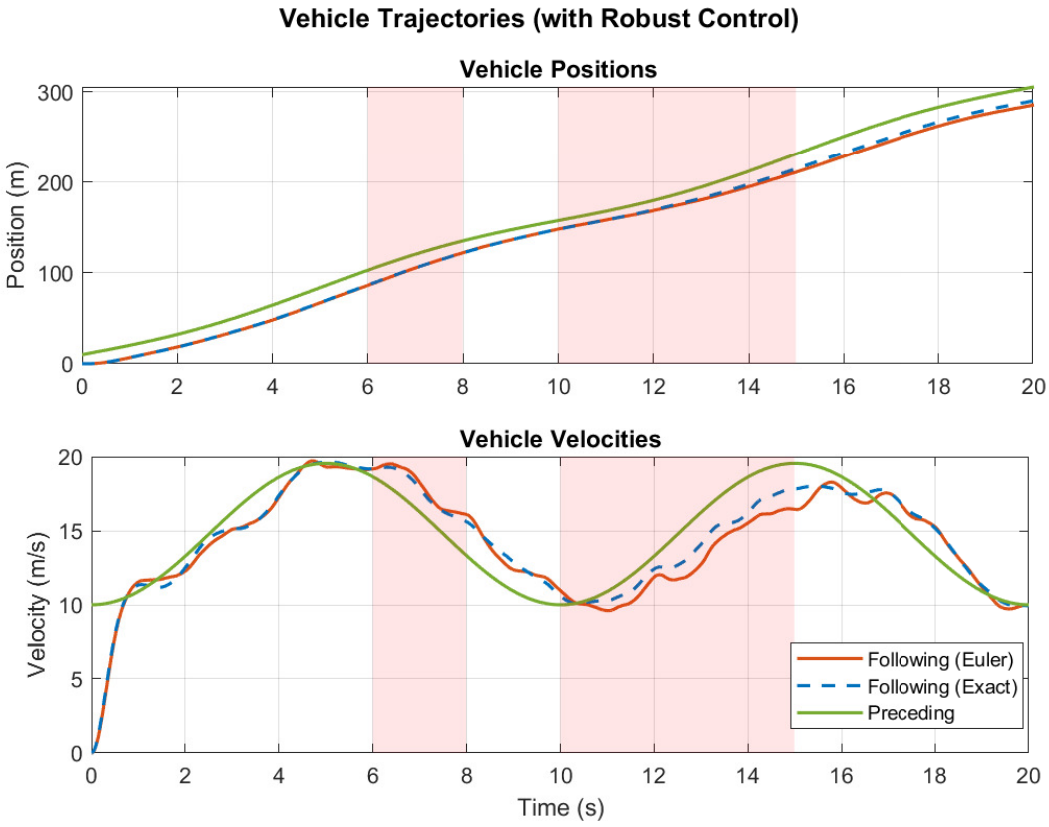

Figure 2.9: Vehicle trajectories of preceding-following vehicle.

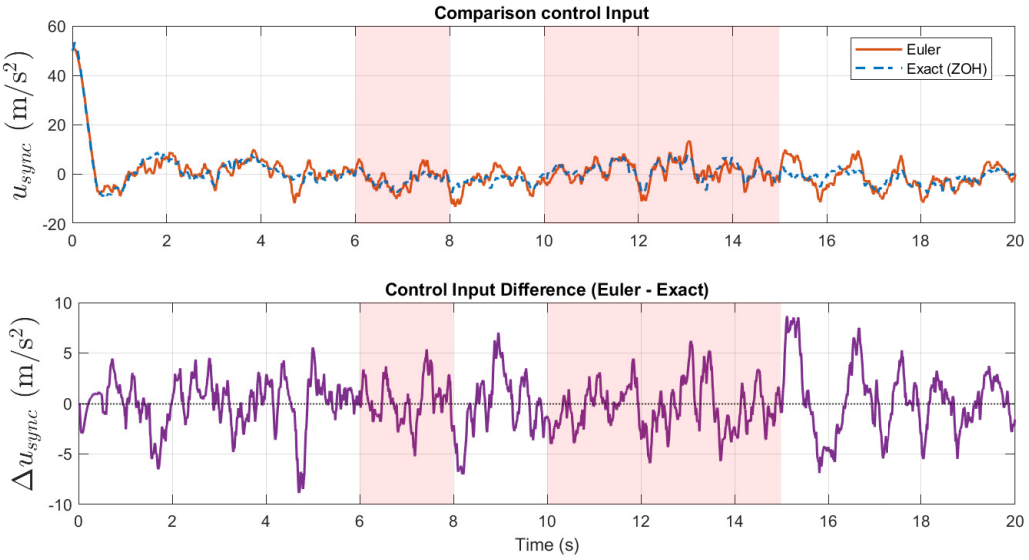

Figure 2.10: Control input of preceding-following vehicle.

and visibly reduces oscillations and noise, with the most pronounced improvement observed for the acceleration estimate.

To quantify this observation, Table 2.3 reports the RMS and MSE values for both discretization

Metric	Euler	Exact (ZOH)
RMS (after warm-up)	4.609962	3.633092
Peak (after warm-up)	13.487141	9.389372

Table 2.2: Control input metrics u_{sync} for Euler and exact (ZOH) discretization (CARLA simulation).

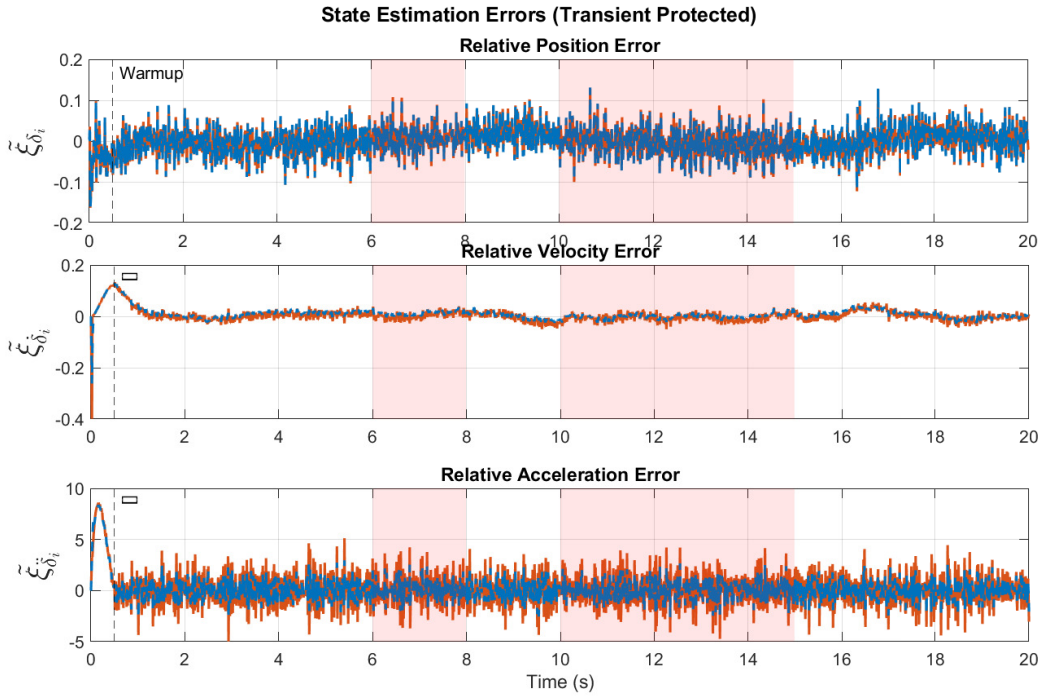

Figure 2.11: State estimation error of 2 discretization method.

methods. While the position error is similar in both cases, the exact discretization reduces the velocity RMS by about 4.5% and the acceleration RMS by about 40%. A similar trend is observed in MSE, where the acceleration MSE decreases by more than 60%. These results support the claim that preserving the exact inter-sample dynamics improves both accuracy and robustness.

Metric	Position	Velocity	Acceleration
RMS (Euler)	0.35637	0.20425	1.508381
RMS (Exact)	0.35600	0.19503	0.912209
MSE (Euler)	0.01270	0.0417	2.275214
MSE (Exact)	0.01267	0.0380	0.832126

Table 2.3: State estimation error metrics for Euler and exact discretization (CARLA simulation).

Figure 2.12 shows the true cyberattack signal and its reconstruction, along with the estimation error. Both discretization strategies enable attack detection; however, the exact discretization yields a smoother reconstruction and a smaller estimation error, which is consistent with the improved state estimates reported above.

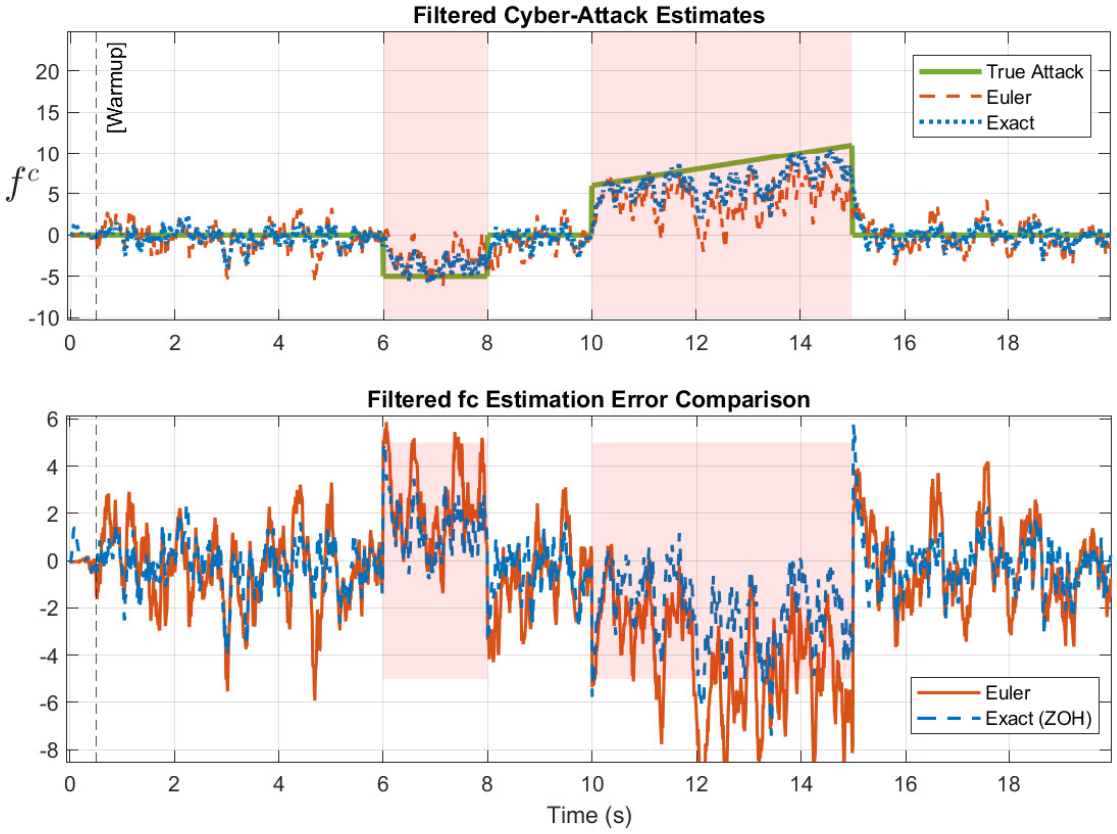

Figure 2.12: Comparison of cyberattack estimation and error.

6 Conclusion

This chapter addressed the problem of resilient state estimation and cyberattack reconstruction for Connected Autonomous Vehicles (CAVs) operating in a Cooperative Adaptive Cruise Control (CACC) platoon. The primary challenge identified was the violation of the rank condition required for standard Unknown Input Observer (UIO) design when using classical Euler discretization.

To overcome this, we first proposed a discrete-time UIO design based on output delay. By shifting the output measurement backward, we recovered the necessary algebraic coupling between the unknown input and the measured output, enabling the simultaneous estimation of vehicle states and attack signals. We derived Linear Matrix Inequality (LMI) conditions to guarantee the Input-to-State Stability (ISS) of the estimation error in the presence of bounded disturbances.

Subsequently, we introduced a refined approach using exact discretization based on the matrix exponential. We demonstrated that the rank condition failure was an artifact of the Euler approximation rather than an intrinsic system limitation. The exact discretization method naturally preserves the higher-order dynamics, restoring the rank condition without the need for artificial delays.

Comparative simulations in both MATLAB and the high-fidelity CARLA simulator validated the effectiveness of both approaches. The results confirmed that while the delayed-output method is effective, the exact discretization approach offers superior performance in terms of convergence speed, estimation

accuracy, and robustness to noise.

Future work will focus on extending these resilient estimation strategies to multi-vehicle platoons with heterogeneous dynamics and investigating the impact of model parameter uncertainties. Additionally, we aim to integrate this observer-based detection with active fault-tolerant control strategies to further enhance the safety and resilience of autonomous transportation systems.

Chapter 3

Learning with Unknown Input Observers for Robust Nonlinear Estimation

Objectives

This chapter introduces a robust hybrid state estimation framework for vehicle motion tracking that combines physics-based guarantees with data-driven adaptability. Standard model-based observers often fail when strict rank conditions are not met, while pure neural network approaches lack stability guarantees. To address this, we propose a two-stage architecture. First, we develop a Generalized Unknown Input Observer (UIO) that utilizes output derivatives to relax the standard rank condition, ensuring the existence of a bounded estimation of unmodeled dynamics. Second, we introduce a Neural Adaptive Observer that treats the UIO estimates as a "teacher" signal. Unlike the UIO, which provides instantaneous signal estimation, the neural observer learns the underlying structure of the uncertainty as a function of the state. This allows the system to predict disturbances along reference trajectories and refine the estimation error asymptotically. The approach is validated via Linear Matrix Inequalities (LMIs) ensuring $\mathcal{H}^1$ and $\mathcal{L}_2$ stability.

Contents

1 Introduction **30**
2 Problem Formulation and Motivation **31**
3 LMI-Based $\mathcal{H}^1$ UIO Design **33**
3.1 System transformation 33
3.2 UIO structure and error dynamics 34
3.3 New LMI-based UIO design conditions 36
4 Output Derivative-Based Generalized UIO **39**
4.1 Output derivative-based generalized model 39
4.2 Regularization of the generalized model 39
4.3 Generalized UIO 40
4.4 Specific cases and discussion 41
5 UIO-Based Neural Online Approximation of Unmodeled Nonlinearity **43**
5.1 Fully UIO-based Learning Architecture 43

5.2 Minimization of the Loss Function . . . 45
6 Continuous Learning Strategy . . . **47**
7 Simulation Results . . . **48**
7.1 Nonlinear Vehicle Plant . . . 48
7.2 LPV Model Used by the Observers . . . 50
7.3 Results and Discussion . . . 55
8 Open Problems and Future Directions . . . **59**
9 Conclusion . . . **60**

1 Introduction

State estimation is a cornerstone of autonomous vehicle control, where safety depends on accurate knowledge of system states and external disturbances. Traditional methods rely on explicit physics-based models [47]. However, in vehicle dynamics, highly nonlinear phenomena- such as variable tire-road friction or aerodynamic drag are difficult to model mathematically, leading to estimation errors that compromise control performance.

Data-driven methods, particularly Neural Networks (NNs), have emerged as powerful tools for approximating these complex nonlinear functions [48, 49]. While NNs offer superior adaptability, they pose significant risks in safety-critical applications. In online learning scenarios, small shifts in input data can cause NNs to behave unpredictably or diverge, lacking the stability guarantees provided by control theory. Consequently, recent research has shifted toward hybrid architectures that embed learning within observer frameworks.

A major limitation in existing hybrid observers is their reliance on the standard observer matching condition. For many vehicle systems, this condition does not hold, making it theoretically impossible to decouple the unknown input from the state using standard techniques. While some methods attempt to bypass this using approximations, they often result in unbounded errors or require expensive additional sensors.

To overcome these limitations, this chapter proposes a layered Teacher-Student estimation architecture consisting of two distinct observers:

- A Generalized UIO (The Teacher): We introduce a regularization technique using output derivatives that ensures the observer exists even when the rank condition fails. This observer provides a robust, physics-guaranteed signal of the unknown input, ensuring the estimation error remains bounded.
- A Neural Adaptive Observer (The Student): While the UIO estimates the current value of the disturbance, it cannot predict how that disturbance behaves at future states (e.g., along a reference trajectory). The Neural Observer utilizes the UIO's signal to learn the unknown dynamics as a function of the state ($\mu_\theta(x)$). This allows for refined precision and enables the controller to anticipate unmodeled dynamics.

This combination offers a specific advantage: the Generalized UIO guarantees the system never diverges (safety), while the Neural Network minimizes the residual error over time (performance). The contributions of this chapter are:

- A Generalized UIO design that relaxes the rank condition using output derivatives ;
- A hybrid learning framework where the UIO acts as a supervisor, enforcing consistency in the neural training loop;
- LMI-based stability conditions that guarantee joint convergence of both the state and model parameters.

2 Problem Formulation and Motivation

In this chapter, we consider the class of continuous-time nonlinear systems in state-space form described by the following equations:

$$\begin{aligned} \dot{x} &= \varphi(x,u) + B\mu_x \\ y &= Cx, \end{aligned} \tag{3.1}$$

where $x \in \mathcal{X} \subseteq \mathbb{R}^{n_x}$ is the state vector, $y \in \mathbb{R}^{n_y}$ is the output measurement, $u \in \mathcal{U} \subseteq \mathbb{R}^{n_u}$ is the control input, and $\mu_x \in \mathbb{R}^{n_\mu}$ is an unknown nonlinear function that encapsulates the system uncertainty including both unmodeled dynamics and external disturbances. The matrices $C \in \mathbb{R}^{n_y \times n_x}$ and $B \in \mathbb{R}^{n_x \times n_\mu}$ are constant and known matrices. The function $\varphi : \mathcal{X} \times \mathcal{U} \to \mathbb{R}^{n_x}$ represents the known nonlinear component of the system.

Remark 3. *For simplicity, we consider systems with linear output. Otherwise, if we have nonlinear output $y = h(x)$, we introduce a new state $\eta(t)$, with $\dot{\eta} \triangleq A_\eta \eta + \gamma y$ and $\eta_0 = \eta(0)$ known. Then, a new system with the augmented vector $\zeta = \begin{bmatrix} \eta \\ x \end{bmatrix}$ may be considered, which has as linear output the vector η.*

Now, let us introduce the following assumptions which are required for our unknown input observer design methods.

Assumption 2. *The output vector y has dimension greater than or equal to the number of unknown terms μ_x; equivalently, $n_\mu \leq n_y$.*

Assumption 3. *The nonlinear function $\varphi(\cdot)$ is γ_φ-Lipschitz continuous on $\mathcal{X}$, uniformly on $u \in \mathcal{U}$.*

Assumption 4. *The unknown nonlinearity $\mu_x(\cdot)$ is Lebesgue measurable and $\mathcal{L}_2$-bounded.*

Remark 4. *Assumption 4 corresponds to a* bounded-energy *uncertainty over $\Omega = [0, +\infty[$, which is standard in $\mathcal{H}_\infty$/ $\mathcal{L}_2$-gain observer analysis. In the vehicle context, μ_x may represent aggregated effects such as unmodeled tire-force nonlinearities, residual parameter mismatches, aerodynamic disturbances, or actuator/sensor fault components. Moreover, since the regularization introduced later contains $\omega_{\delta_1}(t) = \delta_1 \dot{\mu}_x(t)$, the subsequent $\mathcal{H}^1$ performance bound implicitly requires $\mu_x \in \mathcal{H}^1(\Omega)$ (i.e., $\mu_x \in \mathcal{L}_2(\Omega)$ and $\dot{\mu}_x \in \mathcal{L}_2(\Omega)$), which can be interpreted as* bounded-energy variations *of the unknown input.*

The objective of this chapter is to estimate the unmodeled dynamics μ_x. More specifically, we propose to estimate μ_x by combining an unknown input observer (UIO) with a neural network–based approach, leveraging gradient-based methods to better capture the unmodeled components of the system. The key idea is to incorporate the UIO-based estimation into the loss function of the neural network, thereby enhancing residual regularization and ensuring consistency with the UIO. This, in turn, improves the robustness and performance of the overall estimation scheme. Unfortunately, it is not possible to estimate the unknown input, μ_x, if the system fails to satisfy the following main necessary condition:

$$\text{rank}(CB) = \text{rank}(B). \tag{3.2}$$

In addition, to be able to directly construct a UIO for system (3.1) to estimate simultaneously x and μ_x, the constraint (3.2) is not sufficient. For this, we should be able to write the system under the form:

$$\begin{aligned} \mathbb{E}\dot{\zeta} &= \varphi_\zeta(\zeta, u) \\ y &= \mathcal{H}\zeta \end{aligned} \tag{3.3}$$

with

$$\text{rank}\left(\begin{bmatrix}\mathbb{E} \\ \mathcal{H}\end{bmatrix}\right) = n_x + n_\mu. \tag{3.4}$$

For further details on this requirement, the reader is referred to [35, 45, 50, 51, 52] and the references therein.

To address this challenge, various techniques have been proposed in the literature, each offering a different approach to the problem. Without aiming for exhaustiveness, these techniques can be summarized as follows. Nevertheless, the problem remains open, and new ideas or improvements are still possible, although often at the cost of additional assumptions:

- *Inverting the system dynamics:* The system state is first estimated, and the unknown inputs are then obtained by inverting the dynamics [53, 54, 55]. However, the presence of disturbances and nonlinearities in the output signal or in the dynamics can make the problem particularly challenging.

- *Deriving the output vector $y(t)$:* In some cases, the derivatives of the output measurements are required [56, 53]. This leads to the construction of a pseudo-output vector y_{new}, which enables the simultaneous estimation of x and μ_x. For instance, in the linear case without disturbances, one obtains

  $$y_{\text{new}} = C_{\text{new}}x + C_\mu\mu_x,$$

  where $\text{rank}(C_\mu) = n_\mu$. However, this approach is not suitable for nonlinear disturbed systems, since differentiating $y(t)$ introduces additional variables arising from the derivatives of the disturbance vector, as well as new nonlinearities in the pseudo-output vector. Consequently, satisfying the rank condition (3.2) with the new matrices becomes very difficult.

- *Adding sensors:* In some cases, augmenting the system with additional sensors is a natural way to overcome the rank condition (3.2). This approach introduces a new measurement vector y_{new}, where the original output $y(t)$ is used to estimate the state $x(t)$, and the additional outputs y_{new} are exploited to estimate the unknown input, μ_x. For example, in [53] (and references therein), four sensors (i.e., four output measurements) were employed to estimate only two unknown inputs. However, the presence of disturbances can significantly decrease estimation performance. Moreover, additional sensors may be very expensive or, in some cases, unavailable.

- *Proportional–Integral Observer and Null Dynamics:* Some works in the literature have employed a Proportional–Integral Observer (PIO) together with null dynamics imposed on the estimated unknown input [57]. However, this assumption does not reflect the true dynamics of the unknown input, leading to inaccurate estimation. Other approaches assume constant inputs [8], i.e., $\dot{\mu}_x \equiv 0$, but this restriction is overly conservative. Recently, a method for discrete-time systems was

proposed in [58]; however, this approach yields delayed estimates of both the system state and the unknown inputs, which is often impractical to design reliable controllers.

The limitations of the aforementioned methods motivated us to adopt a different approach and propose a simple strategy to estimate the system state and the unknown input without relying on conservative assumptions. The key idea is to recognize that this initial estimation is not final. Rather, the objective is to provide a first-level approximation of x and μ_x, which will subsequently be refined through the neuro-adaptive observer we introduce later. This refinement enhances estimation accuracy and ultimately yields a definitive estimate of the unmodeled nonlinearity, μ_x.

The strategy consists in rewriting system (3.1) without modifying it. Then, the UIO we will propose will be based on reliable approximation of (3.1).

$$\begin{aligned} \dot{x} + E_{\delta_1}\dot{\mu}_x &= \varphi(x,u) + B\mu_x + E\omega_{\delta_1} \\ y &= Cx + D_{\delta_2}\mu_x + D\,\omega_{\delta_2} \end{aligned} \tag{3.5}$$

where $D \in \mathbb{R}^{n_y \times n_\mu}$ and $E \in \mathbb{R}^{n_x \times n_\mu}$ are given constant, full-column-rank matrix specified by the user; $E_{\delta_1} = \delta_1 E, D_{\delta_2} = \delta_2 D$; and $\omega_{\delta_1}(t) = \delta_1 \dot{\mu}_x(t), \omega_{\delta_2}(t) = \delta_2 \mu_x(t)$, with $\delta_j \geq 0$, with $(\delta_1, \delta_2) \neq (0,0)$, chosen sufficiently small to ensure the feasibility of some sufficient conditions that will be stated later. The purpose of this reformulation is to recover the rank condition (3.4), at the expense of introducing the additive terms $\omega_{\delta_j}(t), j = 1, 2$, which are handled as disturbances.

- **Design guideline for E and D:** in practice, E and D can be selected as sparse (often binary) full-column-rank matrices that *inject* the regularization terms into a subset of state/output channels so that the augmented pair $(\mathbb{E}, \mathcal{H})$ satisfies Assumption 5. A simple procedure is to (i) choose D so that $\mathrm{rank}(D) = n_\mu$ (typically by selecting n_μ independent measured outputs), and then (ii) choose E (possibly also sparse/binary) to complete the rank condition (3.4) with minimal additional coupling.

- **Interpretation of δ_1, δ_2:** the scalars δ_1 and δ_2 quantify the trade-off between *rank recovery* (feasibility of Assumption 5) and *disturbance amplification* through the induced terms ω_{δ_1} and ω_{δ_2}.

The next section presents LMI conditions that guarantee accurate estimation of x and μ_x while satisfying an $\mathcal{H}_\infty$ criterion, or more specifically, an $\mathcal{L}_2$-optimality criterion—where the performance bound is proportional to $\delta_j, j = 1, 2$.

3 LMI-Based $\mathcal{H}^1$ UIO Design

This section is devoted to the numerical LMI-based design procedure ensuring the asymptotic estimation of the system state x and the unmodeled dynamics μ_x following a $\mathcal{H}^1-$optimality criterion.

3.1 System transformation

Recall that $\mathcal{H}^1$ is the *Hilbert* space corresponding to the *Sobolev* space, $\mathcal{W}^{1,2}$, of square–integrable functions whose weak first derivatives are also square–integrable. Mathematically, we define the set

$\mathcal{H}^1(\Omega)$ as

$$\mathcal{H}^1(\Omega) := \left\{ \psi \in \mathcal{L}^2(\Omega) \;\middle|\; \frac{\mathrm{d}\psi}{\mathrm{d}t} \in \mathcal{L}^2(\Omega) \right\}$$

with $\Omega = [0 \ +\infty[$ in our case. This space is endowed by the norm $\|.\|_{\mathcal{H}^1}$ defined as follows:

$$\|\psi\|_{\mathcal{H}^1} := \left(\|\psi\|_{\mathcal{L}^2}^2 + \left\| \frac{\mathrm{d}\psi}{\mathrm{d}t} \right\|_{\mathcal{L}^2}^2 \right)^{1/2}.$$

First, system (3.5) can be rewritten under the compact form:

$$\begin{aligned} \mathbb{E}\dot{\zeta} &= \varphi_\zeta(\zeta, u) + \bar{E}\boldsymbol{\omega}_\delta \\ y &= \mathcal{H}\zeta + \bar{D}\boldsymbol{\omega}_\delta \end{aligned} \tag{3.6}$$

where

$$\mathbb{E} := \begin{bmatrix} \mathbb{I}_{n_x} & E_{\delta_1} \end{bmatrix}, \ \mathcal{H} := \begin{bmatrix} C & D_{\delta_2} \end{bmatrix}, \tag{3.7a}$$

$$\bar{E} := \begin{bmatrix} E & 0_{n_x \times n_\mu} \end{bmatrix}, \ \bar{D} := \begin{bmatrix} 0_{n_y \times n_\mu} & D \end{bmatrix}, \tag{3.7b}$$

$$\zeta := \begin{bmatrix} x \\ \mu_x \end{bmatrix}, \ \boldsymbol{\omega}_\delta := \begin{bmatrix} \omega_{\delta_1} \\ \omega_{\delta_2} \end{bmatrix}, \tag{3.7c}$$

$$\varphi_\zeta(\zeta, u) := \begin{bmatrix} \varphi(x, u) + B\mu_x \\ 0_{n_\mu} \end{bmatrix}. \tag{3.7d}$$

Now, let us introduce the following necessary assumption:

Assumption 5. *The matrices E and D are chosen such that $\mathbb{E}$ and $\mathcal{H}$ satisfy the rank condition (3.4).*

The objective is to design a state observer that provides an estimate $\hat{\zeta}$ of ζ, such that the following $\mathcal{H}^1$-optimality inequality holds:

$$\|\tilde{\zeta}\|_{\mathcal{H}^1} \leq \lambda_\delta \ \|\mu_x\|_{\mathcal{H}^1} + \beta \ \|\xi_0\| \tag{3.8}$$

where $\tilde{\zeta} := \zeta - \hat{\zeta}$, λ_δ is the disturbance attenuation level, explicitly depending on δ_1 and δ_2, $\beta > 0$ is a weighting real constant, and ξ_0 is a vector depending on $\tilde{\zeta}(0)$ and $\mu_x(0)$.

3.2 UIO structure and error dynamics

From Assumption 5, there exist two matrices P_ζ and Q_ζ such that

$$P_\zeta \mathbb{E} + Q_\zeta \mathcal{H} = \mathbb{I}_{n_\zeta}. \tag{3.9}$$

where $n_\zeta := n_x + n_\mu$. These matrices are exploited in the following observer structure:

$$\begin{cases} \dot{\eta} &= P_\zeta \varphi_\zeta(\hat{\zeta}, u) + K\left(y - \mathcal{H}\hat{\zeta}\right) \\ \hat{\zeta} &= \eta + Q_\zeta y \end{cases} \tag{3.10}$$

where $\hat{\zeta}$ is the estimate of ζ and $K \in \mathbb{R}^{n_\zeta \times n_y}$ is the observer gain to be determined such that the estimation error, $\tilde{\zeta} := \zeta - \hat{\zeta}$, satisfies the $\mathcal{H}^1$-optimality criterion (3.8) with appropriate λ_δ, β, and ξ_0.

We have

$$\begin{aligned} \tilde{\zeta} &= \zeta - \eta - Q_\zeta y \\ &= \left(\mathbb{I}_{n_\zeta} - Q_\zeta \mathcal{H}\right)\zeta - \eta - Q_\zeta \bar{D}\boldsymbol{\omega}_\delta \\ &\overset{(3.9)}{=\!=} P_\zeta \mathbb{E}\zeta - \eta - Q_\zeta \bar{D}\boldsymbol{\omega}_\delta \end{aligned} \tag{3.11}$$

which gives equivalently

$$\overbrace{\tilde{\zeta} + Q_\zeta \bar{D}\boldsymbol{\omega}_\delta}^{\xi(t)} = P_\zeta \mathbb{E}\zeta(t) - \eta(t). \tag{3.12}$$

It is worth noting that the reformulation (3.12) conveniently avoids the derivative of $\boldsymbol{\omega}_\delta$ in the derivation of the error dynamics.

By using the dynamics (3.6) and (3.10), we obtain

$$\begin{aligned} \dot{\xi} &= P_\zeta\left[\varphi_\zeta(\zeta, u) - \varphi_\zeta(\hat{\zeta}, u)\right] - K\mathcal{H}\tilde{\zeta} \\ &\quad + \left(P_\zeta \bar{E} - K\bar{D}\right)\boldsymbol{\omega}_\delta \\ &= \left(P_\zeta \nabla_\zeta^{\varphi_\zeta}(\boldsymbol{z}, u) - K\mathcal{H}\right)\xi \\ &\quad + \left(\mathcal{E}(\boldsymbol{z}, u) - K\mathcal{D}\right)\boldsymbol{\omega}_\delta \end{aligned} \tag{3.13}$$

where

$$\mathcal{E}(\boldsymbol{z}, u) := \bar{E} - P_\zeta \nabla_\zeta^{\varphi_\zeta}(\boldsymbol{z}, u) Q_\zeta \bar{D}$$

$$\mathcal{D} := \left(\mathbb{I}_{n_y} + \mathcal{H}Q_\zeta\right)\bar{D}.$$

and from the differential mean value theorem [59], we have

$$\varphi_\zeta(\zeta, u) - \varphi_\zeta\left(\hat{\zeta}, u\right) = \nabla_\zeta^{\varphi_\zeta}(\boldsymbol{z}, u)\tilde{\zeta}$$

for a given $\boldsymbol{z}$.

From this point onward, the analysis will be carried out with the vector ξ instead of $\tilde{\zeta}$, and we will return to $\tilde{\zeta}$ at the end to derive the final $\mathcal{H}^1$ bound (3.8).

3.3 New LMI-based UIO design conditions

Before presenting the proposed LMI-based UIO design procedure, we state an intermediate and general result in the following proposition.

Proposition 1. *Let $\vartheta(\cdot)$ be a Lyapunov function such that there exists $\vartheta_{\max} > 0$ such that $\vartheta(z) \leq \vartheta_{\max}\|z\|^2$, for all $z \in \mathbb{R}^{n_\zeta}$. Consider a matrix $\mathcal{S} = \mathcal{S}^\top > 0$ and a real constant $\lambda > 0$ such that the following inequality holds:*

$$\dot{\vartheta}(z) + \|z\|^2 + \dot{z}^\top \mathcal{S}\dot{z} - \lambda\|w\|^2 \leq 0, \forall z \in \mathbb{R}^{n_\zeta}, w \in \mathbb{R}^{2n_\mu} \tag{3.14}$$

with $z \in \mathcal{H}^1$ and $w \in \mathcal{L}^2$. Then, the following inequality is satisfied:

$$\|z\|_{\mathcal{H}^1} \leq \sqrt{\frac{\lambda}{\min\left(1, \lambda_{\min}(\mathcal{S})\right)}}\|w\|_{\mathcal{L}^2} + \sqrt{\frac{\vartheta_{\max}}{\min\left(1, \lambda_{\min}(\mathcal{S})\right)}}\|z_0\|. \tag{3.15}$$

Moreover, if (3.14) is satisfied with $z := \xi$ and $w := \boldsymbol{\omega}_\delta$, where ξ and $\boldsymbol{\omega}_\delta$ are defined by (3.12) and (3.7c), respectively, then the estimation error, $\tilde{\zeta}$, satisfies the $\mathcal{H}^1$ bound (3.8) with λ_δ, β, and ξ_0 given as follows:

$$\lambda_\delta := \delta_2 \sigma_{\max}\left(Q_\zeta D\right) + \max\left(\delta_1, \delta_2\right)\sqrt{\frac{\lambda}{\min\left(1, \lambda_{\min}(\mathcal{S})\right)}} \tag{3.16a}$$

$$\beta := \sqrt{\frac{\vartheta_{\max}}{\min\left(1, \lambda_{\min}(\mathcal{S})\right)}} \tag{3.16b}$$

$$\xi_0 := \tilde{\zeta}(0) + Q_\zeta D \mu_x(0). \tag{3.16c}$$

where $\sigma_{\max}\left(Q_\zeta D\right)$ represents the largest singular value of the matrix $Q_\zeta D$.

Proof. The first part of the proof is relatively straightforward. Before integrating (3.14) to get the norms $\|.\|_{\mathcal{H}^1}$ and $\|.\|_{\mathcal{L}^2}$, take in mind that

$$\min\left(1, \lambda_{\min}(\mathcal{S})\right)\left(\|z\|^2 + \|\dot{z}\|^2\right) \leq \|z\|^2 + \dot{z}^\top \mathcal{S}\dot{z}.$$

Hence, since

$$\int_0^{+\infty}\left(\|z(s)\|^2 + \|\dot{z}(s)\|^2\right)\mathrm{d}s \;=\; \|z\|^2_{\mathcal{H}^1},$$

$$\int_0^{+\infty}\|w(s)\|^2\,\mathrm{d}s \;=\; \|w\|^2_{\mathcal{L}^2},$$

and because $\vartheta(z(t)) \geq 0$ for all $t \geq 0$, implying that

$$\int_0^{+\infty}\dot{\vartheta}(z(s))\,\mathrm{d}s \;=\; \lim_{T\to\infty}\vartheta(z(T)) - \vartheta(z(0)) \;\geq\; -\vartheta(z(0)),$$

we can readily conclude (3.15).

As for the second part of the proof, we will exploit the structure of ξ and $\boldsymbol{\omega}_\delta$. First, ξ and $\boldsymbol{\omega}_\delta$ satisfy (3.15)

proved in the first part. In addition, we have

$$\begin{aligned}\|\tilde{\zeta}\|_{\mathcal{H}^1} &= \left\|\xi - Q_\zeta \bar{D}\boldsymbol{\omega}_\delta\right\|_{\mathcal{H}^1} \\ &\leq \|\xi\|_{\mathcal{H}^1} + \left\|Q_\zeta \bar{D}\boldsymbol{\omega}_\delta\right\|_{\mathcal{H}^1} \\ &= \|\xi\|_{\mathcal{H}^1} + \left\|\begin{bmatrix}0 & Q_\zeta D\end{bmatrix}\boldsymbol{\omega}_\delta\right\|_{\mathcal{H}^1} \\ &= \|\xi\|_{\mathcal{H}^1} + \delta_2 \left\|Q_\zeta D\mu_x\right\|_{\mathcal{H}^1} \\ &\leq \|\xi\|_{\mathcal{H}^1} + \delta_2 \sigma_{\max}\left(Q_\zeta D\right)\|\mu_x\|_{\mathcal{H}^1} \end{aligned} \tag{3.17}$$

and

$$\begin{aligned}\|\boldsymbol{\omega}_\delta\|_{\mathcal{L}^2} &= \sqrt{\delta_1^2\|\dot{\mu}_x\|_{\mathcal{L}^2}^2 + \delta_2^2\|\mu_x\|_{\mathcal{L}^2}^2} \\ &\leq \max\left(\delta_1,\delta_2\right)\sqrt{\|\dot{\mu}_x\|_{\mathcal{L}^2}^2 + \|\mu_x\|_{\mathcal{L}^2}^2} \\ &= \max\left(\delta_1,\delta_2\right)\|\mu_x\|_{\mathcal{H}^1}. \end{aligned} \tag{3.18}$$

Hence, by substituting (3.17) and (3.18) in (3.15), the bound (3.8) is inferred with the parameters given in (3.16a)–(3.16c). □

Before stating the main theorem, notice that from Assumption 3, there exist constant matrices $\mathcal{A}_j \in \mathbb{R}^{n_\zeta \times n_\zeta}$ and functions $\alpha_j(\boldsymbol{z})$, $j = 1,\dots \bar{n}_\zeta$ such that the Jacobian $\nabla_\zeta^{\varphi_\zeta}(\boldsymbol{z},u)$ belongs to the convex polytopic set defined as:

$$\mathcal{H}_\varphi \triangleq \left\{\sum_{j=1}^{\bar{n}_\zeta}\alpha_j(\boldsymbol{z})\mathcal{A}_j, \sum_{j=1}^{\bar{n}_\zeta}\alpha_j(\boldsymbol{z}) = 1, \alpha_j(\boldsymbol{z}) \geq 0\right\} \tag{3.19}$$

where $\mathcal{A}_j \in \mathbb{R}^{n_\zeta \times n_\zeta}$, are the vertices of the polytope $\mathcal{H}_\varphi$.

Now, we are ready to state the main theorem, which provides new LMI conditions ensuring the bound (3.8).

Theorem 2. *Suppose that Assumptions 2, 3, and 4 hold. Let the matrices E and D, together with the scalars δ_1 and δ_2, be chosen such that the Assumption 5 is satisfied. For a given constant $\epsilon > 0$, assume further that there exist a symmetric positive definite matrix $\mathcal{P} \in \mathbb{R}^{n_\zeta \times n_\zeta}$ and a matrix $\mathcal{Q} \in \mathbb{R}^{n_y \times n_\zeta}$ such that the LMI conditions (3.26) are fulfilled. Then, the estimation error $\tilde{\zeta}$, with $K = \mathcal{P}^{-1}\mathcal{Q}^\top$, satisfies the $\mathcal{H}^1$-optimality bound (3.8) with the parameters given in (3.16a)–(3.16c), where $\vartheta_{\max} = \lambda_{\max}(\mathcal{P})$ and $\mathcal{S} = \epsilon\mathcal{P}$ with $\lambda_{\min}(\mathcal{S}) = \epsilon\,\lambda_{\min}(\mathcal{P})$.*

Proof. Consider the quadratic Lyapunov function $\vartheta(\xi) := \xi^\top\mathcal{P}\xi$. Then, the derivative of $\vartheta(.)$ along the trajectories of (3.13) is given as follows:

$$\begin{aligned}\dot{\vartheta}(\xi) = \xi^\top\Big[\Big(P_\zeta\nabla_\zeta^{\varphi_\zeta}(\boldsymbol{z},u) - K\mathcal{H}\Big)^\top\mathcal{P} + \mathcal{P}\Big(P_\zeta\nabla_\zeta^{\varphi_\zeta}(\boldsymbol{z},u) - K\mathcal{H}\Big)\Big]\xi \\ + \xi^\top\mathcal{P}\Big(\mathcal{E}\left(\boldsymbol{z},u\right) - K\mathcal{D}\Big)\boldsymbol{\omega}_\delta + \boldsymbol{\omega}_\delta^\top\Big(\mathcal{E}\left(\boldsymbol{z},u\right) - K\mathcal{D}\Big)^\top\mathcal{P}\xi.\end{aligned} \tag{3.20}$$

$$\begin{bmatrix} \left(P_\zeta \nabla_\zeta^{\varphi_\zeta} - K\mathcal{H}\right)^\top \mathcal{P} + \mathcal{P}\left(P_\zeta \nabla_\zeta^{\varphi_\zeta} - K\mathcal{H}\right) & \left[\mathcal{P} + \left(P_\zeta \nabla_\zeta^{\varphi_\zeta} - K\mathcal{H}\right)^\top \mathcal{S}\right]\left(\mathcal{E} - K\mathcal{D}\right) \\ \left(\mathcal{E} - K\mathcal{D}\right)^\top \left[\mathcal{P} + \mathcal{S}\left(P_\zeta \nabla_\zeta^{\varphi_\zeta} - K\mathcal{H}\right)\right] & -\lambda \mathbb{I}_{2n_\mu} + \left(\mathcal{E} - K\mathcal{D}\right)^\top \mathcal{S}\left(\mathcal{E} - K\mathcal{D}\right) \end{bmatrix} \tag{3.24}$$

$$\begin{bmatrix} \left(P_\zeta \nabla_\zeta^{\varphi_\zeta} - K\mathcal{H}\right)^\top \mathcal{P} + \mathcal{P}\left(P_\zeta \nabla_\zeta^{\varphi_\zeta} - K\mathcal{H}\right) & \mathcal{P}\left(\mathcal{E} - K\mathcal{D}\right) & \left(P_\zeta \nabla_\zeta^{\varphi_\zeta} - K\mathcal{H}\right)^\top \mathcal{S} \\ \left(\mathcal{E} - K\mathcal{D}\right)^\top \mathcal{P} & -\lambda \mathbb{I}_{2n_\mu} & \left(\mathcal{E} - K\mathcal{D}\right)^\top \mathcal{S} \\ \mathcal{S}\left(P_\zeta \nabla_\zeta^{\varphi_\zeta} - K\mathcal{H}\right) & \mathcal{S}\left(\mathcal{E} - K\mathcal{D}\right) & -\mathcal{S} \end{bmatrix} < 0 \tag{3.25}$$

$$\begin{bmatrix} \left(P_\zeta \mathcal{A}_j\right)^\top \mathcal{P} + \mathcal{P}\left(P_\zeta \mathcal{A}_j\right) - \mathcal{H}^\top \mathcal{Q} - \mathcal{Q}^\top \mathcal{H} & \mathcal{P}\mathcal{E}_j - \mathcal{Q}^\top \mathcal{D} & \left(P_\zeta \mathcal{A}_j\right)^\top \mathcal{P} - \mathcal{H}^\top \mathcal{Q} \\ \mathcal{E}_j^\top \mathcal{P} - \mathcal{D}^\top \mathcal{Q} & -\lambda \mathbb{I}_{2n_\mu} & \mathcal{E}_j^\top \mathcal{P} - \mathcal{D}^\top \mathcal{Q} \\ \mathcal{P}\left(P_\zeta \mathcal{A}_j\right) - \mathcal{Q}^\top \mathcal{H} & \mathcal{P}\mathcal{E}_j - \mathcal{Q}^\top \mathcal{D} & -\frac{1}{\epsilon}\mathcal{P} \end{bmatrix} < 0 \tag{3.26}$$

where

$$\mathcal{E}_j := \bar{E} - P_\zeta \mathcal{A}_j Q_\zeta \bar{D}$$

and

$$\begin{aligned} \dot{\xi}^\top \mathcal{S} \dot{\xi} = \xi^\top \left(P_\zeta \nabla_\zeta^{\varphi_\zeta}(\boldsymbol{z}, u) - K\mathcal{H}\right)^\top \mathcal{S} \times \left(P_\zeta \nabla_\zeta^{\varphi_\zeta}(\boldsymbol{z}, u) - K\mathcal{H}\right) \xi \\ + \boldsymbol{\omega}_\delta^\top \left(\mathcal{E}\left(\boldsymbol{z}, u\right) - K\mathcal{D}\right)^\top \mathcal{S}\left(\mathcal{E}\left(\boldsymbol{z}, u\right) - K\mathcal{D}\right)\boldsymbol{\omega}_\delta \\ + 2\xi^\top \left(P_\zeta \nabla_\zeta^{\varphi_\zeta}(\boldsymbol{z}, u) - K\mathcal{H}\right)^\top \mathcal{S}\left(\mathcal{E}\left(\boldsymbol{z}, u\right) - K\mathcal{D}\right)\boldsymbol{\omega}_\delta. \end{aligned} \tag{3.21}$$

Then, we have

$$\dot{\vartheta}(\xi) + \|\xi\|^2 + \dot{\xi}^\top \mathcal{S} \dot{\xi} - \lambda \|\boldsymbol{\omega}_\delta\|^2 = \begin{bmatrix} \xi \\ \boldsymbol{\omega}_\delta \end{bmatrix}^\top \mathbb{M}\left(z, u\right) \begin{bmatrix} \xi \\ \boldsymbol{\omega}_\delta \end{bmatrix} \tag{3.22}$$

where $\mathbb{M}\left(z, u\right)$ is defined in (3.24). By applying Schur lemma, we deduce that $\mathbb{M}(z, u) < 0$ whenever inequality (3.25) holds. Consequently, by setting $\mathcal{S} = \epsilon \mathcal{P}$, introducing the change of variables $\mathcal{Q} := K^\top \mathcal{P}$, and invoking the convexity principle, we conclude that the inequality $\mathbb{M}(z, u) < 0$ is satisfied provided that the LMI conditions (3.26) hold. This, in turn, yields

$$\dot{\vartheta}(\xi) + \|\xi\|^2 + \dot{\xi}^\top \mathcal{S} \dot{\xi} - \lambda \|\boldsymbol{\omega}_\delta\|^2 \leq 0. \tag{3.23}$$

Hence, Proposition 1 applies and the desired result follows.

□

Remark 5. *It is worth emphasizing that the choice $\mathcal{S} = \epsilon\mathcal{P}$ is neither arbitrary nor overly restrictive, although it represents a specific selection. The introduction of the matrix $\mathcal{P}$ serves to recover the decision variable $\mathcal{Q}$ and then to avoid bilinear matrix inequalities, which are generally unsuitable for numerical solvers. The scalar parameter ϵ is included as a feasibility factor to improve the feasibility of the LMI conditions (3.26), and it should be chosen a priori.*

4 Output Derivative-Based Generalized UIO

The main limitation of the previous result is that the proposed method does not guarantee exponential convergence of the estimation error, even when condition (3.2) is satisfied. This represents a drawback of the proposed *regularization* technique and has motivated the development of a more general and robust method that overcomes this shortcoming.

4.1 Output derivative-based generalized model

The key idea consists in introducing a generalized system imbedding the original model, the output y and its derivative. To this end, let us consider $\chi_1 \triangleq y$ and $\chi_2 \triangleq \dot{y}$, which leads to the following generalized system:

$$\left\{\begin{array}{rcl} \dot{\chi}_1 & = & \chi_2 \\ \dot{\chi}_2 & = & C\bar{\varphi}_x(x,u) + C\frac{\partial\varphi}{\partial x}(x,u)B\mu_x + CB\dot{\mu}_x \\ \dot{x} & = & \varphi(x,u) + B\mu_x \\ y_\chi & = & \chi_1 + C_\chi\chi_2 + Cx \end{array}\right. \tag{3.27}$$

where $\bar{\varphi}_x(x,u) \triangleq \frac{\partial\varphi}{\partial x}(x,u)\varphi(x,u)$, and $C_\chi \in \mathbb{R}^{n_y\times n_y}$ is a given weighting matrix associated with the measured derivative $\dot{y}$.

Clearly, if (3.2) is satisfied, then (3.27) can be rewritten in the form of (3.6), for which Assumption 5 holds. In this case, an exponential UIO for (3.27) can be directly constructed if we add χ_2 as output measurement. However, if (3.2) is not satisfied, the construction of an exponential UIO is not possible. In this situation, we can proceed as in the previous section by first regularizing the system (3.27). This approach leads to a design method that is more general than that of the previous section, as it ensures exponential convergence of the UIO whenever condition (3.2) is satisfied and the derivative $\dot{y}$ is used as a measurement.

4.2 Regularization of the generalized model

System (3.27) can be regularized as follows

$$\left\{\begin{array}{rc} \dot{\chi}_1 = & \chi_2 \\ \dot{\chi}_2 + (E_{\delta_1} - CB)\,\dot{\mu}_x = & C\bar{\varphi}_x(x,u) + E\,\omega_{\delta_1} + C\frac{\partial\varphi}{\partial x}(x,u)B\mu_x \\ \dot{x} = & \varphi(x,u) + B\mu_x \\ y_\chi = & \chi_1 + C_\chi\chi_2 + Cx + D_{\delta_2}\mu_x + D\,\omega_{\delta_2} \end{array}\right. \tag{3.28}$$

where the scalars $\delta_1 \geq 0$, $\delta_2 \geq 0$, and the matrices $E \in \mathbb{R}^{n_y \times n_\mu}$ and $D \in \mathbb{R}^{n_y \times n_\mu}$ are the *regularization parameters*, with E and D chosen to be binary, i.e., their entries are restricted to $\{0, 1\}$. This choice is motivated by the aim of controlling the estimation error bound exclusively through the scalar parameters δ_1 and δ_2. Moreover, E and D are selected to satisfy an appropriate rank condition, which will be specified later.

Practical choice: choosing E and D binary amounts to selecting which measured channels are used to restore the rank condition while keeping the design interpretable and sparse. In practice, one may start from a binary D with $\mathrm{rank}(D) = n_\mu$ (select n_μ independent outputs), and then adjust E (binary or structured) so that the resulting augmented matrices satisfy the required rank condition. A concrete selection of such a binary D is given in the numerical vehicle example (Subsubsection *UIO for the LPV Vehicle Model*).

The regularized generalized system (3.28) can be rewritten under the compact form:

$$\begin{aligned} \mathbb{E}\dot{\zeta} &= \varphi_\zeta(\zeta, u) + \bar{E}\boldsymbol{\omega}_\delta \\ y_\chi &= \mathcal{H}\zeta + \bar{D}\boldsymbol{\omega}_\delta \end{aligned} \tag{3.29}$$

where

$$\mathbb{E} := \begin{bmatrix} \mathbb{I}_{n_y} & 0 & 0 & 0 \\ 0 & \mathbb{I}_{n_y} & 0 & -CB \\ 0 & 0 & \mathbb{I}_{n_x} & 0 \end{bmatrix}, \ \mathcal{H} := \begin{bmatrix} \mathbb{I}_{n_y} & C_\chi & C & D_{\delta_2} \end{bmatrix}, \tag{3.30a}$$

$$\bar{E} := \begin{bmatrix} 0 & 0_{n_y \times n_\mu} \\ E & 0_{n_y \times n_\mu} \\ 0 & 0_{n_x \times n_\mu} \end{bmatrix}, \ \bar{D} := \begin{bmatrix} 0_{n_y \times n_\mu} & D \end{bmatrix}, \tag{3.30b}$$

$$\zeta := \begin{bmatrix} \chi_1 \\ \chi_2 \\ x \\ \mu_x \end{bmatrix}, \ \boldsymbol{\omega}_\delta := \begin{bmatrix} \omega_{\delta_1} \\ \omega_{\delta_2} \end{bmatrix}, \tag{3.30c}$$

$$\varphi_\zeta(\zeta, u) := \begin{bmatrix} \chi_2 \\ C\bar{\varphi}_x(x, u) + C\frac{\partial \varphi}{\partial x}(x, u)B\mu_x \\ \varphi(x, u) + B\mu_x. \end{bmatrix} \tag{3.30d}$$

with E_{δ_1}, D_{δ_2}, ω_{δ_1}, and ω_{δ_2} defined as in (3.5).

4.3 Generalized UIO

Here we provide the generalized UIO corresponding to the generalized and regularized system (3.29).

Assumption 6. *The matrices E, D, and C_χ, and the scalars δ_1 and δ_2 are chosen such that $\mathbb{E}$ and $\mathcal{H}$ satisfy the rank condition (3.4).*

Assumption 7. *The function $\varphi_\zeta(\cdot, u)$ defined in (3.30d) is globally Lipschitz, uniformly on u.*

As in the previous section, from Assumption 6, there exist two matrices P_ζ and Q_ζ such that

$$P_\zeta \mathbb{E} + Q_\zeta \mathcal{H} = \mathbb{I}_{n_\zeta}. \tag{3.31}$$

where $n_\zeta := 2n_y + n_x + n_\mu$, and then an observer is constructed as in (3.10) as follows:

$$\begin{cases} \dot{\eta} &= P_\zeta \varphi_\zeta(\hat{\zeta}, u) + K\left(y_\chi - \mathcal{H}\hat{\zeta}\right) \\ \hat{\zeta} &= \eta + Q_\zeta y_\chi \end{cases} \tag{3.32}$$

To avoid repetitions, under Assumption 7, assume that the Jacobian $\nabla_\zeta^{\varphi_\zeta}(\boldsymbol{z}, u)$ belongs to the convex polytopic set $\mathcal{H}_\varphi$ defined in (3.19).

It is unnecessary to restate a new theorem or proposition here. Since we use the same notation as in Section 3, the results of Proposition 1 and Theorem 2 apply directly under Assumptions 6 and 7. Specifically, the observer (3.32) with $K = \mathcal{P}^{-1}\mathcal{Q}^\top$ satisfies the $\mathcal{H}^1$-optimality bound (3.8), with parameters given in (3.16a)–(3.16c), where $\vartheta_{\max} = \lambda_{\max}(\mathcal{P})$ and $\mathcal{S} = \epsilon\mathcal{P}$, with $\lambda_{\min}(\mathcal{S}) = \epsilon\,\lambda_{\min}(\mathcal{P})$. The matrices $\mathcal{P}$, $\mathcal{Q}$, and the scalar ϵ are defined in Theorem 2.

4.4 Specific cases and discussion

This section is devoted to discussing the general result established in Section 4. In addition, several specific cases are analyzed to illustrate the benefits of the generalized UIO in Section 4.3 relative to that of Section 3.

4.4.1 Case $\mathrm{rank}(CB) = \mathrm{rank}(B)$

We show that in this case, exponential convergence of the estimation error to zero can be guaranteed. Indeed, if $\mathrm{rank}(CB) = \mathrm{rank}(B)$, then to satisfy Assumption 6, it suffices to choose an appropriate matrix C_χ, independently of δ_1 and δ_2. We can then set $\delta_1 = \delta_2 = 0$, which implies $\lambda_\delta = 0$ in (3.16a) and $\boldsymbol{\omega}_\delta(t) \equiv 0$ in (3.23). Under these conditions, the bound (3.8) reduces to

$$\|\tilde{\zeta}\|_{\mathcal{H}^1} \leq \beta\,\|\xi_0\|, \tag{3.33}$$

which, combined with the uniform continuity of $\tilde{\zeta}(\cdot)$, implies

$$\lim_{t\to+\infty} \tilde{\zeta}(t) = 0.$$

In other words, we have $\xi(t) = \tilde{\zeta}(t)$, and the LMIs (3.26) ensure (3.23), which reduces to

$$\dot{\vartheta}(\tilde{\zeta}(t)) + \|\tilde{\zeta}(t)\|^2 \leq 0,$$

thus guaranteeing the *exponential convergence of* $\tilde{\zeta}(t)$ *to zero*.

4.4.2 Case $C_\chi = 0$

In this case, the derivative of the output measurement, $\dot{y}$, is not used as an additional input to the observer. Unfortunately, even when $\mathrm{rank}(CB) = \mathrm{rank}(B)$, the only way to satisfy Assumption 6 is to choose an appropriate nonzero matrix D and $\delta_2 > 0$. Consequently, we may set $\delta_1 = 0$ to achieve a tighter $\mathcal{H}^1$ bound; however, exponential convergence of the estimation error to zero cannot be guaranteed.

4.4.3 Case $\mathrm{rank}(CB) < \mathrm{rank}(B)$

In this case, exponential convergence of $\tilde{\zeta}$ to zero cannot be guaranteed; however, an $\mathcal{H}^1$ bound can still be obtained through regularization. By appropriately selecting the matrices E and D, and choosing the scalars δ_1 and δ_2 such that Assumption 6 is satisfied, the $\mathcal{H}^1$ bound (3.8) can be effectively adjusted by tuning the parameters δ_1 and δ_2.

4.4.4 On the use of $\dot{y}$

The generalized UIO (3.32) requires real-time knowledge of the derivative $\dot{y}$, which can be viewed as a drawback since this derivative must be estimated online. Nevertheless, the structure of the proposed observer naturally incorporates the estimation of $\dot{y}$ through the auxiliary state variable χ_2. In particular, when $\mathrm{rank}(CB) = \mathrm{rank}(B)$, the estimate $\hat{\chi}_2$ converges exponentially to χ_2, thereby providing an accurate estimation of $\dot{y}$. This represents a major improvement over conventional UIO design approaches, which typically estimate the unknown inputs by differentiating the estimated states or the measured output y a posteriori.

Table 3.1: Summary of specific cases: assumptions, design choices, and convergence properties.

Case / setting	**Design choice to satisfy Assumption 6**	**Main guarantee**	**Use of $\dot{y}$**
$\mathrm{rank}(CB)$=$\mathrm{rank}(B)$ (classical matching holds)	Pick $C_\chi \neq 0$; can set $\delta_1 = \delta_2 = 0$ (no regularization, $\boldsymbol{\omega}_\delta \equiv 0$)	Exponential convergence of $\tilde{\zeta}(t)$ to 0 (strongest case)	Required by the generalized structure, but estimated internally via $\hat{\chi}_2$
$C_\chi = 0$ (do not inject output derivatives)	Must rely on regularization through $D \neq 0$ and $\delta_2 > 0$ (often take $\delta_1 = 0$ for a tighter bound)	Only an $\mathcal{H}^1$ bound; exponential convergence to 0 cannot be ensured	Not used
$\mathrm{rank}(CB)$<$\mathrm{rank}(B)$ (classical UIO fails)	Regularize: choose E, D, and $\delta_1, \delta_2 > 0$ so that the augmented pair $(\mathbb{E}, \mathcal{H})$ satisfies (3.4)	$\mathcal{H}^1$ bound with tunable attenuation level λ_δ (via δ_1, δ_2); exponential convergence not guaranteed	Typically used if $C_\chi \neq 0$; otherwise not needed

5 UIO-Based Neural Online Approximation of Unmodeled Nonlinearity

As discussed in the previous section, the UIO provides an estimation of the unmodeled nonlinearity μ_x. However, this estimation is instantaneous and does not provide a predictive model of the nonlinearity. To address this, we employ a neural network to learn the function μ_x explicitly. This learned model can then be used for control design or improved state estimation. The UIO scheme developed earlier serves as a reliable source of training data (ground truth proxy) for this online learning process.

Regarding the estimation of the system state x during learning, two approaches can be considered: (1) using the state estimate $\hat{x}$ directly from the existing UIO, or (2) designing a separate neuro-adaptive observer that simultaneously estimates x and the neural network parameters. In this work, we focus on the first approach, where the UIO provides the state estimate used to query the neural network.

We begin by introducing the following assumption regarding the closed-loop system:

Assumption 8. *The system is capable of tracking a known reference trajectory x_{ref} under an observer-based controller of the form:*

$$u := \kappa\left(x_{ref}, u_{ref}, \hat{x}\right) \tag{3.34}$$

where $\hat{x}$ is the state estimate, and u_{ref} is a reference control input such that the pair (x_{ref}, u_{ref}) constitutes an admissible trajectory for the system (3.1).

5.1 Fully UIO-based Learning Architecture

The generalized UIO derived in Section 4 provides an augmented state estimate $\hat{\zeta}$. To facilitate the learning strategy, we partition this vector to isolate the physics-based state estimate, denoted as $\hat{x}_{\text{UIO}}$, and the unknown input estimate, $\hat{\mu}_x$:

$$\hat{\zeta} = \begin{bmatrix} \hat{\chi}_1 \\ \hat{\chi}_2 \\ \hat{x}_{\text{UIO}} \\ \hat{\mu}_x \end{bmatrix} \in \mathbb{R}^{2n_y+n_x+n_\mu}. \tag{3.35}$$

Using these estimates, we introduce a neural network approximation $\mu_\theta(\cdot)$ to capture the unmodeled dynamics. This data-driven model is integrated into a secondary observer structure, referred to as the Neural Observer, to refine the state estimation.

Let $\mu_\theta(\hat{x}_{\text{nn}})$ denote the neural network approximation of μ_x, parameterized by θ:

$$\mu_\theta(\hat{x}_{\text{nn}}) = \mathcal{N}_\theta(\hat{x}_{\text{nn}}, u) \tag{3.36}$$

where $\mathcal{N}_\theta(\cdot)$ is the neural network function. This approximation is incorporated into the observer dynamics as follows:

$$\begin{cases} \dot{\hat{x}}_{\text{nn}} = \varphi(\hat{x}_{\text{nn}}, u) + B\mu_\theta(\hat{x}_{\text{nn}}) + L_{\text{nn}}\left(y - y_{\text{nn}}\right) \\ y_{\text{nn}} = C\hat{x}_{\text{nn}} \end{cases} \tag{3.37}$$

where $\hat{x}_{\text{nn}} \in \mathbb{R}^{n_x}$ is the state of the Neural Observer and L_{nn} is the observer gain to be designed.

The proposed hybrid strategy is illustrated in Figure 3.1. The physics-based UIO uses the measured output y to provide robust initial estimates $\hat{x}_{\text{UIO}}$ and $\hat{\mu}_x$. Simultaneously, the Neural Observer utilizes the

learned model μ_θ to produce a refined state estimate $\hat{x}_{\text{nn}}$. The neural network parameters θ are updated online by minimizing a composite loss function that enforces consistency between the data-driven model and the physics-based UIO estimates.

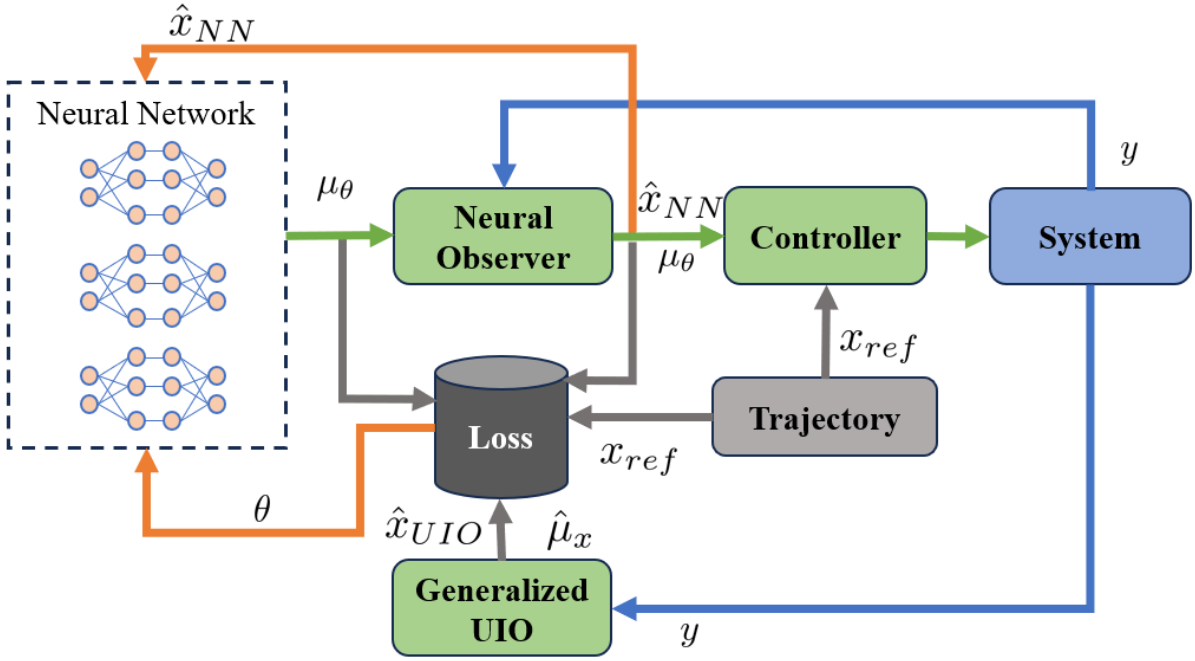

Figure 3.1: Diagram of the proposed hybrid estimation strategy.

The dynamics of the original system (3.1) can be rewritten as:

$$\dot{x} = \varphi(x, u) + B\mu_\theta(\hat{x}_{\text{nn}}) + B\Delta_x(t) \tag{3.38}$$

where $\Delta_x(t) \triangleq \mu_x(t) - \mu_\theta(\hat{x}_{\text{nn}}(t))$ represents the approximation error of the neural network.

5.1.1 Design of the Neural Adaptive Observer

The objective is to determine the observer gain L_{nn} such that the estimation error $\epsilon_{\text{nn}} \triangleq x - \hat{x}_{\text{nn}}$ satisfies an $\mathcal{L}^2$ performance criterion:

$$\|\epsilon_{\text{nn}}\|_{\mathcal{L}^2} \leq \lambda_{\text{nn}} \, \|\Delta_x\|_{\mathcal{L}^2} + \beta_{\text{nn}} \, \|\epsilon_{\text{nn}}(0)\| \tag{3.39}$$

where λ_{nn} and β_{nn} are positive scalars. We consider the quadratic Lyapunov function $V(\epsilon_{\text{nn}}) = \epsilon_{\text{nn}}^\top \mathcal{P} \epsilon_{\text{nn}}$ with $\mathcal{P} > 0$. To satisfy (3.39), it suffices to ensure:

$$\dot{V}(\epsilon_{\text{nn}}) + \epsilon_{\text{nn}}^\top \epsilon_{\text{nn}} - \lambda_{\text{nn}}^2 \Delta_x^\top \Delta_x < 0.$$

The error dynamics are given by:

$$\dot{\epsilon}_{\text{nn}} = \left(\nabla_x^\varphi(\boldsymbol{z}_x, u) - L_{\text{nn}} C\right)\epsilon_{\text{nn}} + B\Delta_x(t) \tag{3.40}$$

where $\nabla_x^{\varphi}(\boldsymbol{z}_x, u)$ is the Jacobian of φ evaluated at some $\boldsymbol{z}_x$. Under Assumption 3, this Jacobian belongs to a convex polytope analogous to $\mathcal{H}_{\varphi}$ defined in (3.19), restricted to the state space $\mathbb{R}^{n_x}$.

The following theorem provides sufficient LMI conditions for the existence of such an observer.

Theorem 3. *Under Assumption 3, if there exist a symmetric positive definite matrix $\mathcal{P} \in \mathbb{R}^{n_x \times n_x}$, a matrix $\mathcal{Q} \in \mathbb{R}^{n_y \times n_x}$, and a positive scalar σ satisfying the following LMI conditions for all vertices $j = 1, \ldots, \bar{n}_x$:*

$$\begin{bmatrix} \left(\mathcal{A}_j^x\right)^\top \mathcal{P} + \mathcal{P}\mathcal{A}_j^x - C^\top \mathcal{Q} - \mathcal{Q}^\top C & \mathcal{P}B \\ B^\top \mathcal{P} & -\sigma \mathbb{I}_{n_\mu} \end{bmatrix} < 0 \tag{3.41}$$

then the observer gain $L_{nn} = \mathcal{P}^{-1}\mathcal{Q}^\top$ ensures that the estimation error ϵ_{nn} satisfies the $\mathcal{L}^2$ criterion (3.39) with $\lambda_{nn} = \sqrt{\sigma}$ and $\beta_{nn} = \sqrt{\lambda_{\max}(\mathcal{P})}$.

Proof. The proof follows standard $\mathcal{L}^2$ stability analysis for LPV systems and is omitted for brevity. □

5.1.2 Optimization of the Learning Parameter θ

To approximate the unknown dynamics $\mu_x(t)$, the neural network parameters θ are optimized to minimize a specific loss function. Since the true value of $\mu_x(t)$ is unknown, we utilize the UIO estimate $\hat{\mu}_x(t)$ as a target. We define a composite loss function that balances tracking performance, measurement consistency, and regularization:

$$\begin{aligned} \mathcal{L}(\theta) = &\underbrace{(\hat{x}_{\text{nn}} - x_{\text{ref}})^\top \mathcal{T}_{\text{ref}} (\hat{x}_{\text{nn}} - x_{\text{ref}})}_{\textit{Tracking Error}} + \underbrace{(y - y_{\text{nn}})^\top \mathcal{T}_y (y - y_{\text{nn}})}_{\textit{Output Error}} \\ &+ \underbrace{(\hat{x}_{\text{nn}} - \hat{x}_{\text{uio}})^\top \mathcal{T}_{\text{uio}} (\hat{x}_{\text{nn}} - \hat{x}_{\text{uio}})}_{\textit{UIO Consistency}} + \underbrace{\lambda \|\mu_\theta(\hat{x}_{\text{nn}}) - \hat{\mu}_x\|^2}_{\textit{Regularization}} \end{aligned} \tag{3.42}$$

where $\mathcal{T}_{\text{ref}}, \mathcal{T}_y, \mathcal{T}_{\text{uio}}$ are positive definite weighting matrices, and $\lambda > 0$ is a scalar weight.

The terms in (3.42) are motivated as follows:

- **Tracking Error:** Penalizes deviations of the neural observer state $\hat{x}_{\text{nn}}$ from the reference trajectory x_{ref}, ensuring the learned model supports the control objective.
- **Output Error:** Enforces consistency between the predicted output y_{nn} and the actual measurement y, providing direct feedback from sensor data.
- **UIO Consistency:** Constrains $\hat{x}_{\text{nn}}$ to remain close to the robust UIO estimate $\hat{x}_{\text{uio}}$, preventing divergence during the early phases of learning.
- **Regularization:** Directly guides the neural network output μ_θ towards the UIO-estimated disturbance $\hat{\mu}_x$, acting as a supervised learning signal.

5.2 Minimization of the Loss Function

This section details the numerical optimization procedure for tuning the neural network parameters θ. We employ a gradient-based approach using a discretized version of the neural observer and sensitivity propagation.

5.2.1 Discretization of the Neural Adaptive Observer

Consider the continuous-time neural observer dynamics:

$$\dot{\hat{x}}_{\text{nn}}(t) = \varphi(\hat{x}_{\text{nn}}(t), u(t)) + B\,\mu_\theta(\hat{x}_{\text{nn}}(t)) + L_{\text{nn}}\big(y(t) - C\hat{x}_{\text{nn}}(t)\big).$$

Applying a forward Euler discretization with sampling period Δt, we obtain the discrete-time update law:

$$\hat{x}_{k+1} = \hat{x}_k + \Delta t\Big(\varphi(\hat{x}_k, u_k) + B\,\mu_\theta(\hat{x}_k) - L_{\text{nn}}C\hat{x}_k + L_{\text{nn}}y_k\Big).$$

This can be written compactly as:

$$\hat{x}_{k+1} = f_{\text{obs}}(\hat{x}_k, \theta, k). \tag{3.43}$$

5.2.2 Gradient Computation via Sensitivity Analysis

The optimal parameters θ are obtained by solving the following optimization problem over a horizon K:

$$\begin{aligned} \min_{\theta} \quad & J(\theta) = \textstyle\sum_{k=0}^{K} \mathcal{L}_k(\hat{x}_k(\theta)) \\ \text{s.t.} \quad & \hat{x}_{k+1} = f_{\text{obs}}(\hat{x}_k, \theta, k). \end{aligned} \tag{3.44}$$

Since the state $\hat{x}_k$ depends implicitly on θ through the observer dynamics, we compute the gradient $\nabla_\theta J$ using sensitivity analysis.

The total gradient of the loss at step k with respect to θ is given by the chain rule:

$$\nabla_\theta \mathcal{L}_k = \frac{\partial \mathcal{L}_k}{\partial \hat{x}_k} S_k + \frac{\partial \mathcal{L}_k}{\partial \mu_k}\left(\frac{\partial \mu_\theta}{\partial \theta} + \frac{\partial \mu_\theta}{\partial \hat{x}_k} S_k\right) \tag{3.45}$$

where $S_k \triangleq \frac{\partial \hat{x}_k}{\partial \theta} \in \mathbb{R}^{n_x \times n_\theta}$ is the sensitivity matrix, and $\mu_k \triangleq \mu_\theta(\hat{x}_k)$.

The partial derivatives of the loss function (3.42) are:

$$\frac{\partial \mathcal{L}_k}{\partial \hat{x}_k} = 2(\hat{x}_k - x_{\text{ref},k})^\top \mathcal{T}_{\text{ref}} - 2(y_k - C\hat{x}_k)^\top \mathcal{T}_y C + 2(\hat{x}_k - \hat{x}_{\text{UIO},k})^\top \mathcal{T}_{\text{uio}} \tag{3.46}$$

$$\frac{\partial \mathcal{L}_k}{\partial \mu_k} = 2\lambda(\mu_\theta(\hat{x}_k) - \hat{\mu}_{x,k})^\top. \tag{3.47}$$

The sensitivity matrix S_k propagates according to the linearized dynamics of the observer:

$$S_{k+1} = S_k + \Delta t\,(A_k S_k + B_k) \tag{3.48}$$

where

$$A_k = \frac{\partial f_{\text{obs}}}{\partial \hat{x}_k} = \frac{\partial \varphi}{\partial \hat{x}_k} + B\frac{\partial \mu_\theta}{\partial \hat{x}_k} - L_{\text{nn}}C \tag{3.49}$$

$$B_k = \frac{\partial f_{\text{obs}}}{\partial \theta} = B\frac{\partial \mu_\theta}{\partial \theta}. \tag{3.50}$$

The Jacobians $\frac{\partial \mu_\theta}{\partial \hat{x}_k}$ and $\frac{\partial \mu_\theta}{\partial \theta}$ are computed via automatic differentiation. The parameters are then updated

using a gradient descent algorithm (e.g., Adam):

$$\theta \leftarrow \theta - \eta \sum_{k=0}^{K} \nabla_\theta \mathcal{L}_k.$$

Remark 6 (Learning stability). *Due to the nonlinear parameterization of deep neural networks, global convergence of the learning parameters θ cannot, in general, be guaranteed using classical adaptive control arguments. Nevertheless, the observer gain is synthesized such that the nominal estimation error dynamics are exponentially stable (i.e., when the approximation error is zero). The neural network enters the estimation error dynamics through the approximation error $\Delta_x(t) := \mu_x(t) - \mu_\theta(\hat{x}_{nn}(t))$, which acts as an additive disturbance. Therefore, the estimation error system is input-to-state stable with respect to Δ_x; in particular, if Δ_x remains bounded during online learning (e.g., by using bounded learning rates and, when needed in practice, weight constraints such as projection/clipping), then all internal estimation signals are uniformly ultimately bounded.*

6 Continuous Learning Strategy

A critical challenge in online learning is the "catastrophic forgetting" phenomenon, where the model loses previously acquired knowledge when trained on new data. In our context, while the unmodeled dynamics μ_x may be state-dependent and time-invariant, the system operates in different regions of the state space over time. Training solely on recent data may degrade performance in previously visited regions.

To address this, we adopt an experience replay mechanism using a fixed-size queue of neural networks, as proposed in [60] and illustrated in Fig. 3.2. The strategy proceeds as follows:

1. A queue of size p maintains historical versions of the neural network model.
2. When new data is available, the current model is updated and added to the queue.
3. If the queue is full, the oldest model is discarded.
4. The effective model used for prediction, $\hat{f}_{\text{nn}}^{(i+1)}$, is a weighted ensemble of the models in the queue:

$$\hat{f}_{\text{nn}}^{(i+1)} = M_\psi \left(\hat{f}_{\text{nn}}^{i}, e^{i+1-p} f_\theta^{(i+1)} \right) \tag{3.51}$$

where $f_\theta^{(i+1)}$ is the $(i+1)$-th network added to the queue, and M_ψ is an aggregation function.

This approach ensures that the learned model retains information from past operating conditions while adapting to new data, thereby enhancing stability and robustness across the entire operating envelope.

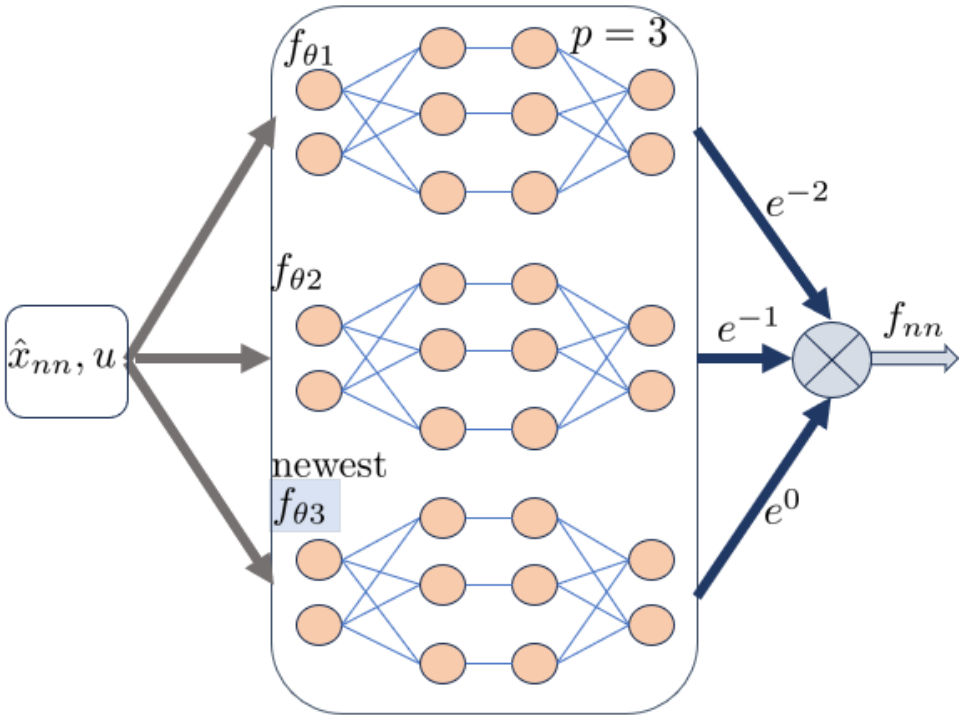

Figure 3.2: Schematic of the continuous learning with forgetting mechanism.

7 Simulation Results

This section evaluates the proposed Teacher–Student estimation architecture through numerical simulations of an autonomous vehicle. The simulated plant includes nonlinear tire-force residuals and parametric mismatch with respect to the model used in the observer design. The objective is to estimate the vehicle lateral dynamics and reconstruct the unknown tire-force nonlinearities from a limited sensor set.

7.1 Nonlinear Vehicle Plant

The simulated plant is a dynamic bicycle model [61]:

$$\dot{v}_x = a - \frac{F_{yf}\sin(\delta)}{m} - \mu g + \dot{\psi} v_y \tag{3.52a}$$

$$\dot{v}_y = \frac{F_{yr}}{m} + \frac{F_{yf}\cos(\delta)}{m} - \dot{\psi} v_x \tag{3.52b}$$

$$\dot{\psi} = r \tag{3.52c}$$

$$\dot{r} = \frac{l_f F_{yf}\cos(\delta)}{I_z} - \frac{l_r F_{yr}}{I_z} \tag{3.52d}$$

$$\dot{X} = v_x\cos(\psi) - v_y\sin(\psi) \tag{3.52e}$$

$$\dot{Y} = v_x\sin(\psi) + v_y\cos(\psi).$$

Here, v_x and v_y are the longitudinal and lateral velocities, ψ is the yaw angle, and $r = \dot{\psi}$ is the yaw rate. The inputs are the longitudinal acceleration a and the steering angle δ. The parameters (m, I_z, l_f, l_r) denote the mass, yaw moment of inertia, and distances from the center of gravity to the front and rear

axles.

The lateral tire forces are decomposed into nominal linear terms and unknown nonlinear residuals:

$$F_{yf} = C_f\alpha_f + f_{yf}(\alpha_f), \qquad F_{yr} = C_r\alpha_r + f_{yr}(\alpha_r), \tag{3.53}$$

with slip angles

$$\alpha_f = \delta - \frac{v_y + l_f r}{v_x}, \qquad \alpha_r = -\frac{v_y - l_r r}{v_x}. \tag{3.54}$$

The functions $f_{yf}(\cdot)$ and $f_{yr}(\cdot)$ represent unmodeled tire dynamics and are treated as unknown inputs to be reconstructed.

7.1.1 QCar Simulation Setup and Residual Injection

The simulated platform is the Quanser QCar with nominal geometric and inertial parameters

$$l = 0.425\ \mathrm{m}, \quad w = 0.192\ \mathrm{m}, \quad m = 2.7\ \mathrm{kg}, \quad I_z = 0.034\ \mathrm{kg\,m^2},$$

and axle distances $l_f = a = 0.13$ m, $l_r = b = 0.13$ m. The observer uses the linear tire model with

$$C_f = C_r = 120\ \mathrm{N/rad}.$$

In the simulation plant, the unknown input is injected as the mismatch between the true nonlinear tire force and this nominal linear model:

$$w_f = F_{yf}^{\mathrm{true}} - C_f\alpha_f, \qquad w_r = F_{yr}^{\mathrm{true}} - C_r\alpha_r, \qquad \mu_x = \begin{bmatrix} w_f \\ w_r \end{bmatrix}. \tag{3.55}$$

Hence, the residual channels in (3.55) are exactly the unknown inputs reconstructed by the UIO/NAO architecture.

The main simulation limits are chosen from the QCar configuration:

$$|\delta| \le 0.52\ \mathrm{rad}, \quad |\dot{\delta}| \le 3.0\ \mathrm{rad/s}, \quad v_x \in [-1.5,\ 2.5]\ \mathrm{m/s}, \quad v_{\mathrm{switch}} = 0.1\ \mathrm{m/s}.$$

For start/stop maneuvers, a low-speed mode is used when $|v_x| < v_{\mathrm{switch}}$: the model switches to a kinematic update (and lateral tire-force terms are faded), which is numerically more robust near standstill. In addition, all terms that require $1/v_x$ use

$$\tilde{v}_x = \max(|v_x|, v_{\mathrm{switch}})\,,$$

so slip-related expressions never divide by a very small speed. The road/tire coefficients are set to $\mu_{\mathrm{road}} = 1.0$ and $\mu = 0.01$ (rolling term in the longitudinal dynamics).

7.2 LPV Model Used by the Observers

The observer design relies on the reduced state $x = [v_x,\ v_y,\ \psi,\ r]^\top$, input $u = [a,\ \delta]^\top$, and measured output $y = [v_x,\ \psi,\ r]^\top$. In the implemented qLPV model, no small-angle approximation is used: the trigonometric terms are kept explicitly through online scheduling variables.

Define the scheduling vector

$$\rho := \begin{bmatrix} \text{inv_}v_x & \sin\delta & \cos\delta & v_x & v_y & \sin\psi & \cos\psi & s_v \end{bmatrix}^\top, \tag{3.56}$$

with

$$\text{inv_}v_x = \frac{1}{\tilde{v}_x}, \qquad \tilde{v}_x := \max(|v_x|, v_{\text{switch}}), \qquad s_v := \text{clip}\left(\frac{\tilde{v}_x - v_{\text{switch}}}{v_{\text{blend}} - v_{\text{switch}}},\ 0,\ 1\right),$$

where $v_{\text{switch}} = 0.1\ \text{m/s}$ and $v_{\text{blend}} = 1.0\ \text{m/s}$. The factor s_v scales lateral stiffness terms at low speed to avoid singular behavior near stop.

The observer model is therefore written as

$$\begin{cases} \dot{x} = A(\rho)x + B(\rho)u + E(\rho)\mu_x(x,u) \\ y = Cx, \end{cases} \tag{3.57}$$

where the unknown input collects the nonlinear tire-force residuals,

$$\mu_x(x,u) = \begin{bmatrix} w_f \\ w_r \end{bmatrix}, \tag{3.58}$$

with residual injection defined in (3.55). The matrices $A(\rho)$, $B(\rho)$, and $E(\rho)$ are computed online from (3.56), while C is constant.

7.2.1 Rank Condition Check (Why a Generalized/Regularized UIO Is Needed)

For (3.57), the unknown input $\mu_x \in \mathbb{R}^2$ enters the dynamics through $E(\rho) \in \mathbb{R}^{4\times 2}$, while the measured output is $y \in \mathbb{R}^3$. A standard condition for unknown-input reconstruction in classical UIO theory must hold over the full scheduling envelope:

$$\text{rank}\big(C\,E(\rho)\big) = \text{rank}\big(E(\rho)\big), \quad \forall\rho. \tag{3.59}$$

In practice, this condition is not uniformly satisfied: for operating points near $\delta \approx 0$, the direct contribution of the front residual to the measured channel v_x is attenuated by $\sin\delta$, and $\text{rank}(CE(\rho))$ can drop below $\text{rank}(E(\rho))$. Therefore, with the sensor set $y = [v_x, \psi, r]^\top$, the classical condition may fail on part of the operating domain. This motivates the generalized/regularized UIO in Section 3, which restores the required augmented rank condition (Assumption 5 and (3.4)) by introducing a controlled regularization of the output equation.

7.2.2 LPV Scheduling and Polytopic Embedding

The qLPV matrices are parameterized by the full scheduling vector (3.56). At each sampling instant, $\rho(t)$ is computed from the measured/estimated state and steering input, then $A(\rho)$, $B(\rho)$, and $E(\rho)$ are updated online.

For LMI-based synthesis, the admissible scheduling domain is bounded and approximated by a convex polytope:

$$\mathcal{A}_\zeta(\rho) \in \mathrm{Co}\{\mathcal{A}_{\zeta,1}, \ldots, \mathcal{A}_{\zeta,\bar{n}}\},$$

where the vertices are obtained by evaluating the augmented Jacobian at selected corners/grid points of the bounded scheduling set (including $\mathrm{inv_}v_x$, $\sin\delta$, $\cos\delta$, and the low-speed scaling factor s_v). The observer gains are then synthesized by enforcing the LMI conditions simultaneously at all selected vertices with a single parameter-independent gain.

7.2.3 Step-by-Step Application of the Generalized UIO to the Vehicle Model

This subsection provides the full, explicit construction of the generalized UIO of Section 3 when applied to the LPV vehicle model (3.57). The development proceeds through four steps: (i) regularization, (ii) augmented matrix construction, (iii) computation of the structural matrices P_ζ and Q_ζ, and (iv) LMI-based gain synthesis.

Step 1: Regularization to recover the rank condition. The teacher component is the regularized UIO of Section 3, which estimates the augmented variable $\zeta = [x^\top, \mu_x^\top]^\top \in \mathbb{R}^{n_\zeta}$, with $n_\zeta = n_x + n_\mu = 4+2 = 6$. Since the classical rank condition (3.59) fails, we regularize the output equation following (3.5):

$$y = Cx + D_{\delta_2}\mu_x + D\,\omega_{\delta_2}, \tag{3.60}$$

with $D_{\delta_2} = \delta_2 D$, $\omega_{\delta_2} = \delta_2\mu_x$, and a binary full-column-rank matrix $D \in \mathbb{R}^{n_y \times n_\mu}$. For this vehicle model ($n_y = 3$, $n_\mu = 2$), we choose

$$D = \begin{bmatrix} 0 & 0 \\ 1 & 0 \\ 0 & 1 \end{bmatrix}, \tag{3.61}$$

so that $\mathrm{rank}(D) = 2 = n_\mu$. This choice injects the regularization into the ψ and r measurement channels, which are physically related to the lateral tire forces through the yaw dynamics.

Since the state dynamics in (3.57) are already first-order, we may set $\delta_1 = 0$ (i.e., $E_{\delta_1} = 0$) and rely only on the output regularization. In this case, the regularized system (3.5) reduces to

$$\begin{cases} \dot{x} = A(\rho)x + B(\rho)u + E(\rho)\mu_x \\ y = Cx + \delta_2 D\mu_x + D\,\omega_{\delta_2}, \end{cases} \tag{3.62}$$

with $\omega_{\delta_2} = \delta_2\mu_x$ treated as a bounded disturbance.

Step 2: Construction of the augmented matrices $\mathbb{E}$ and $\mathcal{H}$. Following (3.7a), we construct the augmented matrices for the vehicle model:

$$\mathbb{E} = \begin{bmatrix} \mathbb{I}_4 & 0_{4\times 2} \end{bmatrix} \in \mathbb{R}^{4\times 6}, \qquad \mathcal{H} = \begin{bmatrix} C & D_{\delta_2} \end{bmatrix} = \begin{bmatrix} 1 & 0 & 0 & 0 & 0 & 0 \\ 0 & 0 & 1 & 0 & \delta_2 & 0 \\ 0 & 0 & 0 & 1 & 0 & \delta_2 \end{bmatrix} \in \mathbb{R}^{3\times 6}. \tag{3.63}$$

The disturbance-related matrices from (3.7b) become (with $\delta_1 = 0$, so $\bar{E}$ vanishes in the first block):

$$\bar{E} = 0_{4\times 4}, \qquad \bar{D} = \begin{bmatrix} 0_{3\times 2} & D \end{bmatrix} = \begin{bmatrix} 0 & 0 & 0 & 0 \\ 0 & 0 & 1 & 0 \\ 0 & 0 & 0 & 1 \end{bmatrix} \in \mathbb{R}^{3\times 4}. \tag{3.64}$$

We now verify the augmented rank condition (3.4) (Assumption 5):

$$\operatorname{rank}\left(\begin{bmatrix} \mathbb{E} \\ \mathcal{H} \end{bmatrix} \right) = \operatorname{rank}\left(\begin{bmatrix} \mathbb{I}_4 & 0_{4\times 2} \\ C & D_{\delta_2} \end{bmatrix} \right). \tag{3.65}$$

Since $\mathbb{I}_4$ has full row rank, the first four rows already span four independent directions. The remaining two columns (5th and 6th) are nonzero in D_{δ_2} (for $\delta_2 > 0$) at rows corresponding to the ψ and r measurements. Therefore,

$$\operatorname{rank}\left(\begin{bmatrix} \mathbb{E} \\ \mathcal{H} \end{bmatrix} \right) = 6 = n_\zeta,$$

confirming that Assumption 5 is satisfied for any $\delta_2 > 0$.

Step 3: Computation of P_ζ and Q_ζ. From the rank condition, there exist $P_\zeta \in \mathbb{R}^{6\times 4}$ and $Q_\zeta \in \mathbb{R}^{6\times 3}$ satisfying (3.9):

$$P_\zeta \mathbb{E} + Q_\zeta \mathcal{H} = \mathbb{I}_6. \tag{3.66}$$

Writing $P_\zeta = \begin{bmatrix} P_1 \\ P_2 \end{bmatrix}$ with $P_1 \in \mathbb{R}^{4\times 4}$ and $P_2 \in \mathbb{R}^{2\times 4}$, and $Q_\zeta = \begin{bmatrix} Q_1 \\ Q_2 \end{bmatrix}$ with $Q_1 \in \mathbb{R}^{4\times 3}$ and $Q_2 \in \mathbb{R}^{2\times 3}$, the condition (3.66) reads:

$$\begin{bmatrix} P_1 + Q_1 C & Q_1 D_{\delta_2} \\ P_2 + Q_2 C & Q_2 D_{\delta_2} \end{bmatrix} = \begin{bmatrix} \mathbb{I}_4 & 0_{4\times 2} \\ 0_{2\times 4} & \mathbb{I}_2 \end{bmatrix}. \tag{3.67}$$

From the $(2,2)$-block, $Q_2 D_{\delta_2} = \mathbb{I}_2$, i.e.,

$$Q_2 \delta_2 D = \mathbb{I}_2 \implies Q_2 = \frac{1}{\delta_2}(D^\top D)^{-1} D^\top = \frac{1}{\delta_2} D^+, \tag{3.68}$$

where D^+ is the Moore–Penrose pseudo-inverse of D. With the binary D in (3.61),

$$D^+ = \begin{bmatrix} 0 & 1 & 0 \\ 0 & 0 & 1 \end{bmatrix}, \qquad Q_2 = \frac{1}{\delta_2} \begin{bmatrix} 0 & 1 & 0 \\ 0 & 0 & 1 \end{bmatrix}. \tag{3.69}$$

From the $(1,2)$-block, $Q_1 D_{\delta_2} = 0$, which gives $Q_1 D = 0$. A natural solution is to set the columns of Q_1 corresponding to the D-active rows equal to zero. With C and D as defined, one may verify that

$$Q_1 = \begin{bmatrix} -1 & 0 & 0 \\ 0 & 0 & 0 \\ 0 & 0 & 0 \\ 0 & 0 & 0 \end{bmatrix} \tag{3.70}$$

satisfies $Q_1 D = 0$, and then $P_1 = \mathbb{I}_4 - Q_1 C$ and $P_2 = -Q_2 C$ are determined accordingly:

$$P_1 = \mathbb{I}_4 - Q_1 C = \begin{bmatrix} 2 & 0 & 0 & 0 \\ 0 & 1 & 0 & 0 \\ 0 & 0 & 1 & 0 \\ 0 & 0 & 0 & 1 \end{bmatrix}, \qquad P_2 = -Q_2 C = -\frac{1}{\delta_2} \begin{bmatrix} 0 & 0 & 1 & 0 \\ 0 & 0 & 0 & 1 \end{bmatrix}. \tag{3.71}$$

The complete matrices are therefore

$$P_\zeta = \begin{bmatrix} P_1 \\ P_2 \end{bmatrix} \in \mathbb{R}^{6\times 4}, \qquad Q_\zeta = \begin{bmatrix} Q_1 \\ Q_2 \end{bmatrix} \in \mathbb{R}^{6\times 3}. \tag{3.72}$$

One can verify that $P_\zeta \mathbb{E} + Q_\zeta \mathcal{H} = \mathbb{I}_6$.

Remark 7 (Non-uniqueness of P_ζ, Q_ζ). *The pair (P_ζ, Q_ζ) is not unique: any solution of the linear system (3.66) is admissible. However, the observer gain K (obtained from the LMI) compensates for the specific choice and produces the same closed-loop error dynamics.*

Step 4: Augmented Jacobian polytope and LMI synthesis. The augmented nonlinear function (3.7d) for the vehicle LPV model (3.57) reads

$$\varphi_\zeta(\zeta, u) = A(\rho)x + B(\rho)u + E(\rho)\mu_x = \begin{bmatrix} A(\rho) & E(\rho) \\ 0_{2\times 4} & 0_{2\times 2} \end{bmatrix} \begin{bmatrix} x \\ \mu_x \end{bmatrix} + \begin{bmatrix} B(\rho)u \\ 0 \end{bmatrix}. \tag{3.73}$$

The Jacobian of φ_ζ with respect to ζ is therefore

$$\nabla_\zeta^{\varphi_\zeta}(\zeta, u) = \begin{bmatrix} A(\rho) & E(\rho) \\ 0_{2\times 4} & 0_{2\times 2} \end{bmatrix} \in \mathbb{R}^{6\times 6}, \tag{3.74}$$

which is parameter-varying through ρ. Using the polytopic embedding of Section 7.2.2, the Jacobian belongs to the polytope

$$\nabla_\zeta^{\varphi_\zeta}(\zeta, u) \in \mathrm{Co}\left\{\mathcal{A}_{\zeta,1}, \ldots, \mathcal{A}_{\zeta,\bar{n}}\right\}, \tag{3.75}$$

with the vertex matrices

$$\mathcal{A}_{\zeta,j} = \begin{bmatrix} A_j & E_j \\ 0_{2\times 4} & 0_{2\times 2} \end{bmatrix} \in \mathbb{R}^{6\times 6}, \qquad j = 1, \ldots, \bar{n}. \tag{3.76}$$

where $A_j := A(\rho_j)$ and $E_j := E(\rho_j)$ are obtained from the selected scheduling vertices/grid points.

The auxiliary disturbance injection matrix at each vertex is computed as

$$\mathcal{E}_j = \bar{E} - P_\zeta \mathcal{A}_{\zeta,j} Q_\zeta \bar{D}, \qquad j = 1, \dots, \bar{n}, \tag{3.77}$$

and the disturbance output matrix is

$$\mathcal{D} = (\mathbb{I}_3 + \mathcal{H} Q_\zeta)\, \bar{D}. \tag{3.78}$$

Step 5: Solving the LMI and extracting the gain. The observer gain $K \in \mathbb{R}^{6\times 3}$ is obtained by solving the LMI problem from Theorem 2. Specifically, one searches for a symmetric positive definite matrix $\mathcal{P} \in \mathbb{R}^{6\times 6}$, a matrix $\mathcal{Q} \in \mathbb{R}^{3\times 6}$, and a scalar $\lambda > 0$ such that the vertex-wise LMI conditions (3.26) hold for $j = 1, \dots, \bar{n}$:

$$\begin{bmatrix} (P_\zeta \mathcal{A}_{\zeta,j})^\top \mathcal{P} + \mathcal{P}\,(P_\zeta \mathcal{A}_{\zeta,j}) - \mathcal{H}^\top \mathcal{Q} - \mathcal{Q}^\top \mathcal{H} & \mathcal{P}\mathcal{E}_j - \mathcal{Q}^\top \mathcal{D} & (P_\zeta \mathcal{A}_{\zeta,j})^\top \mathcal{P} - \mathcal{H}^\top \mathcal{Q} \\ \mathcal{E}_j^\top \mathcal{P} - \mathcal{D}^\top \mathcal{Q} & -\lambda \mathbb{I}_4 & \mathcal{E}_j^\top \mathcal{P} - \mathcal{D}^\top \mathcal{Q} \\ \mathcal{P}\,(P_\zeta \mathcal{A}_{\zeta,j}) - \mathcal{Q}^\top \mathcal{H} & \mathcal{P}\mathcal{E}_j - \mathcal{Q}^\top \mathcal{D} & -\dfrac{1}{\epsilon}\mathcal{P} \end{bmatrix} < 0, \tag{3.79}$$

for a given $\epsilon > 0$. After solving (e.g., using YALMIP/SeDuMi or MATLAB's LMI toolbox), the UIO gain is recovered as

$$K = \mathcal{P}^{-1} \mathcal{Q}^\top \in \mathbb{R}^{6\times 3}. \tag{3.80}$$

The resulting observer dynamics are written as

$$\begin{cases} \dot{\eta} &= P_\zeta \varphi_\zeta(\hat{\zeta}, u) + K\left(y - \mathcal{H}\hat{\zeta}\right) \\ \hat{\zeta} &= \eta + Q_\zeta y, \end{cases} \tag{3.81}$$

and by Theorem 2, the estimation error $\tilde{\zeta} = \zeta - \hat{\zeta}$ satisfies the $\mathcal{H}^1$-optimality bound (3.8) with

$$\lambda_\delta = \delta_2\, \sigma_{\max}(Q_\zeta D) + \delta_2 \sqrt{\frac{\lambda}{\min(1, \epsilon\, \lambda_{\min}(\mathcal{P}))}}, \qquad \beta = \sqrt{\frac{\lambda_{\max}(\mathcal{P})}{\min(1, \epsilon\, \lambda_{\min}(\mathcal{P}))}}. \tag{3.82}$$

Remark 8 (Role of δ_2 in the vehicle application). *The bound (3.82) shows that $\lambda_\delta \to 0$ as $\delta_2 \to 0$. However, taking δ_2 too small increases $\|Q_2\| = 1/\delta_2$ (see (3.69)), which in turn amplifies the influence of output noise through $\hat{\zeta} = \eta + Q_\zeta y$. In practice, δ_2 is chosen as a compromise: large enough for LMI feasibility and reasonable noise sensitivity, small enough for a tight $\mathcal{H}^1$ disturbance attenuation bound.*

Extracting the state and unknown-input estimates. After the UIO runs in real time, the augmented estimate $\hat{\zeta} \in \mathbb{R}^6$ is partitioned as

$$\hat{\zeta} = \begin{bmatrix} \hat{x}_{\text{UIO}} \\ \hat{\mu}_x \end{bmatrix}, \qquad \hat{x}_{\text{UIO}} = \begin{bmatrix} \hat{v}_x \\ \hat{v}_y \\ \hat{\psi} \\ \hat{r} \end{bmatrix} \in \mathbb{R}^4, \quad \hat{\mu}_x = \begin{bmatrix} \hat{f}_{yf} \\ \hat{f}_{yr} \end{bmatrix} \in \mathbb{R}^2. \tag{3.83}$$

The estimate $\hat{\mu}_x$ is then used as the teacher signal in the neural learning loss (3.42) (the "Regularization" term).

7.2.4 Neural Adaptive Observer (NAO) — Application of Theorem 3

The student component is the NAO, which retains the LPV backbone while learning the unknown input through the neural approximation $\mu_\theta(\cdot)$:

$$\dot{\hat{x}}_{\text{nn}} = A(\rho)\hat{x}_{\text{nn}} + B(\rho)u + E(\rho)\mu_\theta(\hat{x}_{\text{nn}}) + L_{\text{nn}}(y - C\hat{x}_{\text{nn}}). \tag{3.84}$$

The gain L_{nn} is designed using Theorem 3. Specifically, one solves the following $\bar{n}$ vertex-wise LMIs for a symmetric positive definite $\mathcal{P}_{\text{nn}} \in \mathbb{R}^{4\times4}$, a matrix $\mathcal{Q}_{\text{nn}} \in \mathbb{R}^{3\times4}$, and a scalar $\sigma > 0$:

$$\begin{bmatrix} A_j^\top \mathcal{P}_{\text{nn}} + \mathcal{P}_{\text{nn}} A_j - C^\top \mathcal{Q}_{\text{nn}} - \mathcal{Q}_{\text{nn}}^\top C + \mathbb{I}_4 & \mathcal{P}_{\text{nn}} E_j \\ E_j^\top \mathcal{P}_{\text{nn}} & -\sigma \mathbb{I}_2 \end{bmatrix} < 0, \qquad j = 1, \dots, \bar{n}. \tag{3.85}$$

The NAO gain is then $L_{\text{nn}} = \mathcal{P}_{\text{nn}}^{-1}\mathcal{Q}_{\text{nn}}^\top$, and Theorem 3 guarantees the $\mathcal{L}^2$ bound (3.39) with $\lambda_{\text{nn}} = \sqrt{\sigma}$ and $\beta_{\text{nn}} = \sqrt{\lambda_{\max}(\mathcal{P}_{\text{nn}})}$. The approximation error $\Delta_x(t) = \mu_x(t) - \mu_\theta(\hat{x}_{\text{nn}}(t))$ acts as an external disturbance, and the estimation error decreases as the neural network learns more accurately.

7.2.5 Gradient Computation Using the Vehicle LPV Model

For the online update of θ, the NAO (3.84) is discretized with a forward Euler step Δt:

$$\hat{x}_{k+1} = \hat{x}_k + \Delta t\Big(A(\rho_k)\hat{x}_k + B(\rho_k)u_k + E(\rho_k)\mu_\theta(\hat{x}_k) + L_{\text{nn}}(y_k - C\hat{x}_k)\Big), \tag{3.86}$$

where ρ_k is computed from $(\hat{x}_k, \delta_k)$ according to (3.56). The sensitivity recursion (cf. Section 5.2.2) used to compute $\nabla_\theta \mathcal{L}$ is

$$S_{k+1} = S_k + \Delta t\,(A_k S_k + B_k)\,, \qquad S_0 = 0, \quad S_k := \frac{\partial \hat{x}_k}{\partial \theta} \in \mathbb{R}^{4\times n_\theta}, \tag{3.87}$$

with

$$A_k = \frac{\partial f_{\text{obs}}}{\partial \hat{x}_k} = A(\rho_k) + E(\rho_k)\frac{\partial \mu_\theta}{\partial \hat{x}_k} - L_{\text{nn}}C \in \mathbb{R}^{4\times4}, \tag{3.88}$$

$$B_k = \frac{\partial f_{\text{obs}}}{\partial \theta} = E(\rho_k)\frac{\partial \mu_\theta}{\partial \theta} \in \mathbb{R}^{4\times n_\theta}. \tag{3.89}$$

This recursion highlights that learning remains explicitly anchored to the physical LPV structure through $A(\rho_k)$ at each sampling instant. The vehicle-specific Jacobians $\frac{\partial \mu_\theta}{\partial \hat{x}_k}$ and $\frac{\partial \mu_\theta}{\partial \theta}$ are computed by automatic differentiation through the neural network.

7.3 Results and Discussion

The following results illustrate the performance of the proposed two-layer Teacher–Student estimation architecture through numerical simulation of the autonomous vehicle scenario described above. The

controller utilizes the state estimates produced by Layer 2 (NAO) as feedback for trajectory tracking.

7.3.1 Trajectory Tracking and Control Inputs

Figure 3.3 presents the vehicle trajectory in the XY-plane alongside the corresponding control inputs. The inset shows the position tracking error, which remains near zero throughout the maneuver, confirming that the state estimates from Layer 2 provide sufficiently accurate feedback for the trajectory-tracking controller. The steering angle and throttle input profiles demonstrate smooth and physically consistent actuation, reflecting the quality of the underlying state estimation.

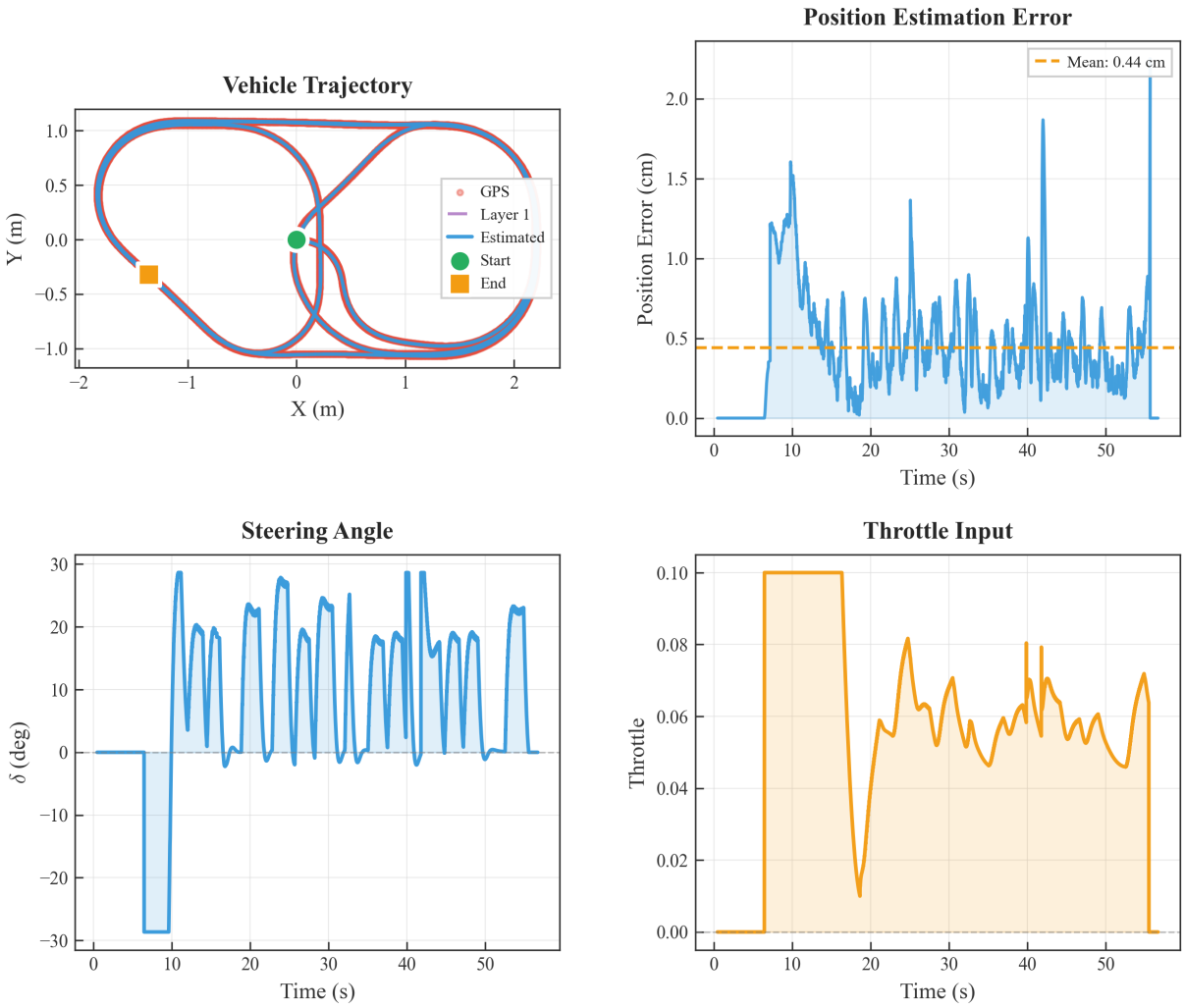

Figure 3.3: Vehicle trajectory in the XY-plane with near-zero position tracking error (inset), and the corresponding steering and throttle control inputs computed using the Layer 2 (NAO) state estimates as feedback.

7.3.2 State Estimation

Figure 3.4 reports the state estimation results for both layers. All estimated states track the true signals closely. The measured channels (v_x, ψ, and r) are recovered with high fidelity, while the unmeasured

lateral velocity v_y—which is the most challenging state to reconstruct—is also well estimated thanks to the observer structure exploiting the coupling in the vehicle dynamics.

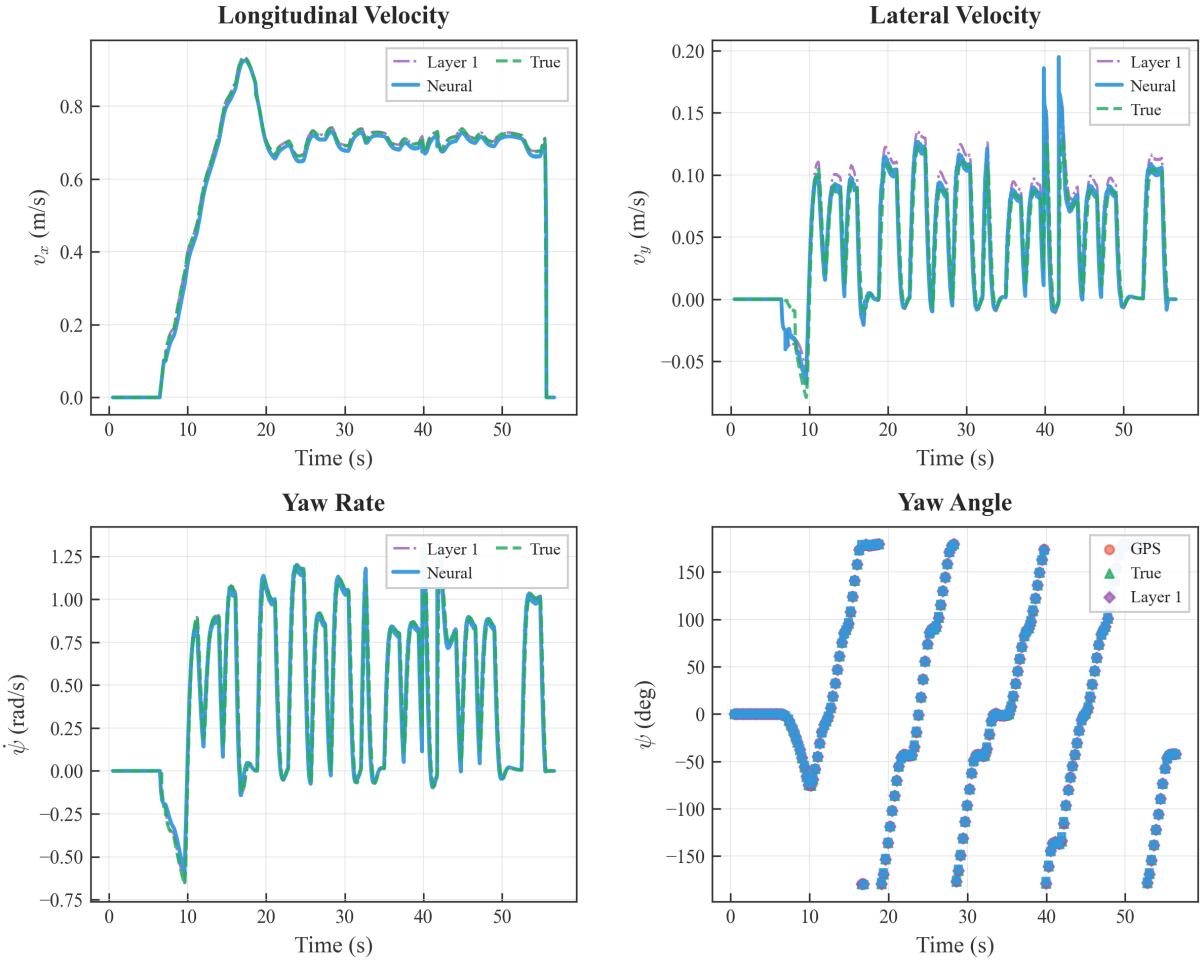

Figure 3.4: State estimation results: all estimated states closely follow the true signals, including the unmeasured lateral velocity v_y.

7.3.3 Tire-Force Residual Estimation

Figure 3.5 presents the reconstruction of the unknown tire-force residuals $\mu_x = [f_{yf},\ f_{yr}]^\top$, comparing the estimates from Layer 1 (UIO) and Layer 2 (NAO). While both layers provide bounded estimates—confirming that the estimation remains stable and does not diverge—Layer 2 exhibits noticeably faster convergence and higher precision in tracking the true residual signals. This improvement is attributed to the neural network's ability to learn the functional relationship $\mu_\theta(\hat{x})$, which refines the instantaneous UIO signal into a predictive model. Importantly, the Layer 2 estimates remain well-constrained, demonstrating that the teacher–student architecture successfully combines the robustness guarantees of the UIO with the adaptability of the neural observer.

Overall, these results validate the proposed two-layer hybrid design: the UIO (Layer 1) provides a stable physics-based supervisory signal with guaranteed bounded estimation, while the NAO (Layer 2) refines the reconstruction of the unknown tire-force residuals with faster convergence and higher precision,

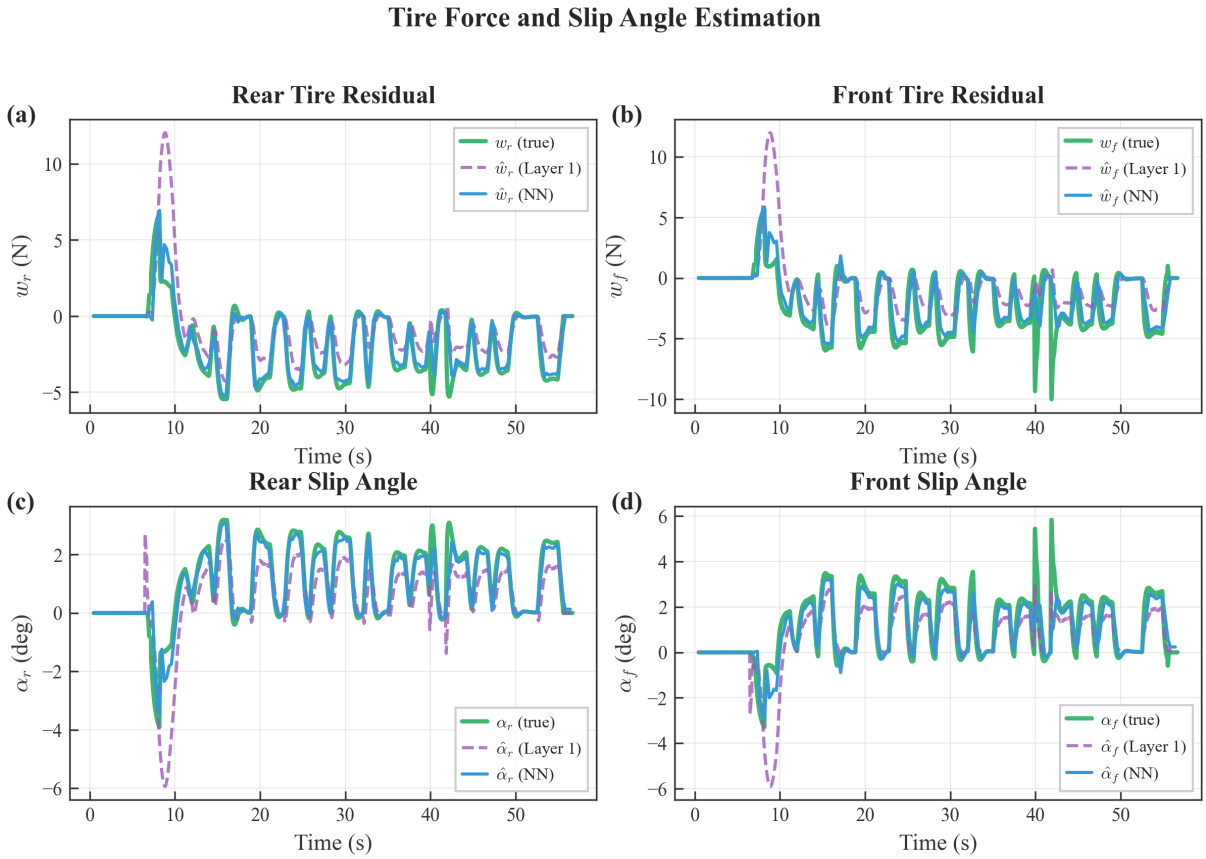

Figure 3.5: Tire-force residual and slip angle estimation: Layer 2 (NAO) achieves faster convergence and higher precision compared to Layer 1 (UIO), while both estimates remain bounded.

ultimately delivering accurate state estimates for closed-loop trajectory tracking.

8 Open Problems and Future Directions

Despite the promising theoretical guarantees and simulation results, several research questions remain open. The following points outline practical and theoretical directions that can improve the applicability of the proposed Teacher–Student estimation architecture.

- **Output-derivative availability and noise amplification.** The generalized/regularized construction is motivated by the need to enrich the output information (cf. rank recovery). In practice, output derivatives may come from IMU signals or filtered differentiators. A key open problem is to quantify the effect of measurement noise and filtering dynamics on the $\mathcal{H}^1$ performance bounds, and to design derivative estimators that preserve the observer guarantees.

- **Guidelines for choosing E, D and tuning (δ_1, δ_2).** While sparse/binary choices of E and D are effective to recover the rank condition, systematic selection procedures that optimize the trade-off between feasibility and disturbance injection remain to be developed. This includes principled tuning of (δ_1, δ_2) as a function of sensor noise, bandwidth limitations, and expected disturbance energy.

- **Beyond $\mathcal{L}_2$-bounded uncertainties.** Assumption 4 (bounded-energy uncertainty) is convenient for analysis, but some automotive disturbances are better modeled as bounded-amplitude or piecewise-smooth signals. Extending the framework to mixed norms (e.g., $\mathcal{L}_\infty$-to-$\mathcal{L}_2$) or incremental input-to-state stability (ISS) type bounds is an interesting direction.

- **Learning conditions and excitation.** The neural adaptive observer uses the UIO estimate as a supervisory signal; however, learning accuracy still depends on the richness of the visited trajectories. Characterizing persistent excitation conditions (or alternative data coverage metrics) that guarantee parameter convergence and good generalization to unseen maneuvers remains an important open issue.

- **Closed-loop interaction and safety guarantees during learning.** In practical deployments, the estimator is embedded in a feedback loop. A challenging direction is to establish end-to-end stability/performance guarantees for the controller–observer–learner interconnection, especially during transient learning phases and under actuator saturation.

- **Discrete-time and embedded implementation.** Real systems operate with sampled measurements and limited compute. Deriving discrete-time counterparts of the $\mathcal{H}^1$ UIO synthesis and the coupled neural adaptation laws—including rigorous treatment of discretization errors and real-time constraints—is required for embedded deployment.

- **Experimental validation and domain shift.** Simulation studies can underestimate issues such as unmodeled sensor biases, delays, and varying road conditions. A natural future direction is validation on real driving datasets and test vehicles, including robustness to domain shift (e.g., different tires, mass loading, and road friction regimes) and the integration of uncertainty quantification for the learned component.

9 Conclusion

This paper presented a robust hybrid estimation framework designed to address the challenges of vehicle motion tracking in the presence of unmodeled nonlinearities. We proposed a layered architecture that integrates a physics-based Generalized Unknown Input Observer (UIO) with a data-driven Neural Adaptive Observer. To overcome the structural limitations of standard observers, specifically when the rank condition $\mathrm{rank}(CB) = \mathrm{rank}(B)$ is not met, we introduced a regularization technique combined with an output-derivative based generalized model. This approach ensures the existence of the observer and provides a reliable initial estimate of the unknown dynamics. This estimate subsequently serves as a supervisor for a neural network, which refines the approximation of complex nonlinearities, such as variable tire-road friction, through online learning. Theoretical analysis demonstrated that the proposed method guarantees $\mathcal{H}^1$ and $\mathcal{L}^2$ stability for the estimation errors, provided that the derived Linear Matrix Inequality (LMI) conditions are satisfied. Open problems and future directions are discussed in Section 8, including experimental validation using real driving data and discrete-time formulations for embedded implementation.

Chapter 4

Resilient Trust–Aware Distributed Observer Design for Connected Vehicle Platoons

Objectives

This chapter proposes a trust-aware distributed observer for vehicle platoons that maintains resilient state estimation under cyberattacks. A behavioral divergence metric evaluates the reliability of shared data, forming a dynamic neighbor set used to adapt observer's weighting gains. Stability conditions are derived via Lyapunov analysis. Simulations under bogus, replay, and DoS attacks demonstrate robust performance and stable platoon behavior.

Contents

1 Introduction . . . **63**
- 1.1 General introduction . . . 63
- 1.2 Graph theory . . . 64
- 1.3 Vehicle mathematical model . . . 64

2 Distributed State Observer Architecture . . . **65**
- 2.1 General structure of the observer . . . 65
- 2.2 On the structure of the observer (4.5) . . . 66
- 2.3 Introduction of a virtual communication graph . . . 67
- 2.4 Main objectives . . . 67

3 Trust Score Framework . . . **67**
- 3.1 Data validity indicator . . . 68
- 3.2 Local trust . . . 68
- 3.3 Distributed trust . . . 71
- 3.4 Target trust and temporal evolution . . . 73
- 3.5 Generalized trust vector . . . 74

4 Weight Design for observer based on the trust . . . **77**
- 4.1 Weight based on the trust . . . 77
- 4.2 Stability of the error . . . 77

5 Simulation Results . . . **80**

5.1 Simulation setup . . . 81
5.2 Attack scenarios . . . 81
5.3 Results . . . 81
5.4 Distributed State Estimation for Platoon Control . . . 83
6 Conclusion and Future Work . . . **89**
6.1 Open Problems and Future Directions . . . 89

1 Introduction

1.1 General introduction

The rapid development of autonomous and connected vehicles has introduced new opportunities to improve road safety, traffic flow, and fuel efficiency. In vehicle platoons-where multiple vehicles coordinate through vehicle-to-vehicle (V2V) communication-accurate distributed state estimation is essential for maintaining stability and efficiency. Each vehicle must reconstruct both its own and others' states using locally sensed data and information exchanged with neighbors. However, this distributed structure also exposes the system to cyber and communication attacks that can disrupt coordination or compromise state estimation [62].

Traditional estimation and control methods generally assume all vehicles are cooperative and trustworthy, which is unrealistic in adversarial environments [63]. Malicious or faulty agents can transmit falsified information, causing estimation errors that propagate through the network. Consequently, resilient estimation strategies capable of identifying and isolating untrustworthy data have become a key research direction in cyber-physical systems (CPS) and distributed multi-agent systems (DMAS).

Existing work on secure estimation and fault detection can be categorized into three main families:

- *Observer-based detection:* compares model-predicted states with sensor measurements to identify anomalies [64, 65]. These methods are effective for detecting deviations but may propagate errors if compromised neighbors provide false data.

- *Consensus-based detection:* relies on cross-validation among agents to identify inconsistent information [18]. While robust under the assumption that most agents are trustworthy, their performance degrades under large-scale coordinated attacks.

- *Trust-based detection:* assigns reliability scores to neighboring agents based on behavioral or statistical consistency. Physical-signal approaches use device fingerprints for authentication [19], while statistical approaches compare communicated data against locally observed behaviors [20]. These methods improve resilience by filtering unreliable inputs before consensus or estimation steps, but they typically require significant computational resources or long-term historical data-making real-time adaptation challenging for dynamic platoons.

Mitigation strategies in the literature often depend on attack detection results. Some switch to fallback modes (e.g., CACC to ACC), while others incorporate trust scores directly into control to down-weight suspicious data [15, 66]. The latter provides finer control adaptation but relies heavily on accurate and timely trust evaluation. To overcome these limitations, we propose a trust-aware distributed observer framework for vehicle platoons. The framework continuously evaluates the trustworthiness of communicated data by comparing reported and predicted behaviors, dynamically adjusting observer weights according to each neighbor's trust score. This mechanism ensures reliable estimation even under cyberattacks or communication faults.

The main contributions of the paper can be summarized in the following items:

- A formal definition of the resilient distributed state estimation problem for connected vehicles under adversarial conditions.

- A behavioral trust model that quantifies each agent's reliability and constructs a dynamic trusted neighbor set.
- A trust-informed distributed observer with provable stability guarantees, validated through simulations under multiple attack scenarios.

By integrating detection, mitigation, and estimation within a unified trust-based layer, the proposed method improves the resilience and stability of cooperative vehicle systems.

1.2 Graph theory

An undirected graph with a nonempty finite set of N nodes can be described by $\mathcal{G} = \{\mathcal{V}, \mathcal{E}, \mathcal{A}\}$ where:

- $\mathcal{V} = \{1, 2, \ldots, N\}$ is the set of nodes.
- $\mathcal{E} \subseteq \mathcal{V} \times \mathcal{V}$ is the set of edges.
- $\mathcal{A} = [a_{ij}] \in \mathbb{R}^{N\times N}$ is the weighted adjacency matrix of $\mathcal{G}$ defined by

$$[a_{ij}] = \begin{cases} a_{ij}, & \text{if } (i,j) \in \mathcal{E}, \\ 0, & \text{otherwise.} \end{cases} \tag{4.1}$$

- The *Laplacian* matrix of $\mathcal{G}$ is denoted as $\mathcal{L} = [l_{ij}] \in \mathbb{R}^{N\times N}$ with

$$l_{ij} = \begin{cases} \sum_{k=1}^{N} a_{ik}, & \text{if } i = j, \\ -a_{ij}, & \text{otherwise.} \end{cases} \tag{4.2}$$

- The set of the neighbors of the node i is defined by $\mathcal{N}_i = \{j \in \mathcal{V} \mid (j,i) \in \mathcal{E}\}$.

1.3 Vehicle mathematical model

The platoon of N vehicles considered in this paper can be modeled as a network of N agents, represented by an undirected communication graph $\mathcal{G} = \{\mathcal{V}, \mathcal{E}, \mathcal{A}\}$. The discrete-time longitudinal dynamics of each vehicle $i \in \mathcal{V}$ are

$$\begin{aligned} x_i(t+1) &= A_{\mathrm{b}} x_i(t) + B_{\mathrm{b}} u_i(t) + \Delta_i(t), \\ y_i(t) &= C_{\mathrm{b}} x_i(t), \end{aligned} \tag{4.3}$$

where $x_i = \begin{bmatrix} s_i & v_i & a_i \end{bmatrix}^\top$ and u_i denote the state and control input of vehicle i, respectively. s_i, v_i, and a_i denote position, velocity, and acceleration. The system matrices are given by

$$A_{\mathrm{b}} = \begin{bmatrix} 1 & T_s & \frac{T_s^2}{2} \\ 0 & 1 & T_s \\ 0 & 0 & 1 - \frac{T_s}{\tau} \end{bmatrix}, \; B_{\mathrm{b}} = \begin{bmatrix} 0 \\ 0 \\ \frac{T_s}{\tau} \end{bmatrix}, C_{\mathrm{b}} = I_3,$$

where T_s is the sampling time and the constant $\tau > 0$ is the nominal engine time lag. $\Delta_i(t)$ captures the modeling differences and uncertainties caused by the difference between the nominal τ and the real value.

Define the collective state as $x = \text{col}\ (x_1, \cdots, x_N)$, the state-space equation of the platoon is

$$\begin{cases} x(t+1) = (I_N \otimes A_\text{b})x(t) + (I_N \otimes B_\text{b})u(t) + \Delta(t) \\ y_i(t) = C_i x(t), \end{cases} \tag{4.4}$$

where $u = \text{col}\ (u_1, \cdots, u_N)$ is the collective control input, $\Delta = \text{col}\ (\Delta_1, \cdots, \Delta_N)$ group unmodeled dynamics and external disturbances and $C_i = \begin{bmatrix} 0 \cdots \underbrace{C_b}_{i\text{th}} \cdots 0 \end{bmatrix}$ is the global output matrix.

Since each vehicle measures its own full states through onboard sensors, ensuring that the pair $(A_\text{b},\ C_\text{b})$ is observable. However, in the context of the platoon dynamic (4.4), the pair $((I_N \otimes A_\text{b}), C_i)$ remain unobservable, motivating the need for distributed estimation through inter-vehicle communication.

2 Distributed State Observer Architecture

The distributed observer provides an effective approach to estimate the full platoon state x. In this section, we introduce a new distributed observer architecture that incorporates trust-function mechanisms, which will be detailed later in Section 3. To achieve full-state estimation of all vehicles, two complementary layers are employed: a Local Observer $(\mathcal{LO})$ that uses onboard sensors, and a Distributed Observer $(\mathcal{DO})$ that fuses information exchanged through communication links. Fig. 4.1 illustrates the architecture of the proposed distributed observer for vehicle platoons.

2.1 General structure of the observer

The distributed state observer architecture considered in this study is characterized by the following set of equations (4.5):

$$(\mathcal{LO}_i) : \hat{x}_0^{(i)}(t+1) = A_\text{b}\hat{x}_0^{(i)}(t) + B_\text{b}u_i(t) + F_i\big(y_i(t) - C_\text{b}\hat{x}_0^{(i)}(t)\big) \tag{4.5a}$$

$$(\mathcal{DO}_i^{(j)}) : \hat{x}_i^{(j)}(t+1) = A_\text{b}\left(\hat{x}_i^{(j)}(t) + \sum_{l\in\mathcal{N}_i} w_{il}^{(j)}(t)\big(\hat{x}_l^{(j)}(t) - \hat{x}_i^{(j)}(t)\big) + w_{i0}^{(j)}(t)\Big(\hat{x}_0^{(j)}(t) - \hat{x}_i^{(j)}(t)\Big)\right) + B_\text{b}\hat{u}_j(t) \tag{4.5b}$$

where

- $\hat{x}_0^{(i)}(t)$ is the state of the local observer $\mathcal{LO}_i$, which will try to track the states of the ith vehicle. It means that
$$\lim_{t\to\infty}\Big(\hat{x}_0^{(i)}(t) - x^{(i)}(t)\Big) = 0. \tag{4.6}$$
- F_i is the gain matrix of the local observer.
- $\mathcal{N}_i$ is the neighbors of the ith vehicle according to the communication graph $\mathcal{G}$.
- $w_{il}^{(j)}(t)$, $l \in \mathcal{N}_i^{(j)}$ is the gain scale to be designed based on the communication topology.
- $\hat{x}_i^{(j)}(t)$ is the state of the distributed observer $\mathcal{DO}_i^{(j)}$, which will try to track the states of the platoon. It means that
$$\lim_{t\to\infty}\big(\hat{x}_i(t) - x(t)\big) = 0, \tag{4.7}$$

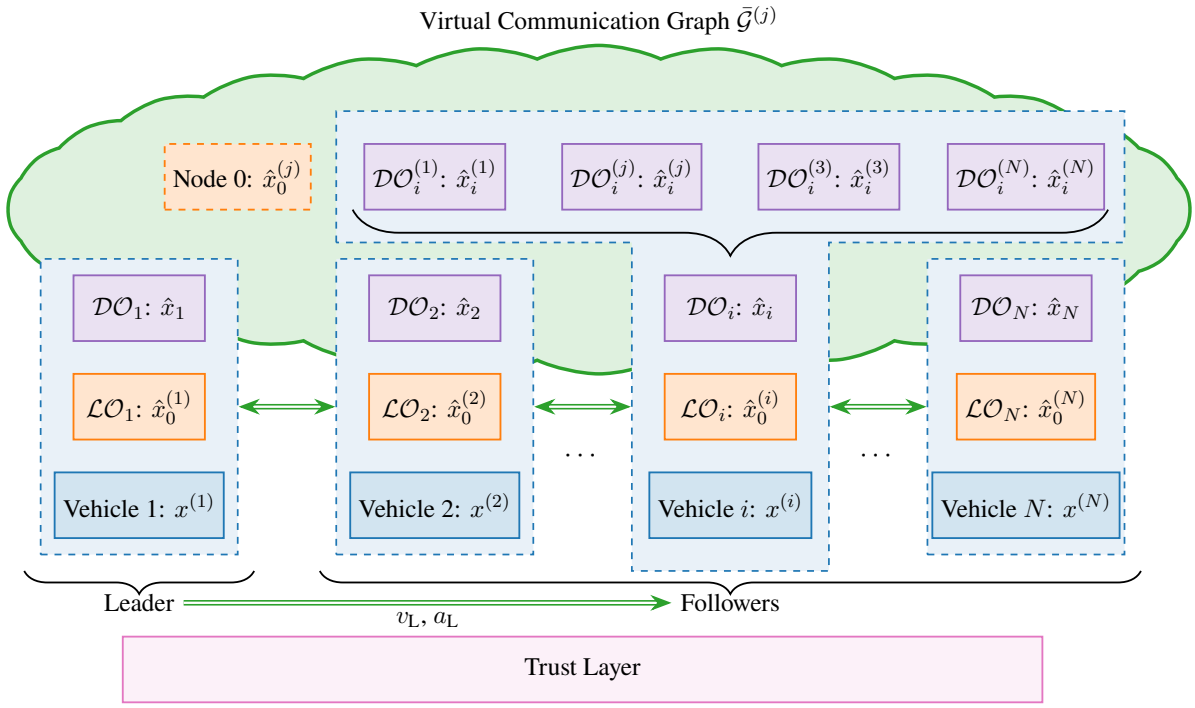

Figure 4.1: Schematic diagram of the estimation method.

where $\hat{x}_i(t) = \text{col}\left(\hat{x}_i^{(1)}(t), \cdots, \hat{x}_i^{(N)}(t)\right)$ is the collective states of all distributed observer.

- $w_{i0}^{(j)}$ is the gain scale to be designed, which is such that

Remark 9. *If a host forms $\hat{u}_j(t)$ (e.g., from a known controller law or an input estimator), the mismatch*

$$\Delta u_j(t) = u_j(t) - \hat{u}_j(t) \tag{4.8}$$

will be treated as part of the disturbance vector. We do not require $\hat{u}_j(t)$ for the $(\mathcal{DO})$ to run; using it only tightens bounds.

2.2 On the structure of the observer (4.5)

The distributed observer $\mathcal{DO}_i^{(j)}$ is designed to estimate the state of each vehicle $j \in \mathcal{V}$ in the platoon from the perspective of vehicle i. The term $\sum_{l\in\mathcal{N}_i} w_{il}^{(j)}\left(\hat{x}_l^{(j)}(t) - \hat{x}_i^{(j)}(t)\right)$ takes into account communication with neighbors $l \in \mathcal{N}_i$ to adjust $\hat{x}_i^{(j)}(t)$ towards a consensus among neighboring estimates of vehicle j's state. The weights $w_{il}^{(j)}$ determine the influence of each neighbor's estimate, promoting consistency across the platoon, which will be designed later. The consensus term alone has a key limitation , it cause all vehicles estimates of a given state $\hat{x}_i^{(j)}(t)$ to converge to a common value. This is theoretically sound only for an ideal platoon with perfectly aligned states. However, practical disturbances, initial condition errors, and imperfect models break this uniformity, rendering a pure consensus estimate inaccurate for any individual vehicle's true state. To mitigate this, the local observer $\mathcal{LO}_i$ provides an accurate estimate of vehicle i's own state, $\hat{x}_0^{(i)}(t)$. The additional anchoring term $w_{i0}^{(j)}\left(\hat{x}_0^{(j)}(t) - \hat{x}_i^{(j)}(t)\right)$ injects this trusted reference, allowing each vehicle to correct model errors and maintain accurate peer estimates.

2.3 Introduction of a virtual communication graph

Each distributed observer $\mathcal{DO}_i^{(j)}$ requires reference information from the local observer $\mathcal{LO}_j$. To formally include this reference, we define a virtual node labeled as node "0" that connects to the vehicle j, where $j \in \mathcal{V}$ and its neighbors $\mathcal{N}_j$ according to the original graph $\mathcal{G}$. The resulting virtual communication graph $\bar{\mathcal{G}}^{(j)} = \{\bar{\mathcal{V}}, \bar{\mathcal{E}}^{(j)}\}$ is constructed as:

$$\begin{aligned} \bar{\mathcal{V}} &= \mathcal{V} \cup \{0\}, \\ \bar{\mathcal{E}}^{(j)} &= \mathcal{E} \cup \{(0,j) | j \in \mathcal{V}\} \cup \{(0,k) | k \in \mathcal{N}_j\}. \end{aligned} \tag{4.9}$$

The adjacency matrix $\bar{\mathcal{A}}^{(j)} \in \mathbb{R}^{(N+1)\times(N+1)}$ corresponding to $\bar{\mathcal{G}}^{(j)}$ is defined as:

$$\bar{\mathcal{A}}^{(j)} = \begin{bmatrix} 0 & 0 \\ w_0^{(j)} & \mathcal{A} \end{bmatrix}, \tag{4.10}$$

where the vector $w_0^{(j)} = \text{col}\left(w_{10}^{(j)}, \cdots, w_{N0}^{(j)}\right) \in \mathbb{R}^N$ defines the connection strengths from node 0 to the distributed observers.

This virtual communication graph provides a unified representation for integrating local estimation (through node 0) and neighbor-based consensus (through graph G), ensuring that every vehicle's local observer acts as a trusted anchor for distributed state estimation.

2.4 Main objectives

Traditional distributed observers use fixed weights w_{il} that assume all data sources are trustworthy. However, in a connected vehicle platoon, compromised nodes may send falsified information. To address this issue, the proposed design incorporates trust-based and time-varying weighting $w_{il}(t)$, allowing each vehicle to dynamically adjust its observer weights according to the reliability of received information. To address this issue, one of the key challenges is to define a quantitative measure of *trust* that captures how reliably a host vehicle can utilize information from its neighbors, despite potential uncertainties or malicious data. Based on this trust, an *adaptive update law* for the gain scaling factor $w_{il}(t)$ is designed, depending on both the computed trust value and the gain matrix F_i of the local observer $(\mathcal{LO}_i)$. This trust mechanism is incorporated into the observer synthesis conditions, presented later in Section 4, ensuring an appropriate ISS convergence bound.

3 Trust Score Framework

To ensure resilient estimation, each vehicle continuously evaluates the reliability of the data it receives. This is achieved through a multi-layer trust framework that quantifies how much a host vehicle i trusts another vehicle l. The overall structure of this trust framework is illustrated in Fig. 4.2.

In this context, we define the following types of trust:

- **Local Trust** $\mathcal{LT}_{i,l}$: evaluates the reliability of the local observer $\mathcal{LO}_l$ data from vehicle l based on consistency and timeliness.
- **Distributed Trust** $\mathcal{DT}_{i,l}$: measures how well the global estimates of l agree with those of i.

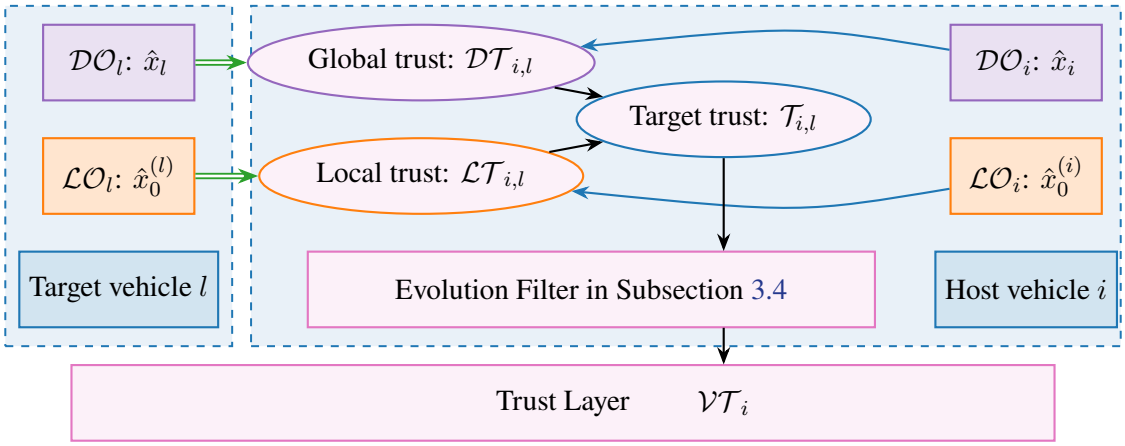

Figure 4.2: Trust framework.

- **Target Trust** $\mathcal{T}_{i,l}$: Combining the Local Trust and Global Trust, the host vehicle i can evaluate the trust score for each target vehicle at time t.
- **Vehicle Trust** $\mathcal{VT}_i$: Smooth evolution of Target Trust scores over time.

In the following subsections, we will explain how to calculate the trust. After that, we will provide more details on how to determine vehicle trust ($\mathcal{VT}_i$) and how to utilize it effectively.

3.1 Data validity indicator

Before trust computation, every received V2V packet data is validated for authenticity and freshness:

$$\delta_{i,l}(t) = \begin{cases} 1, & \text{if message is authenticated and fresh,} \\ 0, & \text{otherwise.} \end{cases} \tag{4.11}$$

Only packets satisfying $\delta_{i,l}(t) = 1$ are used in the following trust evaluation process.

3.2 Local trust

The Local Trust $\mathcal{LT}_{i,l}$ quantifies the confidence that the host vehicle i places in the local observer output of a neighboring vehicle $l \in \mathcal{N}_i$. It is based on three physical-consistency indicators computed from measurable states: velocity, distance, and acceleration. When data are missing, a hold-and-decay rule maintains continuity.

3.2.1 Velocity consistency:

The host estimates the expected velocity of the platoon leader using its last valid packet as a reference value:

$$v_{\text{ref}}(t) = v_{\text{L}}(t - t_{\text{elap}}) + t_{\text{elap}} \cdot a_{\text{L}}(t - t_{\text{elap}}), \tag{4.12}$$

Then, the mismatch score of the target vehicle l with the reference leader can be calculated as

$$v_{l,\text{L}} = \begin{cases} \max\left(1 - \left|\dfrac{\hat{v}_0^{(l)} - v_{\text{ref}}}{v_{\text{ref}}}\right|,\ 0\right), & \text{if } v_{\text{ref}} > 0, \\ \max\left(1 - |\hat{v}_0^{(l)}|,\ 0\right), & \text{otherwise,} \end{cases} \tag{4.13}$$

Table 4.1: Summary of observer notation, trust variables, and index meaning.

Category	Notation	Meaning
Observers	$\mathcal{LO}_i$, $\mathcal{DO}_i$	Local observer at vehicle i (sensor-based), and distributed observer at vehicle i (V2V fusion).
	$\hat{x}_0^{(i)}(t)$	Local state estimate of vehicle i produced by $\mathcal{LO}_i$.
	$\mathcal{DO}_i^{(j)}$, $\hat{x}_i^{(j)}(t)$	Vehicle i's estimate of the target vehicle j's state (distributed layer).
Trust variables	$\delta_{i,l}(t)$	Packet validity indicator (authenticated and fresh).
	$\mathcal{LT}_{i,l}$, $\mathcal{DT}_{i,l}$	Local trust (local-observer consistency) and distributed/global trust (agreement of distributed estimates).
	$\gamma_{i,l}^{\text{self}}$	Self-consistency factor: checks whether the host's own distributed observer global estimate is consistent with local relative measurements.
	$\mathcal{T}_{i,l}$, $\mathcal{VT}_i$	Target trust for vehicle l and its smoothed evolution (vehicle trust).
	O_i, $O_i(j)$	Generalized trust/opinion vector of vehicle i over all platoon members, with entry $O_i(j) \in [0,1]$ the opinion toward vehicle j.
	$w_{il}^{(j)}(t)$, $w_{i0}^{(j)}(t)$	Trust-adaptive gain scaling factors (neighbor l and anchor node 0) used in the distributed observer.
Indices / sets	i	Host vehicle (computes trust and runs $\mathcal{DO}_i$).
	l	Target neighbor whose data is assessed (typically $l \in \mathcal{N}_i$).
	j	Target vehicle whose state is being estimated by $\mathcal{DO}_i^{(j)}$.
	t	Discrete-time index.
	0, N, $\mathcal{N}_i$	Anchor node (local-observer reference), number of vehicles, and neighbor set of vehicle i in the communication graph.

Similarly, the host vehicle $\hat{v}_0^{(i)}$ compares with its neighbors $\hat{v}_0^{(l)}$, the following mismatch score is:

$$v_{l,\mathrm{H}} = \begin{cases} \max\left(1 - \left|\dfrac{\hat{v}_0^{(l)} - \hat{v}_0^{(i)}}{\hat{v}_0^{(i)}}\right|, 0\right), & \text{if } \hat{v}_0^{(i)} > 0, \\ \max\left(1 - |\hat{v}_0^{(l)}|, 0\right), & \text{otherwise,} \end{cases} \tag{4.14}$$

The velocity mismatch is computed as a weighted average of two estimates:

$$\iota_{i,l}^{\text{velocity}} = ((1-\sigma)v_{l,\mathrm{L}} + \sigma v_{l,\mathrm{H}}) \tag{4.15}$$

where the weighted σ is selected based on the index position of the target vehicle l. If the target is

following the host vehicle i, then $\sigma \in (0, 0.3)$. If the target is leading, $\sigma \in (0.7, 1)$.

3.2.2 Distance consistency:

The host vehicle i calculates the distance with respect to the target l as :

$$d_{i,l} = \hat{s}_{\text{x},0}^{(l)} - \hat{s}_{\text{x},0}^{(i)} - L,$$

where L is the length of the vehicle. So the mismatch between the measured distance d from its sensors and the calculated data $d_{k,i}$ is

$$\iota_{i,l}^{\text{distance}} = \max\left(1 - \left|\frac{d_{i,l} - d}{d}\right|, 0\right). \tag{4.16}$$

Assumption 9. *When a vehicle is connected, it has access to basic information about its neighbors, including their type and length.*

3.2.3 Acceleration consistency:

The host vehicle can calculate the expected relative acceleration as

$$a_{\text{recv}}^{\text{rel}} = \hat{a}_0^{(l)} - \hat{a}_0^{(i)}, \qquad a_{\text{expect}}^{\text{rel}} = \frac{v_{\text{rel}}(t) - v_{\text{rel}}(t-n)}{n},$$

where $v_{\text{rel}} = \hat{v}_0^{(l)} - \hat{v}_0^{(i)}$ and n defines the averaging window used to smooth noise. To account for physical context, the mismatch is normalized by both distance and relative velocity:

$$\iota_{i,l}^{\text{accel}} = \max\left(1 - \frac{|a_{\text{recv}}^{\text{rel}} - a_{\text{expect}}^{\text{rel}}|}{a_{\text{th}} \cdot (1 + d_{i,l}/d_{\text{norm}})}, 0\right) \tag{4.17}$$

where:

- a_{th} is a nominal acceleration tolerance,
- $d_{i,l}$ is the inter-vehicle distance,
- d_{norm} are normalization constants reflecting typical spacing in the platoon.

This formulation tightens the trust threshold when vehicles are close or moving fast, where inconsistencies are more critical, and relaxes it when they are farther apart or nearly stationary. It provides smoother and dimensionally consistent trust updates while reducing false trust drops caused by minor sensor fluctuations.

3.2.4 Fusion and update rule:

We combine all three indicators into an integrity measure $\mathcal{LT}_{i,l}$ indicates the trust of local data of the host vehicle i in the target vehicle l at time t:

$$\mathcal{LT}_{i,l}(t) = \begin{cases} f(\iota_{i,l}^{\text{velocity}}, \iota_{i,l}^{\text{distance}}, \iota_{i,l}^{\text{accel}}) & \text{if } \delta_{i,l}(t) = 1 \\ (1-\lambda_h)\mathcal{LT}_{i,l}(t-1), & \text{otherwise} \end{cases} \tag{4.18}$$

where f is a fusion function that combines the three scores. The parameter λ_h defines the slow decay during temporary losses.

Remark 10. *Function f can be a weighted average or a minimum function, depending on the desired sensitivity to individual indicators. The decay λ_h can be varied based on how many consecutive packets are missed. This prevents a single missed packet from instantly reducing trust to zero, while still penalizing prolonged disconnection.*

3.3 Distributed trust

The Distributed Trust follows the same concept as the Local Trust, but is evaluated in the context of distributed estimation data. We denote $\mathcal{DT}_{i,l}$ represents how the host vehicle i trusts the distributed estimation received from target vehicle l, which is defined as

$$\mathcal{DT}_{i,l} = \begin{cases} \gamma_{i,l}^{\text{self}} \cdot \gamma_{i,l}^{\text{local}} \cdot \gamma_{i,l}^{\text{host}} & \text{if } \delta_{i,l}(t) = 1 \\ (1-\lambda_h)\mathcal{DT}_{i,l}(t-1), & \text{otherwise} \end{cases} \tag{4.19}$$

where $\gamma_{i,l}^{\text{host}}$ and $\gamma_{i,l}^{\text{local}}$ are applied to check if the global estimates from neighbor l are consistent with the host's global estimate and the host's local measurements, respectively; $\gamma_{i,l}^{\text{self}}$ checks whether the global estimates from the host's own distributed observer are consistent with the local measurements. They will be illustrated in the following. The resulting $\mathcal{DT}_{i,l}$ is later fused with the local trust to build the target/vehicle trust and ultimately contributes to the generalized trust (opinion) vector O_i in Subsection 3.5.

3.3.1 Consistency with host's global estimate:

To assess whether the global estimate from the target l is trustworthy, the host can compare it directly to its own global estimate. We use the Mahalanobis distance, which normalizes discrepancies based on covariance:

$$\rho_{i,l}^{(j)} = \left(\hat{x}_i^{(j)} - \hat{x}_l^{(j)}\right)^\top \Sigma_{\text{local}}^{-1} \left(\hat{x}_i^{(j)} - \hat{x}_l^{(j)}\right), \tag{4.20}$$

where Σ_{local} is the diagonal covariance matrix which captures variance and correlations between each state channel defined as

$$\Sigma_{\text{local}} = \text{diag}\left(\sigma_1^2, \sigma_2^2, \cdots, \sigma_n^2\right), \tag{4.21}$$

where n is the number of states in the vehicle, and σ_k^2 is the variance of discrepancies about the different states.

And then, add up these differences to get the total discrepancy score across the platoon as the following

$$D_{i,l} = \sum_{j=1}^{N} \rho_{i,l}^{(j)}. \tag{4.22}$$

A small $D_{i,l}$ means the global estimate from vehicle l is close to the host's, suggesting higher trustworthiness.

Based on the total discrepancy score across the platoon, the trust score can be converted to be

$$\gamma_{i,l}^{\text{host}} = \exp\left(-D_{i,l}\right). \tag{4.23}$$

where $\gamma_{i,l}^{\text{host}} \in (0, 1]$. A value near 1 means high trust (small discrepancy), while a value near 0 means low trust (large discrepancy).

3.3.2 Consistency with host's local measurement:

Host vehicle i has relative measurements to nearby vehicles (e.g., distance and relative velocity to a predecessor and a follower) and uses them to check if the distributed estimates received from target l are consistent with these measurements.

Let $y_{i,j}(t) \in \mathbb{R}^{m_{ij}}$ be the relative measurement of vehicle i to vehicle j (e.g., $y_{i,j}(t) = s_j(t) - s_i(t)$ for relative position).

The distributed estimate received from target l should satisfy, ideally:

$$H\big(\hat{x}_l^{(j)}(t) - \hat{x}_l^{(i)}(t)\big) \approx y_{i,j}(t).$$

where $H \in \mathbb{R}^{m_{ij} \times n}$ is the measurement matrix that extracts the relevant states (e.g., position) from the state vector.

Define the error between the predicted relative output and the local measurement as

$$\varepsilon_{i,l}^{(j)}(t) = H\big(\hat{x}_l^{(j)}(t) - \hat{x}_l^{(i)}(t)\big) - y_{i,j}(t), \tag{4.24}$$

Similar with the (4.20), by applying the covariance matrix Σ_{local}, we can get

$$E_{i,l}^{(j)}(t) = \big(\varepsilon_{i,l}^{(j)}(t)\big)^{\top} \Sigma_{\text{local}}^{-1} \varepsilon_{i,l}^{(j)}(t). \tag{4.25}$$

Then, the total consistency error can be get by summing up the errors over all measurable vehicles:

$$E_{i,l}(t) = \sum_{j \in \mathcal{N}_i} E_{i,l}^{(j)}(t). \tag{4.26}$$

A higher $E_{i,l}(t)$ suggests that the distributed estimate of target l contradicts with local sensor relative measurements.

Convert the error into a trust factor as

$$\gamma_{i,l}^{\text{local}}(t) = \exp\left(-E_{i,l}(t)\right), \tag{4.27}$$

where $\gamma_{i,l}^{\text{local}}(t) \in (0, 1]$, with lower values indicating poor consistency.

3.3.3 Self-consistency with host's local measurement:

The host also checks whether its *own* global estimates produced by the distributed observer are consistent with its local relative measurements. Specifically, the host's global estimate should satisfy, ideally,

$$H\big(\hat{x}_i^{(j)}(t) - \hat{x}_i^{(i)}(t)\big) \approx y_{i,j}(t), \quad j \in \mathcal{N}_i.$$

Define the self-consistency error

$$\varepsilon_{i,\text{self}}^{(j)}(t) = H\big(\hat{x}_i^{(j)}(t) - \hat{x}_i^{(i)}(t)\big) - y_{i,j}(t), \tag{4.28}$$

and the corresponding aggregate score

$$E_{i,\text{self}}(t) = \sum_{j \in \mathcal{N}_i} \big(\varepsilon_{i,\text{self}}^{(j)}(t)\big)^\top \Sigma_{\text{local}}^{-1} \varepsilon_{i,\text{self}}^{(j)}(t). \tag{4.29}$$

Then the self-consistency factor is defined as

$$\gamma_{i,l}^{\text{self}}(t) = \exp\left(-E_{i,\text{self}}(t)\right), \tag{4.30}$$

which is shared across all targets l (it depends only on the host's internal consistency at time t).

Remark 11. *We can estimated covariance Σ_{host} and Σ_{local} by collecting the differences in vehicle i from a window of recent received data from l in normal condition. This avoids the need for each node to transmit its own covariance.*

3.4 Target trust and temporal evolution

The target trust combines local and distributed trust into a single scalar indicator for target l:

$$\mathcal{T}_{i,l}(t) = \mathcal{LT}_{i,l} \cdot \mathcal{DT}_{i,l}. \tag{4.31}$$

$\mathcal{T}_{i,l}(t)$ indicates the quality of target l data at the time t , that will facilitate the decision-making process for the host vehicle.

Because this value can vary abruptly, a temporal-evolution mechanism is introduced to obtain a smoother, interpretable estimate.

3.4.1 Discretization into trust quality:

We define a five-level trust quality among $q = 5$ categories: *Unreliable*, *Poor*, *Acceptable*, *Good*, and *Excellent*. When the host vehicle i computes a trust value $\mathcal{T}_{i,l}(t) \in [0, 1]$ for a neighboring vehicle l, the result is discretized into a one-hot vector $r_{i,l}(t) \in \mathbb{R}^q$. For example, if $\mathcal{T}_{i,l}(t) = 0.72$, it falls into the "Good" category (4th level), so $r_{i,l}(t) = [0, 0, 0, 1, 0]^\top$.

3.4.2 Accumulated trust history:

Over time, the accumulated trust vector $R_{i,l}(t)$ for target vehicle l is updated using a weighted aggregation of past interactions:

$$R_{i,l}(t+1) = (1 - \mathcal{T}_{i,l}(t) \cdot \beta) \cdot R_{i,l}(t) + r_{i,l}(t), \tag{4.32}$$

where $\beta \in [0, 1]$ as a tunable weight controls how quickly past experiences decay.

Remark 12. *The choice of β is crucial for effectively capturing the dynamics of trust over time. A higher β places more emphasis on recent observations, allowing the trust score to adapt quickly to changes in behavior. Conversely, a lower β gives more weight to historical data, resulting in a smoother trust evolution that is less sensitive to transient fluctuations.*

3.4.3 Normalized trust distribution:

Finally, at the current step t (in the following, we omit t for simplifying), a normalized trust distribution vector $S_{i,l}(k)$ is computed by incorporating an a priori distribution α and a confidence parameter C:

$$S_{i,l}(k) = \frac{R_{i,l}(k) + C \cdot \alpha(k)}{C + \sum_{j=1}^{q} R_{i,l}(j)}, \tag{4.33}$$

which provides a probabilistic interpretation of the trustworthiness of the target vehicle l, blending historical observations with prior beliefs to produce a robust and adaptive trust estimate.

3.4.4 Expected trust level:

The target vehicle trust score $\mathcal{VT}_{i,l}$ is then calculated as:

$$\mathcal{VT}_{i,l} = \sum_{j=1}^{q} \frac{j-1}{q-1} \cdot S_{i,l}(j). \tag{4.34}$$

While $\mathcal{VT}_{i,l}$ provides a stable, pairwise evaluation between directly connected vehicles, a more global view is required for the observer to weigh all available information. This motivates the definition of a generalized trust vector, introduced next.

3.5 Generalized trust vector

The target trust value $VT_{i,l}$ obtained in the previous subsection quantifies how much the host vehicle i trusts a specific neighbor l. However, for the distributed observer to operate reliably, each vehicle must maintain an opinion about all other vehicles in the platoon, including those beyond its direct communication range. To achieve this, we define a generalized trust vector O_i that aggregates and propagates local trust information in a robust one-hop manner. For vehicle i, the vector is defined as

$$O_i = [O_i(1), O_i(2), \ldots, O_i(N)], \tag{4.35}$$

where O_i represents the current opinion of vehicle i regarding all platoon members, while $O_i(j) \in [0, 1]$ specifies vehicle i's current trust opinion toward vehicle j.

1) Self-Trust. Each vehicle assumes full confidence in its own state:

$$\mathcal{O}_i(i) = 1, \tag{4.36}$$

2) Direct-Neighbor Trust. For every neighbor $j \in \mathcal{N}_i$ with which vehicle i exchanges data directly, the trust opinion is set as :

$$\mathcal{O}_i(j) = \mathcal{VT}_{i,j}, \tag{4.37}$$

where $\mathcal{VT}_{i,j}$ is the smoothed target-trust value derived in the previous subsection.

3) One-Hop Trust Propagation. For any non-neighbor vehicle $j \notin \mathcal{N}_i \cup \{i\}$, the host vehicle i estimates $O_i(j)$ using only information from its direct neighbors $\mathcal{N}_i$.

$$S_{i,j} = \Big\{ \mathcal{O}_k(j) \mid k \in \mathcal{N}_i,\ \mathcal{VT}_{i,k} > \theta_{\min},\ \delta_{i,k}(t) = 1 \Big\} \tag{4.38}$$

Here, $\theta_{\min}$ is the minimum acceptable trust threshold,

Each valid neighbor k is associated with a *credibility weight*

$$\psi_{i,k} = \frac{\mathcal{VT}_{i,k}}{\sum_{p \in S_{i,j}} \mathcal{VT}_{i,p}} \tag{4.39}$$

If the credible set $S_{i,j}$ is non-empty, the propagated opinion is computed using a *weighted median* operator:

$$\mathcal{O}_i(j) = \mathrm{wMed}\big(\{\mathcal{O}_k(j)\}_{k \in S_{i,j}}, \{\psi_{i,k}\}_{k \in S_{i,j}}\big), \tag{4.40}$$

which limits the influence of outliers or manipulated values.

4) Index Distance-Based Fallback. If the credible set $S_{i,j}$ is empty, vehicle i resorts to a *host-centric distance weighting* of all its neighbors:

$$\mathcal{O}_i(j) = \frac{\sum_{k \in \mathcal{N}_i} g_{i,k}\, \mathcal{O}_k(j)}{\sum_{k \in \mathcal{N}_i} g_{i,k}}, \qquad g_{i,k} = \frac{1}{1 + |i - k|}. \tag{4.41}$$

where $|i - k|$ is the index distance between vehicles i and k. The closer a neighbor k is to host i, the larger its influence $g_{i,k}$. This fallback guarantees that the trust vector remains fully populated even when no verified propagated opinion exists.

6) Final Expression. Combining all cases, the complete definition of the generalized trust vector is

$$\mathcal{O}_i(j) = \begin{cases} 1, & j = i, \\ \mathcal{VT}_{i,j}, & j \in \mathcal{N}_i, \\ \mathrm{wMed}\big(\{\mathcal{O}_k(j)\}, \{\psi_{i,k}\}\big), & S_{i,j} \neq \varnothing, \\ \dfrac{\sum_{k \in \mathcal{N}_i} g_{i,k}\, \mathcal{O}_k(j)}{\sum_{k \in \mathcal{N}_i} g_{i,k}}, & S_{i,j} = \varnothing. \end{cases} \tag{4.42}$$

This generalized representation allows each vehicle to maintain a resilient, full-platoon trust profile

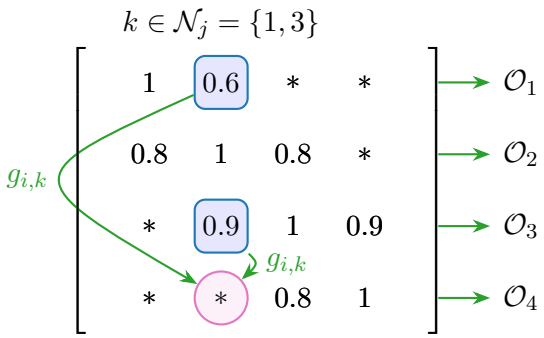

Vehicle $i = 4$ doesn't have the trust for the vehicle $j = 2$

Figure 4.3: Weight based distance for $\mathcal{O}_{i,j}^{\text{dis}}$.

that supports the adaptive observer weight design described in the following section.

4 Weight Design for observer based on the trust

The trust framework provides each vehicle with a set of quantified opinions $\mathcal{O}_{i,j}$ representing the reliability of information from other vehicles. This section shows how these values are used to define adaptive observer weights $w_{il}^{j}(t)$ and establishes conditions for stability of the estimation error dynamics.

4.1 Weight based on the trust

Based on the virtual communication graph $\bar{\mathcal{G}}^{(j)}$ as that includes the local observer node 0, each vehicle i identifies its legitimate neighbors at time t:

$$\begin{aligned}\mathcal{LN}_i^{(j)}(t) = &\Big\{ l \in N_i \mid O_i(l,t) \geq \theta_{\min} \Big\} \\ &\cup \Big(\{0\} \text{ if } \mathcal{LT}_{i,j}(t) \geq \theta_{\min} \Big)\end{aligned} \tag{4.43}$$

To limit the influence of any single neighbor, a normalization factor is introduced.

$$n_{il}^{(j)}(t) = \max\Big\{\kappa, \Big|\mathcal{LN}_i^{(j)}(t)\Big| + 1\Big\} \geq 1, \forall l \in \mathcal{LN}_i^{(j)} \tag{4.44}$$

where $\kappa > 0$ is the parameter to limit the maximum influence from the neighbors of ith vehicle. Then, the observer's weight gain can be chosen as

$$w_{il}^{(j)}(t) = \begin{cases} \dfrac{1}{n_{il}^{(j)}(t)}, & l \in \mathcal{LN}_i^{(j)}(t) \\ 0, & \text{otherwise.} \end{cases} \tag{4.45}$$

According to the weight gain, the communication graph will be switched depending on the time. The following assumption is required.

Assumption 10 (*Jointly connected graph). There exists a scalar constant $T > 0$ such that for all $t \geq 0$, the union graph $\cup_{[t,t+T]}\bar{\mathcal{G}}^{(j)}(t)$ contains a spanning tree.*

Assumption 10 means that for all $t \geq 0$, every node $i \in \mathcal{V}$ is reachable from node "0 in the union graph $\cup_{[t,t+T]}\bar{\mathcal{G}}^{(j)}(t)$. This ensures the connectivity of the proposed switching communication topology, which is required for our observer design method.

4.2 Stability of the error

In this section, we study the stability (ISS) of the estimation error dynamics induced by the observer (4.5). Fix a target vehicle $j \in \mathcal{V}$ and define the local-observer and distributed-observer errors

$$e_0^{(j)}(t) \triangleq \hat{x}_0^{(j)}(t) - x_j(t), \qquad e_i^{(j)}(t) \triangleq \hat{x}_i^{(j)}(t) - x_j(t),\ i \in \mathcal{V}. \tag{4.46}$$

Stack the distributed errors as

$$e_{\mathrm{DO}}^{(j)}(t) \triangleq \operatorname{col}\Big(e_1^{(j)}(t), \ldots, e_N^{(j)}(t)\Big) \in \mathbb{R}^{Nn_x}. \tag{4.47}$$

Using (4.4) and (4.5), the error system can be written as

$$e_0^{(j)}(t+1) = (A_{\mathrm{b}} - F_j C_{\mathrm{b}})\, e_0^{(j)}(t) + d_0^{(j)}(t), \tag{4.48}$$

$$\begin{aligned} e_{\mathrm{DO}}^{(j)}(t+1) = &\left(w_0^{(j)}(t) \otimes A_{\mathrm{b}}\right) e_0^{(j)}(t) \\ &+ \left((I_N - \bar{\mathcal{L}}^{(j)}(t)) \otimes A_{\mathrm{b}}\right) e_{\mathrm{DO}}^{(j)}(t) + d_{\mathrm{DO}}^{(j)}(t), \end{aligned} \tag{4.49}$$

where $w_0^{(j)}(t) = \mathrm{col}\left(w_{10}^{(j)}(t), \ldots, w_{N0}^{(j)}(t)\right) \in \mathbb{R}^N$ collects the weights from the (virtual) local-observer node 0 to all vehicles. The virtual weighted Laplacian $\bar{\mathcal{L}}^{(j)}(t) = [\bar{\ell}_{il}^{(j)}(t)]_{i,l\in\mathcal{V}} \in \mathbb{R}^{N\times N}$ is defined by

$$\bar{\ell}_{il}^{(j)}(t) = \begin{cases} -w_{il}^{(j)}(t), & l \neq i, \\ w_{i0}^{(j)}(t) + \sum\limits_{p\in\mathcal{N}_i} w_{ip}^{(j)}(t), & l = i, \end{cases} \tag{4.50}$$

so that $(I_N - \bar{\mathcal{L}}^{(j)}(t))$ has diagonal entries $1 - w_{i0}^{(j)}(t) - \sum_{p\in\mathcal{N}_i} w_{ip}^{(j)}(t)$, off-diagonal entries $w_{il}^{(j)}(t)$, and its ith row-sum equals $1 - w_{i0}^{(j)}(t) \leq 1$. The disturbance terms collect model mismatch, input mismatch, and measurement noise, and can be written as

$$\begin{aligned} d_0^{(j)}(t) &\triangleq F_j(y_j(t) - C_{\mathrm{b}} x_j(t)) - \Delta_j(t), \\ d_{\mathrm{DO}}^{(j)}(t) &\triangleq (1_N \otimes B_{\mathrm{b}})\left(\hat{u}_j(t) - u_j(t)\right) - \left(1_N \otimes \Delta_j(t)\right), \end{aligned} \tag{4.51}$$

where $1_N \in \mathbb{R}^N$ denotes the all-ones vector. Before stating the main theorem of this section, we need to make the following assumption which is necessary to develop an ISS bound on the estimation errors.

Assumption 11. *The disturbance vectors $d_0^{(j)}(t)$ and $d_{\mathrm{DO}}^{(j)}(t)$ are bounded. That is, there exist $\bar{d}_0 \geq 0$ and $\bar{d}_{\mathrm{DO}} \geq 0$ such that $\|d_0^{(j)}(t)\| \leq \bar{d}_0$ and $\|d_{\mathrm{DO}}^{(j)}(t)\| \leq \bar{d}_{\mathrm{DO}}$, for all $t \geq 0$.*

Now, we are ready to state the following theorem, which provides the main sufficient conditions ensuring the stabilization of the error system (4.48)–(4.49).

Theorem 4. *Consider the error dynamics (4.48)–(4.49) for a fixed target vehicle $j \in \mathcal{V}$ and assume that Assumption 11 holds. Suppose that the following conditions hold:*

1. *(Local observer.) There exists F_j such that the matrix $A_{\ell,j} \triangleq A_b - F_j C_b$ is Schur stable.*
2. *(Nonnegative and normalized weights.) For all $i \in \mathcal{V}$ and all $t \geq 0$, the weights satisfy $w_{i0}^{(j)}(t) \geq 0$, $w_{il}^{(j)}(t) \geq 0$, and*
$$w_{i0}^{(j)}(t) + \sum_{l\in\mathcal{N}_i} w_{il}^{(j)}(t) \leq 1. \tag{4.52}$$
3. *(Uniform contraction of the switched distributed layer.) There exist $\alpha \in (0,1)$ and an induced matrix norm $\|\cdot\|_*$ such that, for all $t \geq 0$,*
$$\left\|(I_N - \bar{\mathcal{L}}^{(j)}(t)) \otimes A_b\right\|_* \leq \alpha. \tag{4.53}$$

Then, the estimation error (4.48)–(4.49) is ISS with respect to $(d_0^{(j)}, d_{\mathrm{DO}}^{(j)})$. *In particular, there exist constants* $c_0, c_1 > 0$ *and* $\lambda \in (0,1)$ *such that, for all* $t \geq 0$,

$$\|e_0^{(j)}(t)\| \leq c_0\, \lambda^t \|e_0^{(j)}(0)\| + c_0\, \bar{d}_0, \tag{4.54}$$

$$\|e_{\mathrm{DO}}^{(j)}(t)\| \leq c_1\, \lambda^t \|e_{\mathrm{DO}}^{(j)}(0)\| + c_1\Big(\|e_0^{(j)}(0)\| + \bar{d}_0 + \bar{d}_{\mathrm{DO}}\Big). \tag{4.55}$$

Proof. Fix $j \in \mathcal{V}$ and define $A_{\ell,j} \triangleq A_{\mathrm{b}} - F_j C_{\mathrm{b}}$.

Step 1 (local observer loop). Since $A_{\ell,j}$ is Schur by Condition (1), there exist constants $c_{\ell,j} > 0$ and $\lambda_{\ell,j} \in (0,1)$ such that $\|A_{\ell,j}^t\|_* \leq c_{\ell,j}\lambda_{\ell,j}^t$ for all $t \geq 0$. Unrolling (4.48) yields

$$e_0^{(j)}(t) = A_{\ell,j}^t e_0^{(j)}(0) + \sum_{k=0}^{t-1} A_{\ell,j}^{t-1-k} d_0^{(j)}(k),$$

and therefore, using Assumption 11,

$$\|e_0^{(j)}(t)\| \leq c_{\ell,j}\lambda_{\ell,j}^t \|e_0^{(j)}(0)\| + \frac{c_{\ell,j}}{1-\lambda_{\ell,j}}\, \bar{d}_0.$$

Step 2 (distributed observer loop). Define

$$A_{\mathrm{DO}}^{(j)}(t) \triangleq (I_N - \bar{\mathcal{L}}^{(j)}(t)) \otimes A_{\mathrm{b}}, \qquad B_0^{(j)}(t) \triangleq w_0^{(j)}(t) \otimes A_{\mathrm{b}},$$

so that (4.49) becomes

$$e_{\mathrm{DO}}^{(j)}(t+1) = A_{\mathrm{DO}}^{(j)}(t) e_{\mathrm{DO}}^{(j)}(t) + B_0^{(j)}(t) e_0^{(j)}(t) + d_{\mathrm{DO}}^{(j)}(t).$$

By Condition (2), each entry of $w_0^{(j)}(t)$ lies in $[0,1]$, so $w_0^{(j)}(t)$ ranges in a compact set. Since the mapping $w \mapsto w \otimes A_{\mathrm{b}}$ is continuous, there exists $\bar{B}_0 > 0$ such that $\|B_0^{(j)}(t)\|_* \leq \bar{B}_0$ for all $t \geq 0$. Next, define the state transition matrices

$$\Phi(t,k) \triangleq \begin{cases} I, & t = k, \\ A_{\mathrm{DO}}^{(j)}(t-1)\cdots A_{\mathrm{DO}}^{(j)}(k), & t > k, \end{cases}$$

for which Condition (3) implies $\|\Phi(t,k)\|_* \leq \alpha^{t-k}$ for all $t \geq k$. Unrolling the recursion gives

$$e_{\mathrm{DO}}^{(j)}(t) = \Phi(t,0) e_{\mathrm{DO}}^{(j)}(0) + \sum_{k=0}^{t-1} \Phi(t,k+1)\Big(B_0^{(j)}(k) e_0^{(j)}(k) + d_{\mathrm{DO}}^{(j)}(k)\Big),$$

so that, using Assumption 11,

$$\|e_{\mathrm{DO}}^{(j)}(t)\| \leq \alpha^t \|e_{\mathrm{DO}}^{(j)}(0)\| + \sum_{k=0}^{t-1} \alpha^{t-1-k}\Big(\bar{B}_0\, \|e_0^{(j)}(k)\| + \bar{d}_{\mathrm{DO}}\Big).$$

Define $\lambda \triangleq \max\{\alpha, \lambda_{\ell,j}\} \in (0,1)$. From Step 1, $\|e_0^{(j)}(k)\| \leq c_{\ell,j}\lambda_{\ell,j}^k \|e_0^{(j)}(0)\| + \frac{c_{\ell,j}}{1-\lambda_{\ell,j}}\bar{d}_0$ for all $k \geq 0$,

hence

$$\sum_{k=0}^{t-1} \alpha^{t-1-k} \|e_0^{(j)}(k)\| \le c_{\ell,j} \|e_0^{(j)}(0)\| \sum_{k=0}^{t-1} \alpha^{t-1-k} \lambda_{\ell,j}^k + \frac{c_{\ell,j}}{1-\lambda_{\ell,j}} \bar{d}_0 \sum_{k=0}^{t-1} \alpha^{t-1-k}.$$

Using $\alpha^{t-1-k}\lambda_{\ell,j}^k \le \lambda^{t-1}$ and the identity $\sum_{t=1}^{\infty} t\lambda^{t-1} = (1-\lambda)^{-2}$, we obtain

$$\sum_{k=0}^{t-1} \alpha^{t-1-k} \lambda_{\ell,j}^k \le \frac{1}{(1-\lambda)^2}, \qquad \sum_{k=0}^{t-1} \alpha^{t-1-k} \le \frac{1}{1-\alpha}.$$

Combining these bounds yields an explicit inequality of the stated ISS form. Absorbing the resulting constants into (c_0, c_1) completes the proof. □

Remark 13 (Checking Condition (4.53)). *Condition (4.53) is a uniform contraction requirement on the switched distributed layer. A simple sufficient check can be obtained with the induced ∞-norm: since $I_N - \bar{\mathcal{L}}^{(j)}(t)$ is nonnegative and its ith row-sum equals $1 - w_{i0}^{(j)}(t)$, one has*

$$\|I_N - \bar{\mathcal{L}}^{(j)}(t)\|_\infty = \max_{i\in\mathcal{V}} \left(1 - w_{i0}^{(j)}(t)\right), \qquad \|(I_N - \bar{\mathcal{L}}^{(j)}(t)) \otimes A_b\|_\infty \le \|I_N - \bar{\mathcal{L}}^{(j)}(t)\|_\infty \, \|A_b\|_\infty.$$

Thus, if there exists $\underline{w}_0 > 0$ such that $w_{i0}^{(j)}(t) \ge \underline{w}_0$ for all i and all t, and $(1-\underline{w}_0)\|A_b\|_\infty < 1$, then (4.53) holds with $\alpha = (1-\underline{w}_0)\|A_b\|_\infty$.

Remark 14. *(Limitations of the Stability Guarantees). The ISS guarantees of Theorem 4 rely critically on (i) bounded influence of each neighbor ensured by trust-based weight normalization (Condition 4.52), and (ii) uniform contraction of the switched distributed layer (Condition (4.53)), which in practice requires persistent anchoring (directly or indirectly) through the local observer node.*

These conditions may be violated under the following scenarios:

- *Stealthy Byzantine attacks, where adversarial vehicles generate physically consistent but biased data, maintaining high trust and inducing convergence to an incorrect equilibrium.*
- *Colluding attacks, in which multiple compromised vehicles mutually reinforce false estimates, undermining trust propagation mechanisms.*
- *Persistent DoS or network partition attacks, which permanently disconnect vehicles from anchoring local observers, rendering absolute state reconstruction impossible.*

These scenarios correspond to fundamental identifiability limits of distributed estimation and cannot be addressed without additional assumptions such as cryptographic authentication, majority-honest agents, or infrastructure-based anchoring.

5 Simulation Results

This section evaluates the performance of the proposed trust-aware distributed observer for a connected vehicle platoon under various cyberattack scenarios. The main objectives of the simulation are to:

- Assess the observer resilience to falsified and delayed information.

- Analyze the evolution of trust scores for detecting and isolating malicious nodes.
- Quantify estimation performance degradation under different types of attacks.

5.1 Simulation setup

The simulation considers a platoon of four fully connected vehicles, where each vehicle exchanges information with all others through vehicle-to-vehicle (V2V) communication. All vehicles share similar nominal parameters, with small modeling variations treated as uncertainties.The proposed trust-aware distributed observer runs onboard each vehicle to estimate states and evaluate the reliability of shared data. Table 4.2 summarizes the main parameters used for the vehicle model and the trust framework.

Table 4.2: Main simulation parameters.

Parameter	Value	Description
T_s	0.1 s	Sampling time
τ	1.5 s	Engine lag constant
w_v, w_d, w_a	1.2, 2.0, 0.9	Local trust weights
$\beta_{\text{trust}}, C, k$	0.5, 0.2, 5	Trust decay and regularization
d_{norm}	15 m	Normalization constants
$\theta_{\min}$	0.5	Minimum trust threshold
N	4	Number of vehicles

5.2 Attack scenarios

To assess the robustness of the vehicle platooning system, six attack cases are defined, as summarized in Table 4.3. All attacks are launched by the leader vehicle and broadcast to every follower in the platoon. Each attack is active during the interval $[10, 15]$ s. For reproducibility , the observer is evaluated under the assumption that the follower controllers are known, thereby isolating and emphasizing the observer capability to detect and mitigate malicious data. The parameter p denotes the probability of the attack or fault occurrence.

Table 4.3: Six attack cases in the scenario.

Case	Type	Target	Parameters
1	Bias	Position	bias = -5 m
2	Faulty	Position	int. = 10, $p = 0.3$
3	Bias	Velocity	bias = -2 m/s
4	Faulty	Velocity	int. = 2.5, $p = 0.3$
5	Faulty	Acceleration	int. = 1.0, $p = 0.3$
6	Drop	All	$p_{\text{drop}} = 0.5$

5.3 Results

Figure 4.4 presents a heatmap of the normalized impact scores for each vehicle across all six attack cases. The normalized impact score is obtained by dividing the raw combined error by the maximum observed

combined error across all vehicles and attack scenarios. This normalization enables a clear comparison of the relative severity of each attack on individual vehicles.

To quantitatively assess the influence of different cyberattack scenarios, both raw combined errors and normalized impact scores were analyzed. The raw combined error provides a direct measure of deviation in distance, velocity, and acceleration estimation, whereas the normalized impact score offers a more balanced indicator of overall system degradation relative to nominal operating performance.

Across all cases, the DoS attack (Case 6) exhibited the highest normalized impact score (0.872), confirming it as the most severe attack scenario. This high value reflects a significant degradation in estimation accuracy and control performance during the 5-second attack window. In contrast, the velocity bias attack (Case 3) with a bias of -2 m/s produced the lowest normalized impact score (0.240), indicating minimal influence on system stability and tracking capability.

From the vehicle perspective, V4 was identified as the most affected vehicle, reaching the maximum normalized impact score (0.872), whereas vehicle V2 demonstrated the highest resilience, with the lowest average impact score (0.362). This suggests that V4 local dynamics or communication dependencies make it more sensitive to external disruptions, while V2 maintains more stable performance under varying attack conditions.

Overall, the relatively low mean normalized impact scores across all cases indicate that the proposed trust-aware distributed observer effectively mitigates diverse types of cyberattacks and maintains accurate state estimation for each vehicle in the platoon.

In Figure 4.5, the trust score evolution for the DoS attack (Case 6) is illustrated. During the attack period $[10, 15]$ s, these 3 vehicles (V2, V3, V4) exhibit a noticeable drop in trust values below the threshold of 0.5, indicating successful detection of the communication disruption. Once the attack ceases, the trust scores gradually recover, demonstrating the system ability to restore confidence and resume normal operation. This behavior confirms the effectiveness of the proposed trust mechanism in identifying and isolating malicious data in real time.

While the heatmap in Figure 4.4 provides an aggregate view across scenarios, the following figures offer a time-domain perspective that is more informative for control: they show how quickly the observer rejects corrupted information and the magnitude of the resulting transient estimation errors during the attack window.

Figure 4.6 reports the estimation errors in longitudinal position, velocity, and acceleration for the four-vehicle platoon. Across all vehicles, the errors remain centered around zero and bounded over the full horizon, with the largest excursions occurring during the attack interval $[10, 15]$ s. In particular, the velocity channel exhibits short spikes (consistent with packet drops or corrupted updates), but these transients do not persist: once the trust mechanism down-weights unreliable links, the errors return to their nominal range. The acceleration estimates remain well-behaved after the initial transient, indicating that the observer/controller interface is sufficiently smooth for closed-loop operation.

Figure 4.7 complements the error plots by showing representative state trajectories over time. The platoon reaches a common cruising speed and the acceleration settles close to zero after a short transient, indicating convergence to a steady formation. Moreover, the lateral position and heading remain bounded, suggesting that the disturbances introduced by the considered attacks do not induce unstable motion. Together, Figures 4.6–4.7 show that the trust-aware distributed observer provides bounded, quickly

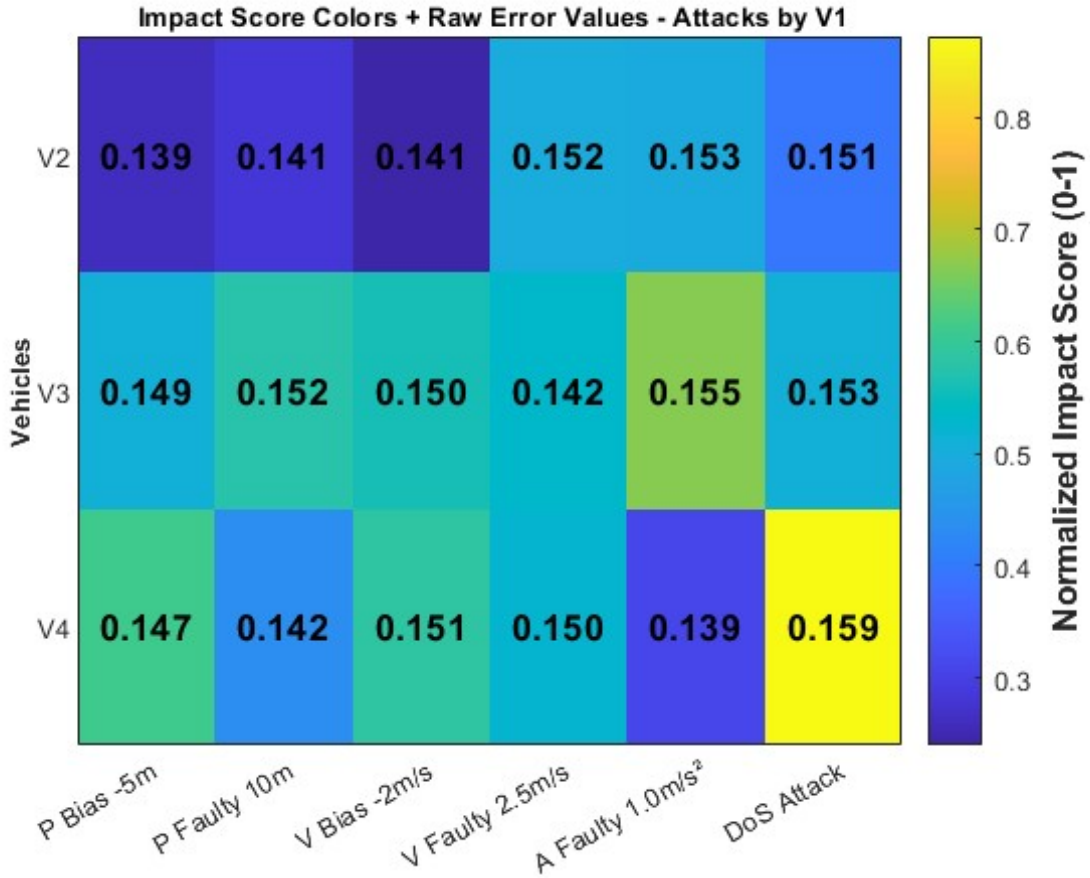

Figure 4.4: Heatmap of normalized impact scores for all vehicles and attack cases.

recovering estimates that can be safely used by the platoon controller in the next subsection.

5.4 Distributed State Estimation for Platoon Control

This subsection closes the loop by using the proposed trust-aware observers in a longitudinal platoon controller. After evaluating estimation accuracy and trust evolution under the attack cases in Section 5.2, we now study how these estimates translate into *closed-loop* safety and performance. The controller follows a constant time headway spacing (CTHS) policy and combines (i) a purely local car-following controller (IDM) and (ii) a cooperative controller (CACC) that exploits trusted V2V information. The trust/opinion mechanism in Section 3 is used to modulate the contribution of the cooperative layer so that the platoon can gracefully degrade to local control when communication becomes unreliable.

5.4.1 Notation

We denote the longitudinal position, velocity, and acceleration of vehicle i by s_i, v_i, and a_i. The observers provide the following state estimates used by the controllers:

- **Local estimate ($\mathcal{LO}_i$):** $\hat{x}_0^{(i)} = [\hat{s}_0^{(i)}, \hat{v}_0^{(i)}, \hat{a}_0^{(i)}]^\top$.

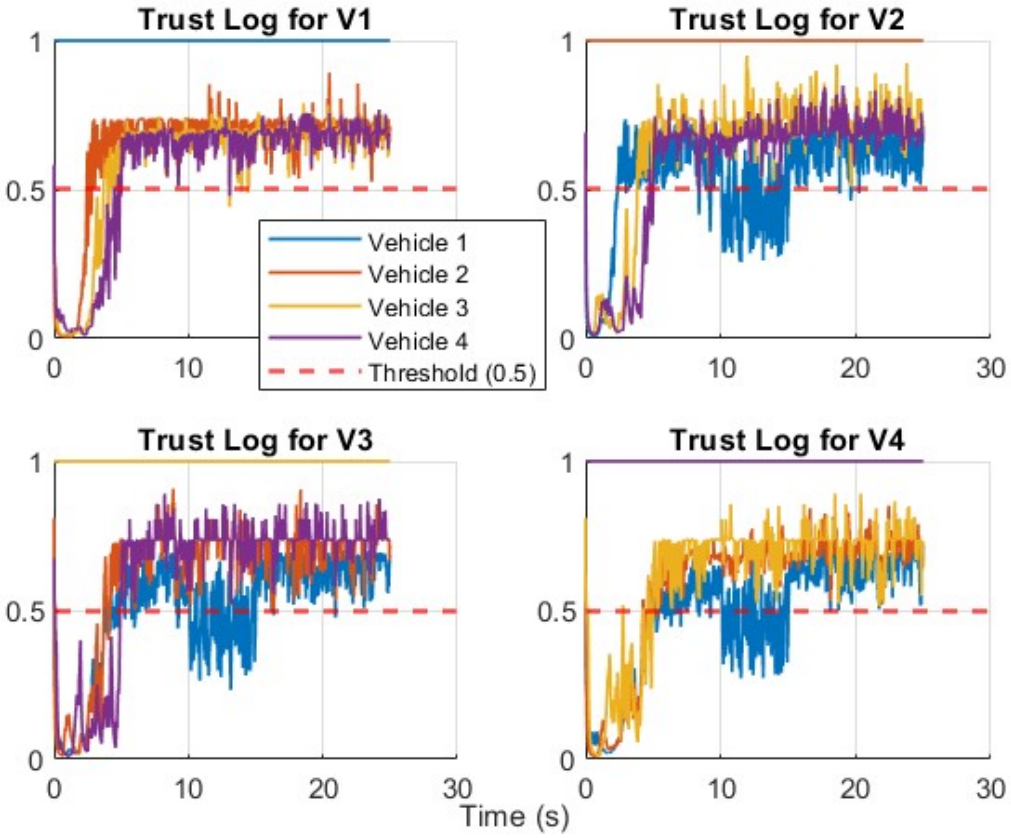

Figure 4.5: Trust score evolution during DoS attack (***Case 6***).

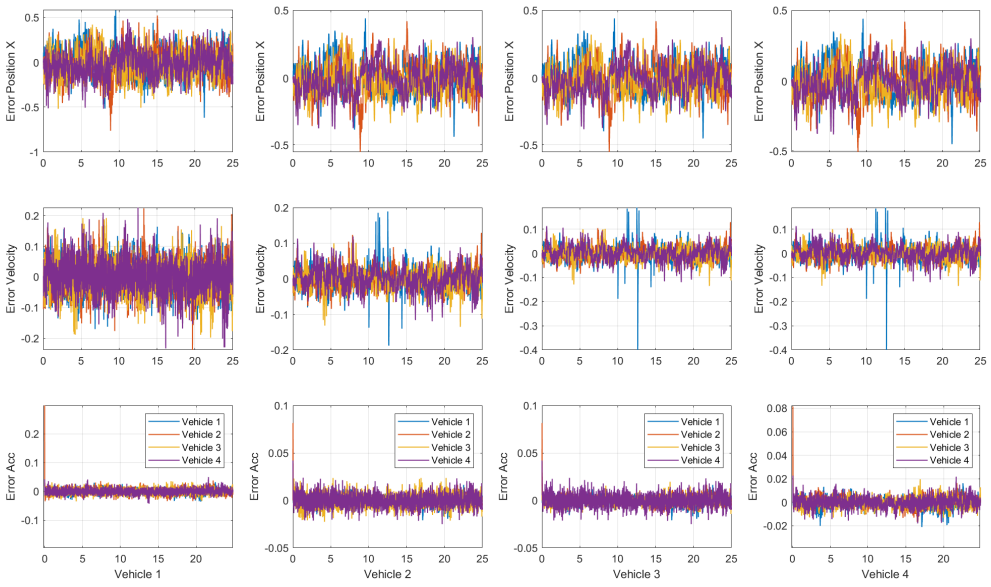

Figure 4.6: State-estimation errors for all vehicles.

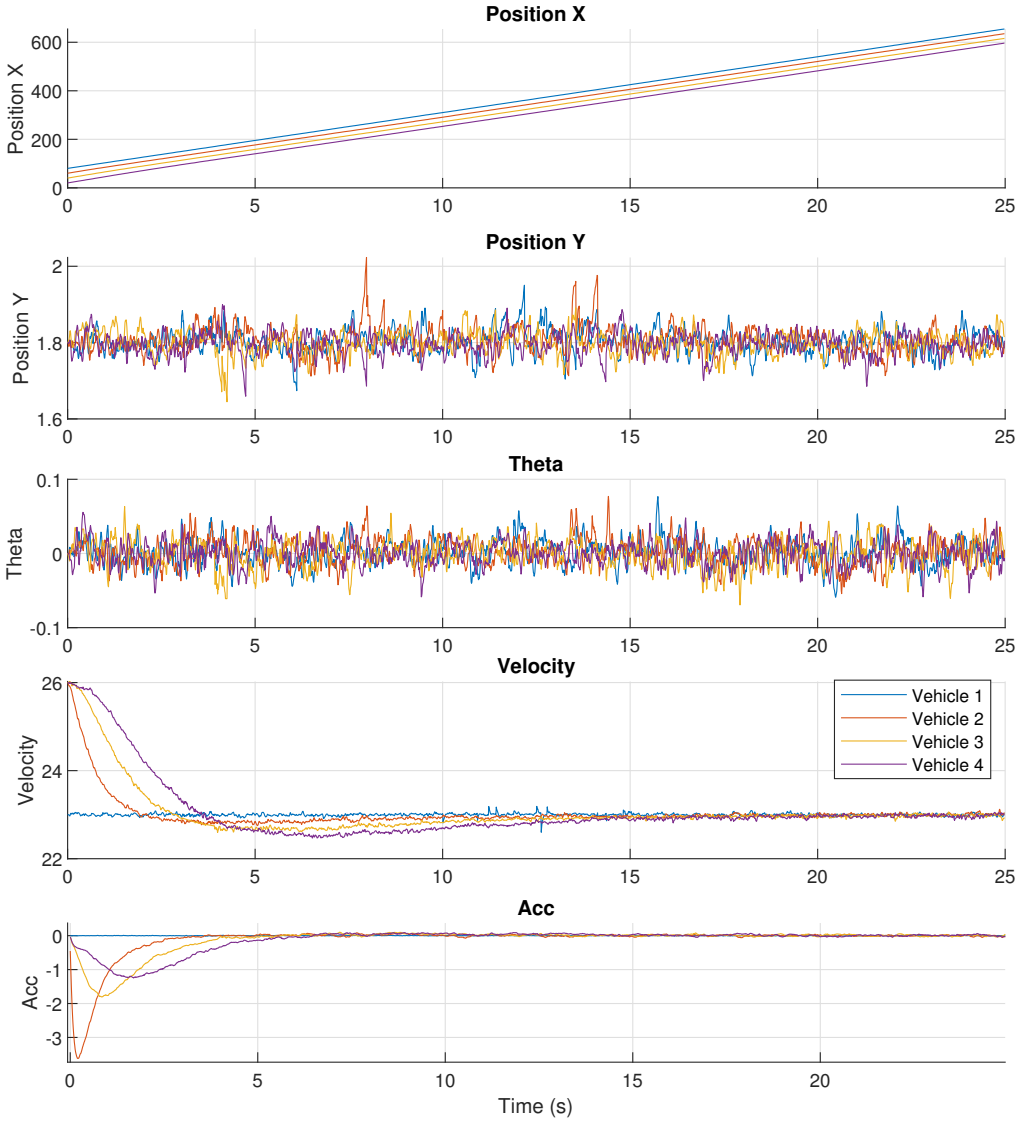

Figure 4.7: State trajectories of the four-vehicle platoon (vehicle 4 is the tail vehicle).

- **Distributed estimate ($\mathcal{DO}_i^{(j)}$):** $\hat{x}_i^{(j)} = [\hat{s}_i^{(j)}, \hat{v}_i^{(j)}, \hat{a}_i^{(j)}]^\top$, i.e., the state of vehicle j reconstructed onboard vehicle i.

Under the CTHS policy, the desired bumper-to-bumper spacing to the immediate predecessor is $d + h\,\hat{v}_0^{(i)}$, where d is the standstill distance and h is the time headway.

5.4.2 Inner/Local Controller: Intelligent Driver Model (IDM)

The IDM is used as an inner controller for local longitudinal control. It computes the desired acceleration using ego-state estimates from the local observer $\mathcal{LO}_i$ together with relative measurements to the

predecessor obtained from onboard sensing. The IDM acceleration for vehicle i is given by:

$$a_{\text{IDM},i} = a_{\max}\left[1 - \left(\frac{\hat{v}_0^{(i)}}{v_0}\right)^{\delta} - \left(\frac{s^*(\hat{v}_0^{(i)}, \Delta v_{i-1,i})}{s_{i-1,i}}\right)^2\right], \tag{4.56}$$

where:

- $\hat{v}_0^{(i)}$ is the estimated velocity of vehicle i from $\mathcal{LO}_i$.
- $s_{i-1,i} = s_{i-1} - s_i - L$ is the (measured) distance to the predecessor, with L the vehicle length.
- $\Delta v_{i-1,i}$ is the (measured) relative velocity to the predecessor.
- $s^*(\hat{v}_0^{(i)}, \Delta v_{i-1,i}) = s_0 + T\hat{v}_0^{(i)} + \frac{\hat{v}_0^{(i)}\Delta v_{i-1,i}}{2\sqrt{a_{\max} b_{\text{comf}}}}$ is the desired minimum gap.
- $a_{\max}$, b_{comf}, δ, v_0, s_0, and T are model parameters: maximum acceleration, comfortable deceleration, free-flow exponent, desired velocity, minimum gap, and time headway, respectively.

This inner loop remains fully local (no reliance on V2V) and therefore provides a natural fallback mode during communication degradation or when upstream information is deemed untrustworthy.

5.4.3 Cooperative Controller: Cooperative Adaptive Cruise Control (CACC)

The CACC layer enhances coordination by leveraging information from multiple preceding vehicles via the distributed observer $\mathcal{DO}_i$. For vehicle i, the CACC control input is:

$$\begin{aligned} u_{\text{CACC},i}(k) = \sum_{j=1}^{i-1}[&\kappa_s\left(\hat{s}_i^{(j)}(k) - \hat{s}_0^{(i)}(k) - d_{i,j}(k)\right) \\ &+\kappa_v\left(\hat{v}_i^{(j)}(k) - \hat{v}_0^{(i)}(k)\right) + \kappa_a\left(\hat{a}_i^{(j)}(k) - \hat{a}_0^{(i)}(k)\right)] \end{aligned} \tag{4.57}$$

where:

- $\hat{s}_i^{(j)}(k)$, $\hat{v}_i^{(j)}(k)$, $\hat{a}_i^{(j)}(k)$ are the estimated position, velocity, and acceleration of vehicle j from $\mathcal{DO}_i^{(j)}$.
- $\hat{s}_0^{(i)}(k)$, $\hat{v}_0^{(i)}(k)$, $\hat{a}_0^{(i)}(k)$ are the ego-state estimates of vehicle i from $\mathcal{LO}_i$.
- $d_{i,j}(k) = (i-j)\big(d + h\hat{v}_0^{(i)}(k)\big)$ is the desired distance between vehicles j and i under CTHS, where d is the standstill gap and h is the time headway.
- κ_s, κ_v, κ_a are control gains for position, velocity, and acceleration errors, respectively.

This formulation ensures that vehicle i adjusts its behavior based on the estimated states of all preceding vehicles, promoting consensus and stability across the platoon.

5.4.4 Final Controller

The final control input blends the IDM and CACC layers to balance local safety and cooperative performance. The target acceleration is:

$$a_{\text{target},i} = (1 - \gamma(t))a_{\text{IDM},i} + \gamma(t)u_{\text{CACC},i}, \tag{4.58}$$

where $\gamma(t) \in [0, 1]$ is selected from the trust/opinion score in Section 3. Intuitively, low trust should yield $\gamma(t) \approx 0$ (IDM-dominated behavior), while reliable communication should yield $\gamma(t) \approx 1$ (CACC-dominated behavior). In this study we use $\gamma(t) = mean(\mathcal{O}_i)$. To avoid chattering and abrupt transitions in the mixed controller, a first-order filter is applied:

$$u_i(t) = u_i(t-1) + \tau_f(a_{\text{target},i} - u_i(t-1)), \tag{4.59}$$

where τ_f is the filter time constant.

5.4.5 Expected Distance (Spacing)

To validate the control strategy, we derive the expected steady-state spacing:

- **IDM Steady-State Spacing**: When $a_{\text{IDM},i} = 0$ and $\Delta v_{i-1,i} = 0$:

$$1 - \left(\frac{\hat{v}_0^{(i)}}{v_0}\right)^{\delta} = \left(\frac{s_0 + T\hat{v}_0^{(i)}}{s_{i-1,i}}\right)^2,$$

  yielding:

$$s_{i-1,i} = \frac{s_0 + T\hat{v}_0^{(i)}}{\sqrt{1 - \left(\frac{\hat{v}_0^{(i)}}{v_0}\right)^{\delta}}}.$$

- **CACC Steady-State Spacing**: For the CTHS policy, when the platoon reaches consensus (all velocities equal), the spacing between vehicle i and $i-1$ is:

$$\boxed{s_i = d + \frac{h\,\hat{v}_0^{(i)}}{i-1}\,.}$$

These expressions provide steady-state references for interpreting the simulation results. Beyond estimation errors, the expected closed-loop outcomes are (i) smooth acceleration commands (no abrupt switching), (ii) bounded spacing errors around the CTHS reference, and (iii) collision-free behavior during the attack interval, with graceful performance degradation when cooperative information is down-weighted by trust.

Figures 4.8 and 4.9 shows the acceleration commands for vehicles 2 and 3. The trust-modulated γ blending and the filter time constant $\tau_f = 0.2$ yield smooth transitions between the local (IDM) and cooperative (CACC) contributions, avoiding abrupt control jumps.

Figure 4.10 reports the relative distance in the platoon (difference between the position of a follower

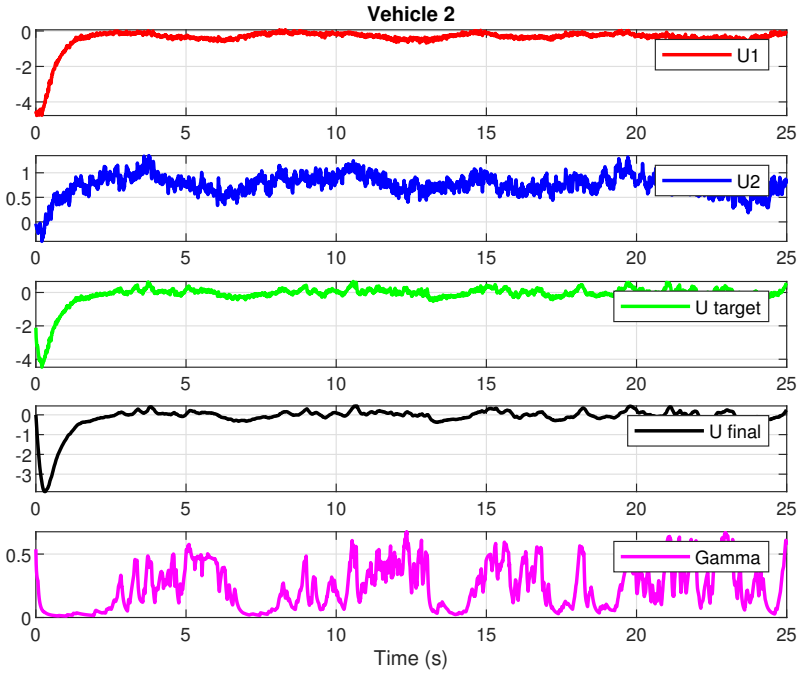

Figure 4.8: Acceleration command (controller output) for vehicles 2.

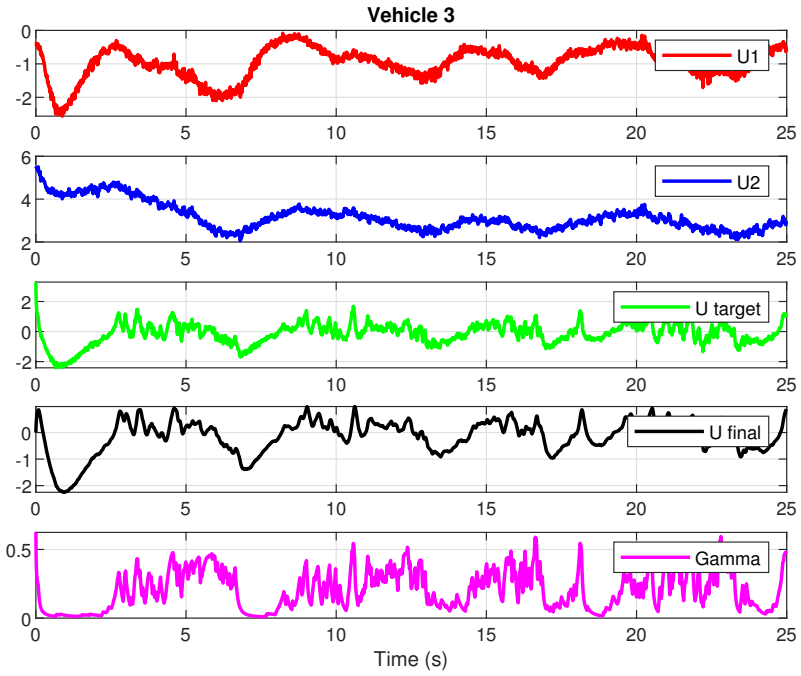

Figure 4.9: Acceleration command (controller output) for vehicles 3.

and its predecessor). Even under the considered attack scenario, the spacing remains positive and close to the CTHS reference, indicating robust distance regulation and collision avoidance.

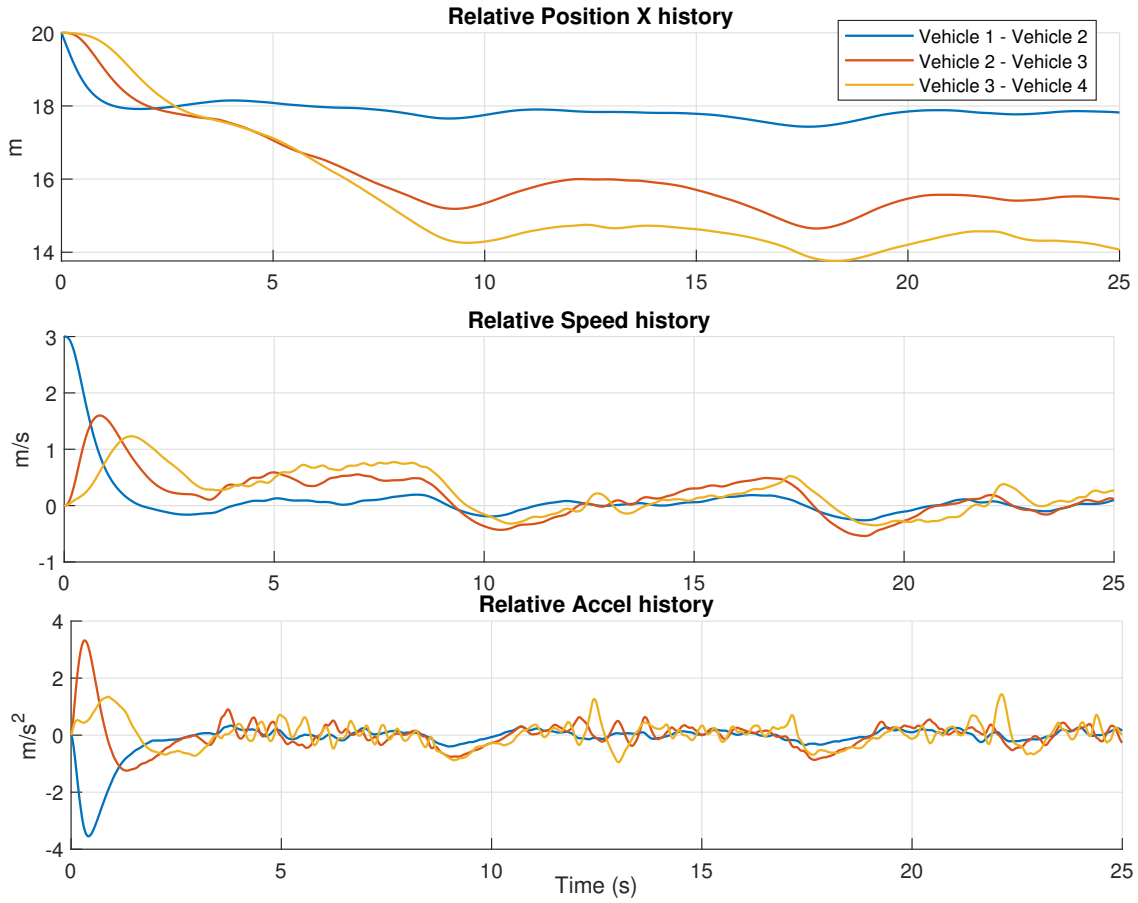

Figure 4.10: Relative distance to the predecessor in the platoon.

6 Conclusion and Future Work

This paper presented a distributed observer-based platoon control framework capable of maintaining stability and safety under cyberattacks. The approach combines local and distributed observers with a trust evaluation mechanism to assess the reliability of inter-vehicle data, ensuring robust operation even with compromised nodes.

6.1 Open Problems and Future Directions

The analysis in this chapter focuses on stability and boundedness (ISS) under bounded disturbances and a trust-driven switching topology. Several open problems remain before such architectures can be made both sharper (less conservative) and more resilient in practice:

- **Matrix-valued (channel-wise) trust weights.** In (4.5)–(4.45), the coupling weights $w_{il}^{(j)}(t)$ are scalar and therefore apply the same attenuation to all state channels. A promising extension is to replace them with *matrix* gains $W_{il}^{(j)}(t) \in \mathbb{R}^{n_x \times n_x}$ (e.g., diagonal or block-diagonal), allowing the trust mechanism to down-weight only the corrupted channels (e.g., acceleration) while preserving reliable channels (e.g., position). This leads to a matrix-weighted virtual Laplacian and stability conditions of the form $\|\mathcal{A}_{\mathrm{DO}}^{(j)}(t)\|_* \leq \alpha < 1$ for a suitably defined induced norm, or equivalently LMI-type contraction constraints on the lifted (block) error dynamics.

- **Trust/detection delay and rollback mechanisms.** In realistic networks, trust values are computed from time windows and may be delayed; consequently, false data can enter the distributed observer before a node is flagged, degrading the estimate. Moreover, abruptly cutting a node can temporarily reduce information flow and worsen estimation during the transition. A natural direction is to equip each host with a *rollback buffer*: store a fixed window of past estimates and received packets. When the trust of a node drops below threshold, roll back to time $t - T_{\mathrm{w}}$ (window length) and re-propagate the observer using (i) only trusted neighbors and (ii) model-based prediction/local-observer anchoring to bridge the missing information. This resembles fixed-lag smoothing with trust-aware data rejection and could mitigate transient corruption while preserving stability, provided the reset/rollback map is bounded and updates satisfy a dwell-time or bounded-variation condition.

  Contamination rollback (compact recipe). If a neighbor $l^\star$ is flagged at time t, undo the last K steps by keeping a buffer of the *innovation terms* appearing in (4.5b). For each step k, store $\hat{x}_i^{(j)}(k)$ and

$$\eta_{il}^{(j)}(k) \triangleq w_{il}^{(j)}(k)(\hat{x}_l^{(j)}(k) - \hat{x}_i^{(j)}(k)), \quad l \in \mathcal{N}_i,$$
$$\eta_{i0}^{(j)}(k) \triangleq w_{i0}^{(j)}(k)(\hat{x}_0^{(j)}(k) - \hat{x}_i^{(j)}(k)),$$

  as well as the input term $\hat{u}_j(k)$. When $l^\star$ is flagged, set $x \leftarrow \hat{x}_i^{(j)}(t-K)$ and replay for $k = t-K, \ldots, t-1$ using the same observer update but excluding $l^\star$ (or a malicious set $\mathcal{M}$):

$$x \leftarrow A_{\mathrm{b}}\Big(x + \sum_{l \in \mathcal{N}_i \setminus \mathcal{M}} \eta_{il}^{(j)}(k) + \eta_{i0}^{(j)}(k)\Big) + B_{\mathrm{b}}\hat{u}_j(k),$$

  and finally set $\hat{x}_i^{(j)}(t) \leftarrow x$.

- **Data-driven trust and learned uncertainty (with model-based safety layer).** Machine learning can be used to *learn the mapping from signals to reliability*, while keeping the stability guarantee in the model-based layer by enforcing bounded weights. Concretely: (i) learn a calibrated trust score or anomaly probability from a feature vector built from innovation/residual signals (e.g., $\hat{x}_l^{(j)} - \hat{x}_i^{(j)}$, $\varepsilon_{i,l}^{(j)}$, packet age/loss, and consistency indicators), using change-point detection, self-supervised prediction, or lightweight sequence models; (ii) learn state-dependent covariance/uncertainty (heteroscedastic models) to adapt Σ_{local} and thresholding; and (iii) implement the learned output only through a saturation/projection step that maps it to admissible weights satisfying Condition (2) and preserving contraction in Condition (3).

Future work will also focus on enhancing the trust mechanism by coupling it more closely with the controller, enabling trust evaluation for non-neighboring vehicles, and improving adaptability under dynamic communication topologies. We will also investigate machine-learning based trust estimation.

Chapter 5

Vehicle experiments and Board electronic

Objectives

This chapter reports the experimental validation workflow and the implementation results obtained on the Quanser QCar2/QLabs platform. It first presents the virtual-to-real experimental methodology, the platform architecture (sensing, perception, V2V communication, software stack), and the longitudinal/lateral control loops used to reproduce cooperative driving. Finally, this chapter introduces the custom embedded electronic board designed to host the proposed estimation and trust mechanisms on a real vehicle, and discusses the firmware validation and the integration roadmap.

Contents

1 Vehicle Experiments **92**
1.1 Experimental methodology: from virtual validation to real trials 92
2 Quanser QCar2/QLabs experimental platform **93**
2.1 Virtual environment and scenario definition 93
2.2 Measurements and perception pipeline 94
2.3 V2V communication and modular software architecture and Attack design 95
3 Control architecture **97**
3.1 Longitudinal control: cooperative cruise control 97
3.2 Lateral control: extended look-ahead to reduce corner cutting 98
3.3 MPC for following path 98
4 Custom embedded electronic board for future onboard deployment **98**
4.1 Motivation and design objectives 98
4.2 Architectural Alignment with State-of-the-Art 99
4.3 Architecture and PCB design 100
4.4 Firmware structure and first validation tests 102
4.5 Integration roadmap with thesis algorithms 105
5 Conclusion **106**

1 Vehicle Experiments

1.1 Experimental methodology: from virtual validation to real trials

The experimental validation strategy follows a modular pipeline centered on (i) platoon modeling, (ii) cooperative control, (iii) distributed observation, and (iv) incremental validation on a realistic platform. In practice, the workflow is decomposed into five phases:

- **Phase 1 – Environment setup:** configuration of the virtual environment under Ubuntu and deployment of the Quanser Virtual Environment container to connect QLabs and QCar2.
- **Phase 2 – V2V communication and software architecture:** implementation of inter-vehicle communication via UDP and development of a modular Python architecture.
- **Phase 3 – Longitudinal and lateral control:** two complementary control loops are implemented: (i) longitudinal control to regulate speed and inter-vehicle distance, and (ii) lateral control to track the road/trajectory.
- **Phase 4 – Observer and trust system:** development of a distributed observer to estimate the fleet states even in presence of delays and information losses; integration of a trust system that weights the reliability of received data and dynamically adapts the fusion mechanism.
- **Phase 5 – Full integration and real-time validation:** complete integration and real-time testing in QLabs; the transfer to physical scenarios on real QCar2 is prepared as a next step.

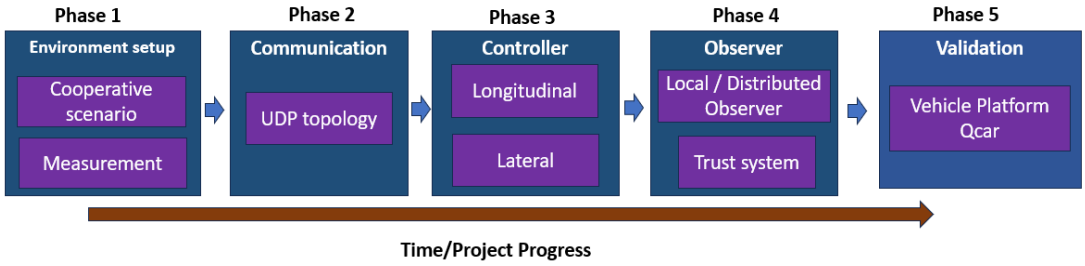

Figure 5.1: Modular Experimental Phases.

The objective of the real-trial preparation is to design an *embedded intelligent soft sensor* able to estimate non-measured quantities and detect disturbances related to cyberattacks and/or sensor faults. This embedded soft sensor associates perception measurements to surrounding vehicles, reconstructs critical variables, and distinguishes physical anomalies from malicious perturbations.

Beyond the modular phases described above, the experiments rely on a coordinated workflow that links code development, simulation, and real-world testing. A containerized development environment is used to write and package the Python control and estimation code. Once a new controller or observer is ready, the container sends the code to a Graphical Ground Station. This application acts as the central hub for the experiments: it runs the cooperative control and planning algorithms, visualizes trajectories and state estimates in real time, and forwards commands to the test platform. When working with the QLabs simulator, the ground station interfaces with the QLabs Virtual Environment, which is a digital

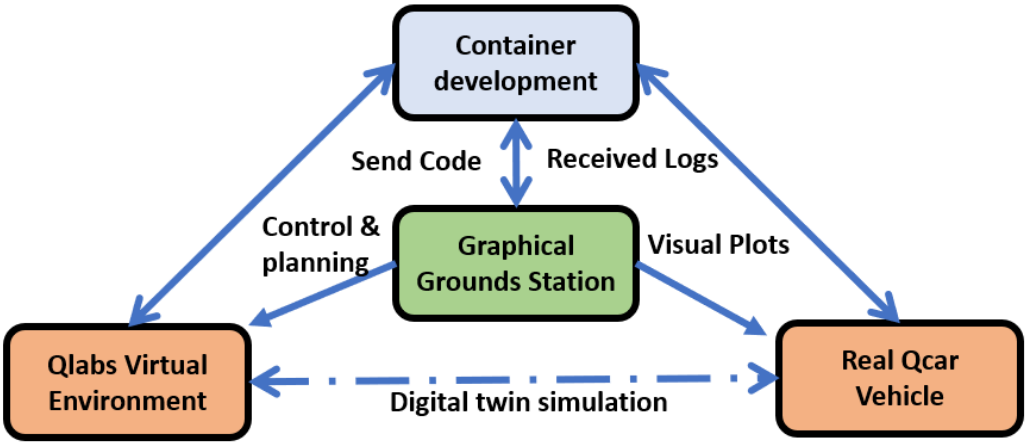

Figure 5.2: Experimental workflow for the virtual validation on QLabs/QCar2 and preparation of real trials.

twin of the physical QCar platform. The virtual QCar behaves the same way as the real hardware and exposes the same sensors and actuators, so control software can be measured and tested in simulation before deployment.

During a simulation trial, the ground station sends high-level control commands (e.g., desired speed and spacing) to the virtual environment and receives simulated sensor data and vehicle states. This allows the researcher to verify the platoon behaviour, tune the cooperative adaptive cruise control and look-ahead steering loops, and adjust observer parameters. Because the digital twin mirrors the physical self-driving car studio, the same code can then be executed on the real QCar with minimal changes. In physical tests, the ground station sends visual plots and user commands to the vehicle while logging the on-board measurements, estimated distances and trust indicators. The logs collected during real trials are sent back to the containerized development environment, where they are analysed to refine the models and software. This feedback loop—code development $\rightarrow$ ground-station execution $\rightarrow$ virtual trials $\rightarrow$ physical trials $\rightarrow$ log analysis—enables safe, incremental validation: controllers and observers are first validated in a realistic digital twin, then applied to the real vehicle. Bridging and blending code between the virtual and physical platforms allows researchers to explore new scenarios and behaviours while ensuring that the resulting algorithms are robust when transferred to hardware. The GitHub repository `https://github.com/kslhuy/QCar2_Cran` contains all algorithms developed in this thesis.

2 Quanser QCar2/QLabs experimental platform

2.1 Virtual environment and scenario definition

The QLabs environment is configured with two connected vehicles: a *leader* vehicle tracking a predefined closed-loop trajectory and a *follower* vehicle reproducing cooperative platoon behavior. The leader trajectory is defined via a set of waypoints that form a closed loop. In the reported experiments, a desired speed of $0.5\,\mathrm{m/s}$ is selected to generate a smooth and repeatable reference motion for the follower. The scenario includes typical road elements (ground, walls, pedestrian crossing), making it closer to real

driving conditions.

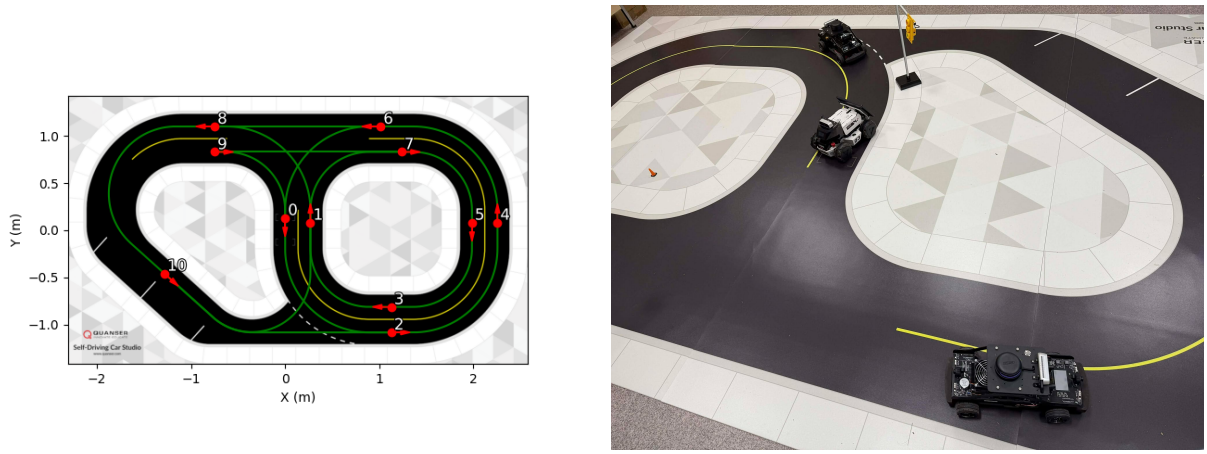

Figure 5.3: QLabs map and example of selected waypoints for the vehicle.

2.2 Measurements and perception pipeline

Designing trust-aware distributed estimation requires a clear definition of the measurements and metadata available on the QCar2 platform. In this work, the data sources include: onboard sensors, perception modules (LiDAR-camera fusion), and V2V exchanged states. Table 5.1 summarizes the measurements used in the reported experiments.

Two critical quantities for cooperative control and trust assessment are the inter-vehicle distance d and the relative speed Δv. They are obtained via a LiDAR-camera fusion pipeline, which can be summarized as follows:

- Image segmentation: YOLOv8-seg is used to extract object masks (vehicles, pedestrians).
- Post-processing: mask erosion reduces false positives.
- LiDAR projection: 3D LiDAR points are projected into the image plane using intrinsic/extrinsic calibration matrices.
- Data association: projected points are associated to segmented objects, yielding a 2D-3D coupling.
- Spatial clustering: DBSCAN filters and groups fused points.
- 3D estimation: PCA computes 3D bounding boxes and relative positions.
- Final quantities: distance d is deduced from relative position; relative speed is obtained from time-derivative of d.

Table 5.1: Summary of measurements and metadata available on QCar2/QLabs used for control, estimation, and trust evaluation.

Category	Measurement / metadata	Source	Usage
Onboard sensors (raw)	Position (x, y) and timestamp	QLabs virtual GPS (GPSSync API)	Time alignment and trajectory matching
Onboard sensors (raw)	Acceleration and angular rate	IMU (accelerometers, gyros)	Instantaneous vehicle dynamics
Onboard sensors (raw)	2D point cloud	LiDAR (RPLiDAR A2, $12\,\mathrm{m}$)	360° obstacle sensing
Onboard sensors (raw)	RGB/depth images	Cameras (RealSense D435, CSI 360°)	Visual perception
Onboard sensors (raw)	Wheel speed and steering angle	Motor encoder and steering servo	Inputs for longitudinal/lateral control
Derived kinematics	Position, orientation (ψ)	QLabs global state	Absolute vehicle state in the map
Derived kinematics	Longitudinal speed (v)	Encoder + Kalman filter	Smoothed speed estimate
Derived kinematics	Longitudinal acceleration (a)	Derivative of v (Kalman) or IMU	Longitudinal acceleration estimate
Relative variables	Inter-vehicle distance (d)	LiDAR-camera fusion pipeline	Reliable distance for cooperative control
Relative variables	Relative speed (Δv)	Temporal derivative of d	Rate of change of inter-vehicle gap
V2V metadata	Neighbor states (p, v, a)	Periodic V2V messages	Cooperative/distributed estimation
V2V metadata	Link quality	Packet loss rate, delays	Communication reliability for trust

2.3 V2V communication and modular software architecture and Attack design

2.3.1 Design of V2V communication

Beyond control and estimation algorithms, the overall system requires a robust communication layer. The V2V stack is organized into three functional layers, as illustrated in Figure 5.4:

1. **Application layer**: high-level cooperative functions (platoon controller, distributed observer, trust manager) consume and produce vehicle state messages.

2. **Session layer**: handles message reliability through acknowledgments (ACK/NACK), periodic heartbeats for neighbor-presence detection, and a virtual-GPS-based time synchronization service that timestamps every packet.

3. **Transport layer**: UDP sockets transmit and receive datagrams at a fixed period (typically $T_s = 100\,\mathrm{ms}$). Separate threads handle transmission and reception to avoid blocking.

At each communication period, a vehicle broadcasts a state packet containing:

- vehicle identifier (id);
- position (x, y) and heading ψ;
- longitudinal speed v and acceleration a;

- synchronized timestamp t.

When a packet is received, an ACK is returned to the sender; if no ACK arrives within a timeout, the message is flagged as lost. In parallel, a heartbeat mechanism periodically checks for missing neighbors: if no message (nor heartbeat) is received from a neighbor for a configurable interval, that neighbor is marked as unavailable and excluded from the cooperative estimation until communication resumes. These mechanisms ensure temporal consistency and data integrity, which are prerequisites for the distributed observer and trust framework.

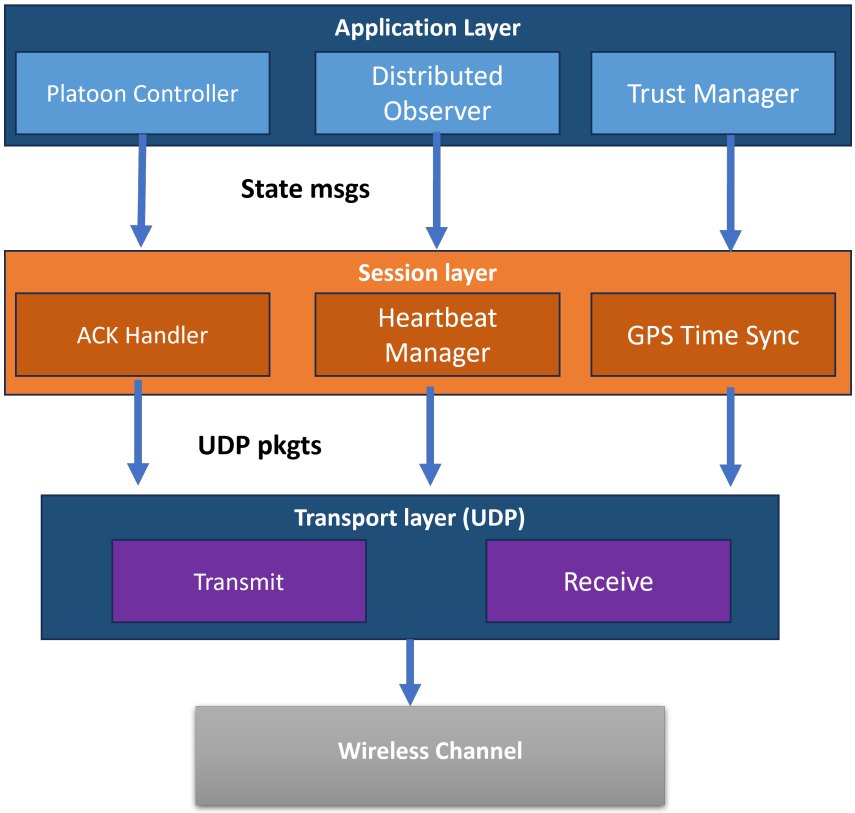

Figure 5.4: Layered architecture of the V2V communication stack used in the QLabs experiments.

2.3.2 Attack injection mechanism

To evaluate the robustness of the distributed observer and trust framework under adversarial conditions, a configurable *attack injector* is integrated into the communication layer. The injector intercepts outgoing or incoming V2V packets and applies one of several perturbation models before the data reach the application layer. Figure 5.5 illustrates the injection pipeline.

Injection modes. Three attack families are supported:

1. **Bias injection**: a constant offset δ is added to one or more state variables (e.g., $\tilde{v} = v + \delta_v$).
2. **Random fault**: with probability p, the transmitted value is replaced by a random sample drawn from a uniform distribution of configurable intensity.

3. **Data drop (DoS)**: with probability p_{drop}, the packet is discarded entirely, simulating a denial-of-service or severe packet-loss scenario.

Injection parameters. Each attack scenario is defined by:

- *attacker ID*: the vehicle whose outgoing messages are corrupted;
- *target variables*: which state components are affected (position, velocity, acceleration, or all);
- *attack window*: the time interval $[t_{start}, t_{end}]$ during which the attack is active;
- *attack parameters*: bias magnitude δ, fault intensity, or drop probability p_{drop}.

The injector can operate transparently (victim vehicles are unaware) or be logged for post-experiment analysis. This flexibility enables systematic benchmarking of the trust-aware estimation framework across a wide range of adversarial conditions.

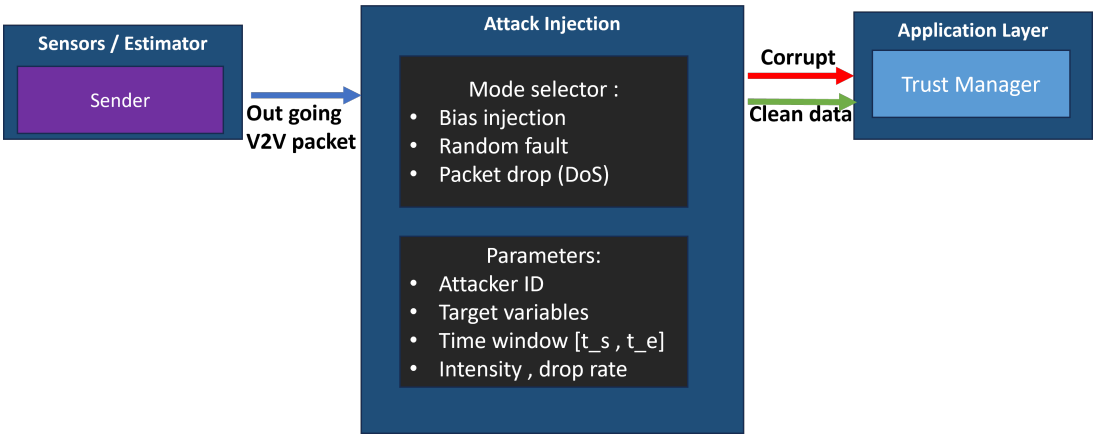

Figure 5.5: Attack injection mechanism integrated into the V2V communication layer.

3 Control architecture

We have separated 2 types of controllers: one for path following (MPC) and one for vehicle following (CACC). To follow a vehicle, the control system can have separated longitudinal and lateral control loops, which are respectively CACC and ELC.

3.1 Longitudinal control: cooperative cruise control

The longitudinal control loop is based on Cooperative Adaptive Cruise Control (CACC) to regulate both velocity and inter-vehicle spacing. The control input combines locally measured quantities (e.g., speed/acceleration) with cooperative information received via V2V (e.g., predecessor acceleration), and relies on the perception-derived distance d and relative speed Δv. This chapter focuses on the experimental integration and validation aspects; the detailed CACC modeling and resilient observer-based compensation are developed in earlier chapters.

3.2 Lateral control: extended look-ahead to reduce corner cutting

In curves, follower vehicles tend to exhibit *corner cutting* (reduced turning radius compared to the leader), which can induce lateral offsets and affect the effective inter-vehicle spacing. To mitigate this effect, an Extended Look-Ahead Controller (ELC) is implemented. The idea is to define a virtual pursuit point P^* located ahead of the preceding vehicle by a look-ahead distance d_{LA} and laterally shifted by d_{lat}. The follower then computes its steering command using this virtual target rather than the preceding vehicle's center of gravity. This improves curve tracking and helps maintain the spacing policy (e.g., constant time-gap) in both straight and curved roads.

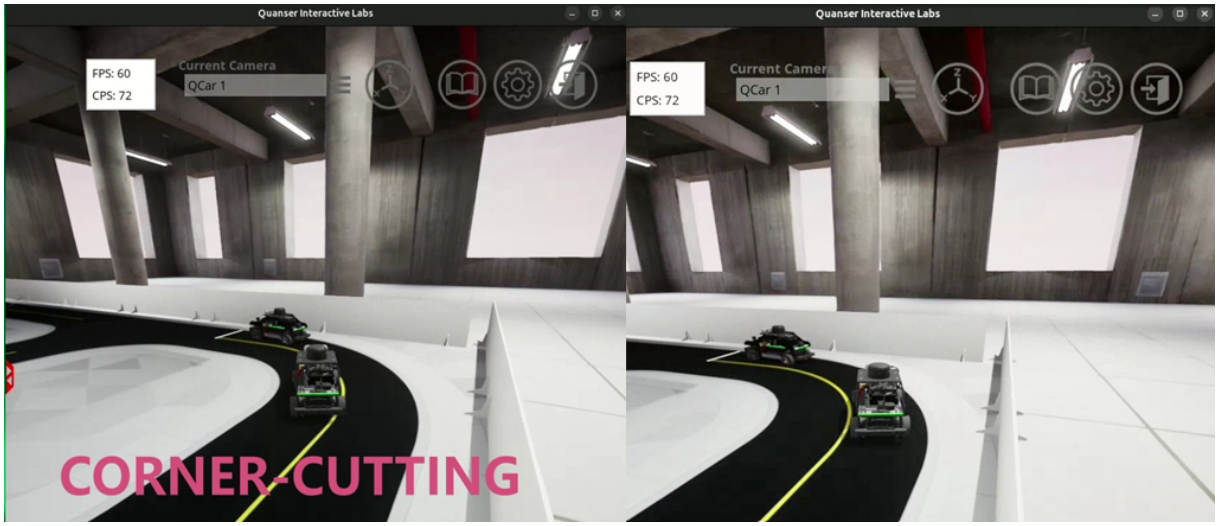

Figure 5.6: Effect of extended look-ahead on corner cutting in curves.

3.3 MPC for following path

The MPC for path following is designed to track a reference trajectory defined by the leader's waypoints while respecting the vehicle's kinematic constraints and ensuring smooth control actions. This also supports the lateral control loop by providing a reference heading and curvature that the look-ahead controller can use to compute steering commands. The MPC optimization problem is solved at each control step, using the current state estimate and the reference trajectory to compute the optimal steering and acceleration commands to minimize tracking error.

4 Custom embedded electronic board for future onboard deployment

4.1 Motivation and design objectives

Transitioning from simulation-based validation and small-scale experiments to real vehicle trials requires an onboard implementation of the proposed estimation and trust mechanisms. Running all software on a central vehicle computer (e.g., industrial PC or NVIDIA Jetson) is useful for proof-of-concept, but it is less practical for deployment across heterogeneous platforms. In practice, OS scheduling and middleware layers often hide low-level timing behavior, creating non-deterministic delays that affect

high-rate estimation loops. Portability is also reduced when the implementation depends on a specific vehicle sensing stack, since testbeds such as QCar and full-scale passenger cars use different sensors and communication buses (CAN, Automotive Ethernet, etc.).

In this thesis, the embedded board is therefore treated as an *intelligent soft sensor* and an edge estimation node. It reconstructs non-measured variables, checks cooperative-data consistency, and provides state/trust indicators to higher-level control and decision layers. This choice is also driven by practical constraints: directly measuring all cooperative-control quantities (relative distance/speed/acceleration, heading, road-adhesion proxies, etc.) is costly, and some variables are not accessible with standard instrumentation. Model-based observers can recover missing information online, but only with deterministic timing, consistent timestamping, and reliable access to local sensing and V2V data. Accordingly, the VEHALSECU effort targets a compact onboard module for state estimation and cyberattack-aware consistency monitoring under reduced sensing and intermittent/corrupted V2V communication [67]. Within an RCP workflow, the module can first operate in monitoring-only mode, then be progressively integrated into closed-loop operation after validation.

4.2 Architectural Alignment with State-of-the-Art

To bridge academic research and industrial automotive practice, the hardware selection prioritizes data integrity, precise synchronization, and interoperability with established robotics frameworks (e.g., ROS 2 / micro-ROS). The objective is to keep research flexibility while approaching the integration constraints of commercial telematics units.

Commercial Off-the-Shelf (COTS) landscape and motivation. Recent COTS V2X products already offer mature features for deployment use cases. Representative examples include the Cohda MK6 (strong positioning and V2X-Locate capabilities) [68], the Commsignia OB4 (high-throughput HSM integration for large-scale signed messaging) [69], and modular platforms such as the Unex SOM-351U for Tier-1 style integration flows [70]. Infrastructure-side deployments also rely on interoperable RSU solutions in European C-ITS programs, including NeoGLS-class setups in C-Roads testing contexts [71]. These product lines evolve under standards and regulatory frameworks such as 3GPP NR V2X [72], SAE J2735 message dictionaries [73], and the DSRC-to-C-V2X transition reflected in recent spectrum policy updates [74]. However, for research labs and early prototypes, accessibility remains limited by cost, procurement, closed software stacks, and integration constraints. This gap motivates a custom embedded board: not to replace commercial OBUs/RSUs, but to provide an open and portable platform for observer, trust, and cyber-resilience experimentation before industrial transfer.

Component Selection and Functional Requirements. The specific functional requirements are mapped to state-of-the-art component categories as follows:

- **Real-Time Processing Core:** To guarantee deterministic execution of the estimation loops (target $\approx 100\,\mathrm{Hz}$), the design leverages high-performance microcontrollers (e.g., **ARM Cortex-M7** series such as the STM32H7 or NXP i.MX RT). Unlike standard Linux-based embedded computers, these cores provide bare-metal or RTOS-based execution with negligible interrupt latency, essential for synchronizing sensor acquisition with V2V message arrival.

Table 5.2: Examples of COTS V2X products relevant to this thesis motivation.

Product	Best for	Key differentiator
Cohda MK6	Research and urban-canyon operation	High-accuracy positioning (V2X-Locate) [68]
Commsignia OB4	Large-scale fleet deployment	High-throughput HSM for message signing [69]
Unex SOM-351U	Tier-1 hardware integration	Modular PCIe form factor for custom PCB integration [70]
NeoGLS RSU class	European infrastructure deployment	Alignment with C-Roads and French/European interoperability contexts [71]

- **High-Fidelity Inertial Sensing:** The board integrates a 6-DoF Industrial-grade Inertial Measurement Unit (IMU) (e.g., **Bosch BMI088** or **TDK InvenSense ICM-42688**). Selected for their vibration robustness and low bias instability, these sensors represent the current standard for automotive electronic stability control (ESC) and navigation support, offering a significant upgrade over consumer-grade MEMS found in basic development kits.
- **Precision Positioning and Timing:** A multi-constellation GNSS receiver (e.g., **u-blox F9 series**) is employed not only for absolute positioning but as a precise time source. By utilizing the GNSS Timepulse (1PPS signal) to discipline the microcontroller's internal clock, the board ensures that all local data and V2V messages are timestamped to a global reference (UTC), a critical requirement for cooperative perception and sensor fusion in multi-agent systems.
- **Wireless V2X/V2V Interface:** While full-scale automotive deployments use C-V2X (3GPP PC5) or DSRC (802.11p), this research platform uses a modular Wi-Fi interface (e.g., **Espressif ESP32** or dedicated 802.11 modules) to emulate V2V functionality. This module handles the physical layer broadcast of state vectors, allowing the main processor to focus on estimation logic. For future-proofing, the hardware interface (UART/SPI) is designed to be compatible with commercial C-V2X modules (e.g., from Quectel or u-blox) for seamless migration to standard automotive protocols.
- **Data Integrity and Connectivity:** Robust logging is handled via an SDIO interface to high-speed storage, enabling "black box" recording of raw sensor data for offline replay. External connectivity includes both USB for development and robust vehicle buses (CAN/CAN-FD) to broadcast the "trust indicators" and estimated states to the vehicle's central planning unit.

Overall, this modular architecture enables the board to verify incoming cooperative data before forwarding estimates and trust indicators to trajectory-level functions.

4.3 Architecture and PCB design

The development process is structured into four phases: (i) functional needs analysis and block-architecture definition, (ii) electronic CAD design, (iii) prototyping and embedded programming, and

(iv) experimental verification with rigorous test protocols. The design identifies required sensors, the target microcontroller family, and the main communication protocols (**SPI**, **I^{2}C**, **UART**, and **Wi-Fi 6**).

Sizing and interface selection. To keep the embedded implementation compatible with the thesis algorithms, the architecture includes a first-order sizing step: expected sensor sampling rates and message rates are translated into throughput and storage requirements, guiding memory and logging choices [67]. In practice, this leads to (i) separating time-critical sensor acquisition from less deterministic communication bursts and (ii) keeping an onboard storage path for raw and intermediate signals used in offline analysis.

Communication choice for the first prototype. Several V2V candidates were considered (DSRC / ITS-G5, C-V2X, and Wi-Fi-based solutions). For the first experimental prototype on a scaled test platform, Wi-Fi 6 was retained because it is comparatively accessible to implement while still providing sufficient short-range V2V performance; it also simplifies early integration before migration to more automotive-oriented stacks if required [67]. The electronic design is implemented in KiCad and routed on a **4-layer PCB**, which offers two main benefits: (i) dedicated reference planes to control return paths and reduce EMI, and (ii) improved power distribution and decoupling compared with 2-layer prototypes. Following the layout strategy reported in [67], inner layers are used as continuous planes (ground and the main 3.3 V distribution) to stabilize return paths and supply impedance while freeing outer layers for routing and component placement. This 4-layer choice also reflects a compromise between routability/EMC and manufacturing cost: while additional layers can further ease routing and improve isolation, they were not retained for the first prototype iteration [67].

Functional blocks. At a high level, the board architecture (Figure 5.8) can be described as a composition of:

- a **real-time processing unit** (microcontroller + memory resources) responsible for scheduling tasks, running the embedded observer/trust logic, and managing peripherals;
- a **communication subsystem** supporting short-range V2V exchange (Wi-Fi) and wired diagnostic/telemetry links (UART);
- a **sensing and timing subsystem** interfacing inertial and positioning/time-reference signals through SPI/I^{2}C/UART, and providing timestamping for data consistency;
- a **power subsystem** that converts the vehicle supply to regulated rails for digital logic and RF modules, with attention to inrush current, ripple, and protection.

Electrical and layout considerations. Beyond functional connectivity, the PCB is designed to be compatible with an onboard environment where noisy actuators, switching regulators, and RF emissions may coexist. The main layout guidelines are summarized below:

- **Power integrity:** short decoupling loops close to IC supply pins, separation of noisy switching nodes from sensitive analog/RF areas, and adequate bulk capacitance for transient loads.

- **Grounding and return paths:** continuous ground reference planes and stitching vias to reduce loop areas, ensuring that high-frequency return currents follow controlled paths.
- **High-speed / RF routing:** controlled-impedance routing and keep-out zones for the Wi-Fi/RF section, plus careful placement of the GNSS/RF components to minimize coupling.
- **Robust I/O:** ESD-aware connector placement and protection where needed (especially for external cables), as well as clear separation between internal buses (SPI/I^2C) and external-facing ports.

These rules are used to keep power quality, EMC behavior, and RF/high-frequency routing robust in onboard conditions.

Table 5.3: Embedded board design targets for thesis-to-vehicle transfer (high-level, implementation-dependent).

Design aspect	Target / rationale
Real-time behavior	Deterministic scheduling for periodic estimation tasks (e.g., $\sim 100\,\mathrm{Hz}$) and bounded latency for event-driven message handling.
Interfaces	Support SPI/I^2C/UART for sensors and debugging; support Wi-Fi for V2V exchange of compact state packets and link-quality metadata.
Time consistency	Timestamping and time-reference handling to align sensor samples and received packets before fusion and trust evaluation.
Robustness	Health monitoring (watchdog, peripheral status), logging/telemetry hooks, and safe fallback behavior when links or sensors degrade.
PCB constraints	4-layer stack-up to improve grounding and EMC; separation of RF/power/sensitive areas; routing practices compatible with on-board EMI constraints.

4.4 Firmware structure and first validation tests

To validate hardware early and reduce integration risk, initial firmware developments are performed on development modules before deployment on the final board. The software is prepared using STM32CubeMX and STM32CubeIDE, with RTOS integration. The firmware remains modular and follows the same main functions as in QLabs experiments (sensing, communication, estimation, trust update), while respecting embedded constraints (bounded memory, fixed timing, robust I/O).

Traceability and experiment reproducibility. Because the goal is to transition from simulation to real-world deployment, a key practical requirement is the ability to *trace* what happened during a run: raw sensor samples, timestamps, received packets, link-quality indicators, intermediate observer quantities, and final state/trust outputs. This motivates onboard logging (e.g., SD storage) and lightweight telemetry channels so that the observer behavior can be audited offline and compared against simulation baselines [67].

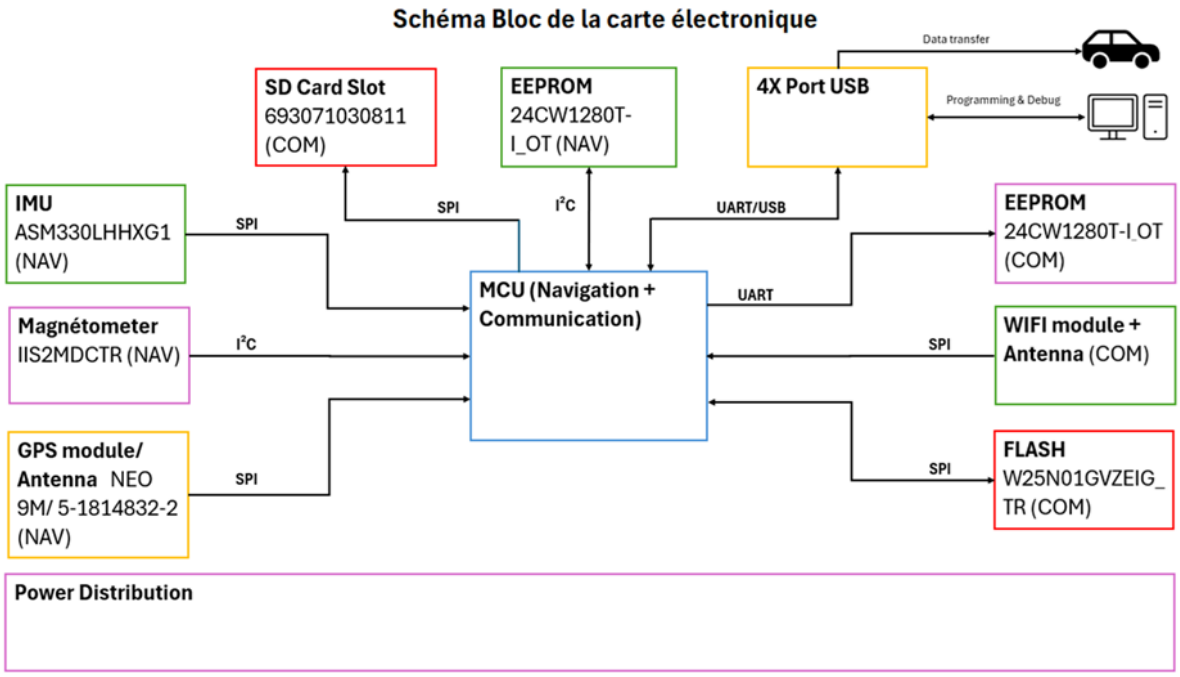

Figure 5.7: Block architecture.

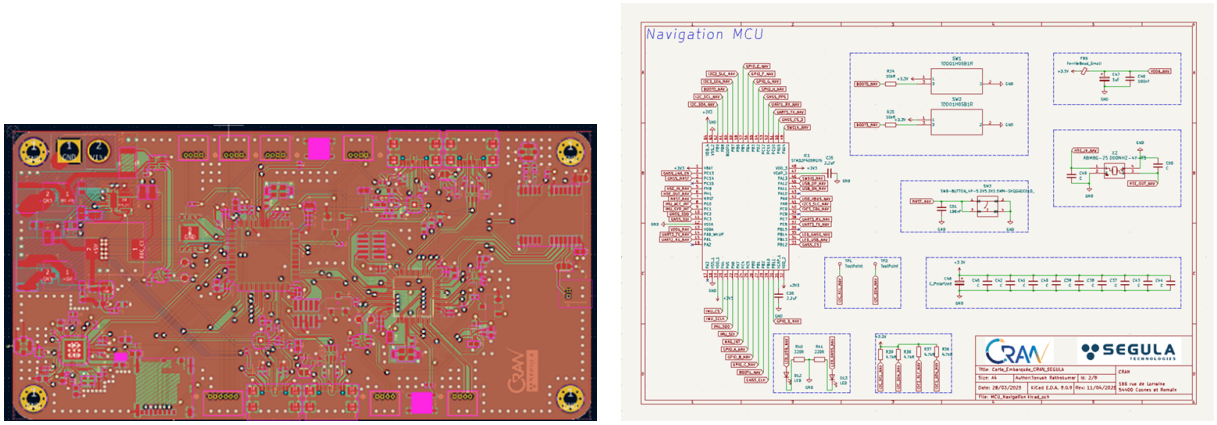

Figure 5.8: Embedded board design: KiCad PCB implementation.

RTOS organization. From a scheduling point of view, two categories of tasks are distinguished:

- **Periodic tasks** (time-triggered), responsible for sensor acquisition, filtering, and state propagation at a fixed rate.
- **Event-driven tasks** (message-triggered), responsible for reception/transmission handling and for updating distributed estimates when new V2V data arrive.

This separation is aligned with the needs of the trust-aware distributed observer: local estimation must remain stable even when communication becomes intermittent, while V2V updates can be processed opportunistically and explicitly timestamped.

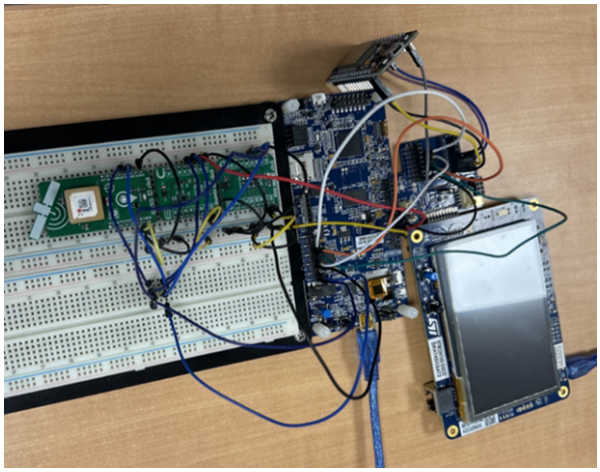

(a) Prototype validation using development kits (firmware bring-up and I/O tests).

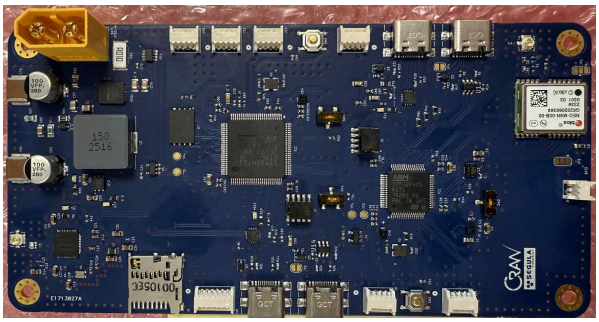

(b) Manufactured embedded board intended for onboard deployment.

Figure 5.9: Prototype validation and manufactured embedded board.

Data flow and software services. At a functional level, the firmware implements the following services:

- acquire environment data from onboard sensors;
- structure data in a dynamic list adapted to real-time processing;
- communicate with neighbor vehicles to exchange environmental and state data;
- fuse received information with local measurements for a coherent view;
- transmit consolidated variables to the vehicle system for decision making.

The sensing layer provides unified data structures with numerical values and metadata (timestamps, validity flags, optional quality indicators). The communication layer handles packet framing/serialization and exposes link-quality hooks (packet counters, estimated loss, delay statistics). At application level, the embedded "observer/soft-sensor" consumes these inputs and outputs consistent state estimates plus trust-related indicators for logging or transmission to the vehicle control stack.

Verification philosophy. The first firmware iterations focus on hardware bring-up and repeatable subsystem tests before enabling closed-loop operation. This staged approach validates peripherals with controlled stimuli and debug traces before moving to multi-task real-time execution. Initial protocols confirm:

- sensor data readout and transmission via UART;
- stable RTOS scheduler operation at 100 Hz;
- correct interrupt and asynchronous task handling;
- compatibility between configured peripherals and the target hardware.

These checks indicate that the platform can sustain required sampling/communication rates and that timing-critical sections (interrupt handlers, DMA transfers when used, inter-task synchronization) remain reliable in continuous operation.

Bring-up and interface test protocol. The verification procedure follows a hierarchical approach. First, power integrity is checked through inspection/continuity, progressive power-up with current limiting, and ripple measurements on regulated rails. Second, interfaces are validated with repeatable transactions: UART loopback/telemetry, I^2C bus scan and register reads, SPI transfers to a known peripheral (or synthetic pattern), then GNSS acquisition and Wi-Fi association with basic packet tests (IP assignment, ping, packet sending) [67].

Bench measurements complement software checks and provide quantitative confidence in the electrical design. Reported results include a regulated $3.3\,\mathrm{V}$ rail close to nominal with limited ripple, stable bidirectional UART communication (e.g., $115200\,\mathrm{baud}$), GNSS fix acquisition within tens of seconds with meter-level horizontal accuracy, and a functional Wi-Fi 6 link with throughput on the order of tens of Mbit/s in a test setup [67].

4.5 Integration roadmap with thesis algorithms

The embedded platform supports a staged transfer of the estimation and resilience mechanisms developed throughout the thesis:

- implementing the local observer as a periodic real-time task (sensor acquisition, filtering, state update);
- implementing the distributed observer and trust update as event-driven tasks synchronized with V2V message reception;
- maintaining time consistency via timestamping (synchronized clock) and heartbeat/ACK mechanisms;
- ensuring safe degradation modes under detected faults/attacks by down-weighting or isolating untrusted neighbors.

The transfer follows three stages: First, the embedded platform is used as a data concentrator and logger to validate sensing and timestamping on the vehicle. Second, the local observer is activated onboard, producing filtered kinematic estimates and residuals for fault detection. Third, V2V exchange is enabled and the distributed observer is executed, initially in a monitoring mode (estimating and logging without affecting control), then progressively coupled to the decision/control layer once stability and robustness are confirmed.

Two practical aspects are key to a successful transfer:

- **Computational budgeting:** profiling of task execution times and memory usage to ensure that worst-case execution times remain compatible with the selected sampling periods.

- **Numerical robustness:** careful management of numeric scaling, saturation, and data validation (outlier rejection, missing-data handling) to avoid observer divergence when inputs are corrupted or delayed.

At the hardware level, the reported design identifies future optimization axes, including RF matching network tuning, via-loss reduction, improved high-frequency routing, and more refined power management. From an experimental perspective, these optimizations will be coupled with extended stress tests (continuous operation, communication congestion, and perturbation injection) to verify that the embedded implementation preserves the key properties demonstrated in simulation: stable local estimation, timely trust degradation under attacks, and recovery once the perturbation ends.

5 Conclusion

This chapter presented the experimental workflow and results obtained on the Quanser QCar2/QLabs platform. The full software stack (communication, perception, control, estimation) was integrated and validated in real time. Nominal experiments confirm accurate local state reconstruction and coherent distributed estimation of the whole fleet. Under representative attack scenarios (biases, random faults, and DoS drops), the trust-aware fusion mechanism detects inconsistencies and mitigates their impact, with the DoS case being the most severe according to the reported normalized impact score. Finally, a custom embedded electronic board was designed and prototyped as a hardware foundation for future real-vehicle deployment of the proposed observers and cyber-resilience mechanisms.

Conclusion and Perspectives

1 General Conclusion

This thesis addressed the problem of resilience in autonomous and connected vehicles through the development of advanced state estimation algorithms. As autonomous driving systems increasingly rely on interconnected sensors, embedded computation, and wireless communications, their vulnerability to sensor faults, modeling uncertainties, and cyber-attacks has become a major safety concern. In particular, false data injection attacks targeting vehicle-to-vehicle communication channels pose a serious threat to cooperative driving functionalities such as Adaptive Cruise Control (ACC), Cooperative Adaptive Cruise Control (CACC), and vehicle platooning.

The main objective of this research was to design estimation frameworks capable of maintaining reliable state information under adverse conditions, thereby ensuring safe and robust control performance. To this end, several complementary observer-based approaches were developed, analyzed, and validated within the context of autonomous and connected vehicle systems.

First, a discrete-time unknown input observer was proposed to estimate both vehicle states and malicious disturbances affecting communication signals. By employing an advanced discretization strategy and appropriate state transformations, the observer overcomes classical existence constraints and significantly reduces estimation delay. This contribution enables fast and accurate reconstruction of cyber-attack signals, allowing the controller to compensate for their effects in real time rather than merely detecting their presence.

Second, to address nonlinearities and modeling uncertainties inherent to vehicle dynamics, a neural network-based observer was introduced. This observer integrates learning capabilities into a model-based estimation framework, allowing online adaptation to unknown dynamics and external perturbations. The proposed architecture preserves stability while improving estimation accuracy in scenarios where classical models alone are insufficient, such as aggressive maneuvers or varying road conditions.

Third, the estimation framework was extended to cooperative and distributed scenarios involving vehicle platoons and mixed traffic environments. A distributed observer architecture combined with a trust management mechanism was developed to evaluate the reliability of information received through vehicle-to-vehicle communication. This approach limits the influence of compromised or unreliable data and enhances the collective resilience of the platoon, preventing the propagation of malicious effects from a single vehicle to the entire formation.

The proposed methods were extensively validated through high-fidelity simulations using MAT-

LAB/Simulink, CARLA, and Quanser QLabs environments. Various scenarios were considered, including nominal operation, sensor faults, communication disturbances, and cyber-attacks. The results demonstrate that the developed estimation algorithms significantly improve robustness, estimation accuracy, and safety compared to conventional approaches. Furthermore, the preparation for embedded implementation confirms the feasibility of deploying the proposed observers in real-time automotive systems.

Overall, this thesis contributes novel theoretical developments and practical solutions for resilient autonomous and connected vehicles. By combining model-based estimation, learning techniques, and cooperative trust mechanisms, it provides a unified framework capable of addressing both physical and cyber-related uncertainties in modern intelligent transportation systems.

2 Outlook and Perspectives

Although the results obtained in this thesis represent a significant step toward resilient autonomous driving, several promising research directions remain open and deserve further investigation.

A first perspective concerns large-scale experimental validation. While the proposed algorithms were tested in realistic simulation environments and prepared for embedded implementation, full-scale experiments on real vehicles in diverse traffic conditions would provide valuable insights into their real-world performance. Such experiments could include highway platooning, urban driving, and interaction with non-cooperative road users.

A complementary perspective is the full onboard implementation of the proposed resilient estimation and trust mechanisms on an embedded platform. In particular, the custom electronic board introduced in Chapter 6 was designed as a future hosting target for the observers developed in the thesis (unknown-input observers, neuro-adaptive observers, and trust-aware distributed observers). Future work will consist in porting the estimation stack to the embedded RTOS environment (task scheduling at $100\,\mathrm{Hz}$, timestamped V2V messaging, and robust I/O handling), and validating the resulting closed-loop performance on the QCar2 platform and, ultimately, on full-scale vehicles. This step will enable a rigorous assessment of real-time constraints (latency, packet losses, sensor noise), computational load, and energy consumption, while providing a practical path from simulation-grade validation to deployable automotive-grade solutions.

A second perspective involves extending the estimation framework to cooperative perception systems. Future autonomous vehicles will increasingly rely on shared perception data, such as camera images, LiDAR point clouds, and radar detections exchanged through V2V and V2I communications. Integrating resilient estimation algorithms with cooperative perception would enable robust fusion of heterogeneous data sources while mitigating the impact of corrupted or delayed information.

Another important direction concerns the interaction between estimation, control, and decision-making layers. In this thesis, the focus was placed on state estimation and its role in ensuring reliable control. Future work could explore tighter integration between resilient observers and higher-level planning or decision-making modules, allowing autonomous vehicles to adapt their behavior dynamically in response to detected threats or uncertainty levels.

From a methodological standpoint, further research could investigate advanced learning techniques, such as adaptive neural ordinary differential equations or hybrid physics-informed learning models,

to enhance estimation accuracy while maintaining stability guarantees. Additionally, incorporating uncertainty quantification into the estimation process could provide confidence measures that inform both control actions and trust management strategies.

Finally, extending the proposed framework to multi-agent traffic networks and infrastructure-assisted systems represents a long-term perspective. In such systems, vehicles, roadside units, and cloud services collaborate to optimize traffic flow and safety. Developing scalable, resilient estimation algorithms capable of operating across multiple layers of this ecosystem remains a challenging and impactful research direction.

In conclusion, the work presented in this thesis lays a solid foundation for resilient estimation in autonomous and connected vehicles. It opens the door to numerous future developments aimed at enhancing safety, reliability, and trust in next-generation intelligent transportation systems.

List of Publications

Peer-Reviewed Journal Articles

Q. H. Nguyen, O. Sadki, H. Rafaralahy, M. Haddad, A. Zemouche. "*Cyberattack Detection by Using a Discrete-Time Model-Based Unknown Input Observer*". IEEE Control Systems Letters 8, 856-861, 2024.

International Conference Papers

Q. H. Nguyen, S. Meng, M. Haddad, H. Rafaralahy, A. Zemouche. "*Neural Observer-Based Learning for Robust State Estimation*". The International Conference on Electrical and Computer Engineering (ICEECE), Madagasca, 2025.

S. Bougherara, **Q. H. Nguyen**, M. Haddad, H. Rafaralahy, A. Zemouche. "*Application of Discrete-Time Unknown Input Observers for Cyberattack Detection in Connected CACC Vehicles*". (ICEECE), Madagasca, 2025.

S. Meng, **Q. H. Nguyen**, A. Zemouche, F. Meng, F. Zhang. "*Distributed High-Gain Observer for Nonlinear Connected Autonomous Vehicle*". 2025 American Control Conference (ACC).

O. Sadki, **Q. H. Nguyen**, A. Zemouche, H. Rafaralahy, M. Haddad. "*Cyberattack Estimation in Intelligent Transportation System by Using an Adaptive High Order Sliding Mode Differentiator*". 2025 33rd Mediterranean Conference on Control and Automation (MED).

Q. H. Nguyen, O. Sadki, H. Rafaralahy, M. Haddad, A. Zemouche. "*Cyberattack Detection by Using a Discrete-Time Model-Based Unknown Input Observer*". CDC, 2024.

Article Submitted for Publication

Q. H. Nguyen, S. Meng, M. Haddad, H. Rafaralahy, A. Zemouche. "*Resilient Trust–Aware Distributed Observer Design for Connected Vehicle Platoons.*". 23rd IFAC World Congress, 2026 (Submitted).

Q. H. Nguyen, S. Meng, M. Haddad, H. Rafaralahy, A. Zemouche. "*Control-Oriented Trust-Aware Observer Design for Connected Vehicle Platoons.*". IEEE Transactions on Intelligent Transportation Systems (Preparation).

Poster Presentations

Q. H. Nguyen, O. Sadki, H. Rafaralahy, M. Haddad, A. Zemouche. "*Cyberattack Detection by Using a Discrete-Time Model-Based Unknown Input Observer*". (ACC), 2024.

Bibliography

[1] MARTIN CORLESS and JAY TU. "State and Input Estimation for a Class of Uncertain Systems". *Automatica* 34.6 (1998), pp. 757–764 (cit. on p. 2).

[2] Hongyan Guo, Dongpu Cao, Chen Hong, Chen Lv, Huaji Wang, and Siqi Yang. *Vehicle Dynamic State Estimation: State of the Art Schemes and Perspectives*. 2018 (cit. on p. 2).

[3] Ehsan Hashemi, Reza Zarringhalam, Amir Khajepour, William Melek, Alireza Kasaiezadeh, and Shih-Ken Chen. "Real-time estimation of the road bank and grade angles with unknown input observers". *Vehicle System Dynamics* 55.5 (2017), pp. 648–667. eprint: https://doi.org/10.1080/00423114.2016.1275706 (cit. on p. 2).

[4] Yuxiao Zhang, Alexander Carballo, Hanting Yang, and Kazuya Takeda. "Perception and Sensing for Autonomous Vehicles under Adverse Weather Conditions: A Survey". *ISPRS Journal of Photogrammetry and Remote Sensing* 196 (2023), pp. 146–177 (cit. on p. 3).

[5] Alexey Dosovitskiy, German Ros, Felipe Codevilla, Antonio Lopez, and Vladlen Koltun. "CARLA: An Open Urban Driving Simulator". *Proceedings of the 1st Annual Conference on Robot Learning*. 2017, pp. 1–16 (cit. on p. 4).

[6] Xiaofei Sun, F. Richard Yu, and Ping Zhang. "A Survey on Cyber-Security of Connected and Autonomous Vehicles (CAVs)". *IEEE Transactions on Intelligent Transportation Systems* 23.7 (2022), pp. 6240–6259 (cit. on p. 4).

[7] Zhiyang Ju, Hui Zhang, Xiang Li, Xiaoguang Chen, Jinpeng Han, and Manzhi Yang. "A Survey on Attack Detection and Resilience for Connected and Automated Vehicles: From Vehicle Dynamics and Control Perspective". *IEEE Transactions on Intelligent Vehicles* 7.4 (2022), pp. 815–837 (cit. on pp. 4, 7).

[8] W. Jeon, Z. Xie, A. Zemouche, and R. Rajamani. "Simultaneous cyber-attack detection and radar sensor health monitoring in connected ACC vehicles". *IEEE Sensors Journal* 21.14 (2020), pp. 15741–15752 (cit. on pp. 4, 6, 11, 32).

[9] Q. H. Nguyen, O. Sadki, H. Rafaralahy, M. Haddad, and A. Zemouche. "Cyberattack Detection by Using a Discrete-Time Model-Based Unknown Input Observer". *IEEE Control Systems Letters* 8 (2024), pp. 856–861 (cit. on pp. 5, 6, 23).

[10] Dengfeng Pan, Xiaohua Ge, Derui Ding, and Qing-Long Han. "Observer-Based Resilient Control of CACC Vehicle Platoon Against DoS Attack". *Automot. Innov. 6, 176-189 (2023)* (2023) (cit. on pp. 5, 11).

[11] P. Cheng, J. Pan, and Y. Zhang. "Adaptive unknown input observer-based detection and identification method for intelligent transportation under malicious attack". *Measurement and Control* 56.7-8 (2023), pp. 1377–1386 (cit. on pp. 5, 11).

[12] Tianci Yang and Chen Lv. "A Secure Sensor Fusion Framework for Connected and Automated Vehicles Under Sensor Attacks". *IEEE Internet of Things Journal* 9.22 (2022), pp. 22357–22365 (cit. on pp. 5, 6).

[13] A. Biroon, P. Bagheri, and M. Pirani. "False Data Injection Attack in a Platoon of Cooperative Adaptive Cruise Control Vehicles and Its Impact on String Stability". *IEEE Transactions on Intelligent Transportation Systems* 23.2 (2022), pp. 1755–1763 (cit. on pp. 5, 6).

[14] Hamza Fawzi, Paulo Tabuada, and Suhas Diggavi. "Secure estimation and control for cyber-physical systems under adversarial attacks". *IEEE Transactions on Automatic Control* 59.6 (2014), pp. 1454–1467 (cit. on p. 5).

[15] Aquib Mustafa, Hamidreza Modares, and Rohollah Moghadam. "Resilient synchronization of distributed multi-agent systems under attacks". *Automatica* 115 (2020), p. 108869 (cit. on pp. 5, 63).

[16] Ruixuan Zhao, Guitao Yang, Thomas Parisini, and Boli Chen. *Distributed Unknown Input Observer Design with Relaxed Conditions: Theory and Application to Vehicle Platooning*. 2025. arXiv: 2509.08783 [eess.SY] (cit. on p. 5).

[17] Ruixuan Zhao, Guitao Yang, Peng Li, and Boli Chen. *Bridging Centralized and Distributed Frameworks in Unknown Input Observer Design*. 2025. arXiv: 2509.08914 [eess.SY] (cit. on p. 5).

[18] Guitao Yang, Hamed Rezaee, Andrea Serrani, and Thomas Parisini. "Sensor Fault-Tolerant State Estimation by Networks of Distributed Observers". *IEEE Transactions on Automatic Control* 67.10 (2022), pp. 5348–5360 (cit. on pp. 5, 63).

[19] Michal Yemini, Angelia Nedić, Andrea J. Goldsmith, and Stephanie Gil. "Characterizing Trust and Resilience in Distributed Consensus for Cyberphysical Systems". *IEEE Transactions on Robotics* 38.1 (2022), pp. 71–91 (cit. on pp. 5, 63).

[20] Yiyang Wang, Neda Masoud, and Anahita Khojandi. "Real-Time Sensor Anomaly Detection and Recovery in Connected Automated Vehicle Sensors". *IEEE Transactions on Intelligent Transportation Systems* 22.3 (2021), pp. 1411–1421 (cit. on pp. 6, 63).

[21] Woongsun Jeon, Ankush Chakrabarty, Ali Zemouche, and Rajesh Rajamani. "LMI-based neural observer for state and nonlinear function estimation". *International Journal of Robust and Nonlinear Control* 34.10 (2024), pp. 6964–6984. eprint: https://onlinelibrary.wiley.com/doi/pdf/10.1002/rnc.7327 (cit. on p. 6).

[22] Ayoub Farkane, Mohamed Boutayeb, Mustapha Oudani, and Mounir Ghogho. "An Adaptive Physics-Informed Neural Network Observer for state estimation in nonlinear dynamical systems". *Engineering Applications of Artificial Intelligence* 162 (2025), p. 112655 (cit. on p. 6).

[23] Yi-Lin Li, Run-Ze Li, Yi-Ping Liu, and Yu Chen. "A hybrid physics-data driven approach for vehicle dynamics state estimation". *Mechanical Systems and Signal Processing* 223 (2025), p. 112249 (cit. on p. 6).

[24] Chenkai Tan, Yingfeng Cai, Hai Wang, and Xiaoqiang Sun. "Vehicle State Estimation Combining Physics-Informed Neural Network and Unscented Kalman Filtering on Manifolds". *Sensors* 23.15 (2023), p. 6665 (cit. on p. 6).

[25] Pragyan Dahal, Simone Mentasti, Luca Paparusso, Stefano Arrigoni, and Francesco Braghin. "RobustStateNet: Robust ego vehicle state estimation for Autonomous Driving". *Robotics and Autonomous Systems* 172 (2024), p. 104585 (cit. on p. 6).

[26] Hasan Abdl Ghani, Hind Laghmara, Sofiane Ahmed Ali, Samia Ainouz, Xing Gao, and Redouane Khemmar. "Continuous-Discrete Time Neural Network Observer for Nonlinear Dynamic Systems Application to Vehicle Systems". *IFAC-PapersOnLine* 56.2 (2023) (cit. on p. 6).

[27] Kong Yao Chee and M. Ani Hsieh. "LEARNEST: LEARNing Enhanced Model-based State ESTimation for Robots using Knowledge-based Neural Ordinary Differential Equations" (2023), pp. 11590–11596 (cit. on p. 6).

[28] Yan Wang, Jingyu Hu, Fa'an Wang, Haoxuan Dong, Yongjun Yan, Yanjun Ren, et al. "Tire Road Friction Coefficient Estimation: Review and Research Perspectives". *Chinese Journal of Mechanical Engineering* 35 (2022), p. 6 (cit. on p. 6).

[29] Jinheng Han, Junzhi Zhang, Chen Lv, Ruihai Ma, and Henglai Wei. "Estimation of Road Friction Coefficient via the Data Enforced Unscented Kalman Filter". *Chinese Journal of Mechanical Engineering* 38 (2025), p. 195 (cit. on p. 6).

[30] Tianli Gu, Bo Li, Zhenqiang Quan, Shaoyi Bei, and Xiaoqiang Sun. "A novel estimation method for tire-road friction coefficient using intelligent tire and tire dynamics". *Mechanical Systems and Signal Processing* 235 (2025), p. 112872 (cit. on p. 6).

[31] Karanjit Kalsi, Jianming Lian, Stefen Hui, and Stanislaw H. Żak. "Sliding-Mode Observers for Systems with Unknown Inputs: A High-Gain Approach". *Automatica* 46.2 (2010), pp. 347–353 (cit. on p. 6).

[32] Fanglai Zhu. "State estimation and unknown input reconstruction via both reduced-order and high-order sliding mode observers". *Journal of Process Control* 22.1 (2012), pp. 296–302 (cit. on pp. 6, 15).

[33] Mukai Zhang, Badriah Alenezi, Stefen Hui, and Stanislaw H. Żak. "Unknown Input Observers for Discretized Systems With Application to Networked Systems Corrupted by Sparse Malicious Packet Drops". *IEEE Control Systems Letters* 5.4 (2021), pp. 1261–1266 (cit. on pp. 6, 22).

[34] O. Sadki, Q.H. Nguyen, A. Zemouche, H. Rafaralahy, and M. Haddad. "Cyberattack Estimation in Intelligent Transportation System by Using an Adaptive High Order Sliding Mode Differentiator". *2025 33rd Mediterranean Conference on Control and Automation (MED)*. 2025, pp. 43–48 (cit. on p. 6).

[35] A. Chaouche, A. Zemouche, M. Ramdani, K. Chaib Draa, and D. Delattre. "Unknown input estimation algorithms for a class of LPV/nonlinear systems with application to wastewater treatment process". *Proceedings of the Institution of Mechanical Engineers, Part I: Journal of Systems and Control Engineering* 236.7 (2022), pp. 1372–1385 (cit. on pp. 7, 14, 32).

[36] L. Hassan, A. Zemouche, and M. Boutayeb. "Robust Unknown Input Observers for Nonlinear Time-Delay Systems". *SIAM Journal on Control and Optimization* 51.4 (2013), pp. 2735–2752. eprint: https://doi.org/10.1137/11085181X (cit. on p. 7).

[37] Fanping Bu and Ching-Yao Chan. "Adaptive and Cooperative Cruise Control". *Handbook of Intelligent Vehicles*. Ed. by Azim Eskandarian. London: Springer London, 2012, pp. 191–207 (cit. on p. 11).

[38] A. Khalil, M. Al Janaideh, K.F. Aljanaideh, and D. Kundur. "Fault detection, localization, and mitigation of a network of connected autonomous vehicles using transmissibility identification". *2020 American Control Conference (ACC)*. IEEE. 2020, pp. 386–391 (cit. on p. 11).

[39] X. Huang and X. Wang. “Detection and isolation of false data injection attack in intelligent transportation system via robust state observer”. *Processes* 10.7 (2022), p. 1299 (cit. on p. 11).

[40] E. Mousavinejad, F. Yang, Q.L. Han, X. Ge, and L. Vlacic. “Distributed cyber attacks detection and recovery mechanism for vehicle platooning”. *IEEE Transactions on Intelligent Transportation Systems* 21.9 (2019), pp. 3821–3834 (cit. on p. 11).

[41] Joe Diether Cabelin, Paul Vincent Alpano, and Jhoanna Rhodette Pedrasa. “SVM-based Detection of False Data Injection in Intelligent Transportation System”. *2021 International Conference on Information Networking (ICOIN)*. 2021, pp. 279–284 (cit. on p. 11).

[42] Dengfeng Pan, Xiaohua Ge, Derui Ding, and Qing-Long Han. “Simultaneous Cyber Attack Estimation and Radar Spoofing Attack Detection for Connected Automated Vehicles”. *IECON 2023- 49th Annual Conference of the IEEE Industrial Electronics Society* (2023), pp. 1–6 (cit. on p. 11).

[43] Y. Yamamoto, N. Kuze, and T. Ushio. “Attack detection and defense system using an unknown input observer for cooperative adaptive cruise control systems”. *IEEE Access* 9 (2021), pp. 148810–148820 (cit. on p. 11).

[44] R. Rajamani and C. Zhu. “Semi-autonomous adaptive cruise control systems”. *IEEE Transactions on Vehicular Technology* 51.5 (2002), pp. 1186–1192 (cit. on pp. 12, 13, 17).

[45] H. Trinh and T. Fernando. *Functional observers for dynamical systems*. Vol. 420. Springer Science & Business Media, 2011 (cit. on pp. 14, 32).

[46] A. Dabroom and H.K. Khalil. “Numerical differentiation using high-gain observers”. *Proceedings of the 36th IEEE Conference on Decision and Control*. Vol. 5. 1997, 4790–4795 vol.5 (cit. on p. 15).

[47] Tim D. Barfoot. “State Estimation for Robotics”. 2017 (cit. on p. 30).

[48] F. Abdollahi, H.A. Talebi, and R.V. Patel. “A stable neural network-based observer with application to flexible-joint manipulators”. *IEEE Transactions on Neural Networks* 17.1 (2006), pp. 118–129 (cit. on p. 30).

[49] Mona Buisson-Fenet, Valery Morgenthaler, Sebastian Trimpe, and Florent Di Meglio. “Joint State and Dynamics Estimation With High-Gain Observers and Gaussian Process Models”. *IEEE Control Systems Letters* 5.5 (2021), pp. 1627–1632 (cit. on p. 30).

[50] Ali Zemouche and Mohamed Boutayeb. “Nonlinear-observer-based $\mathcal{H}_\infty$ synchronization and unknown input recovery”. *IEEE Trans. Circuits Syst. I. Regul. Pap.* 56.8 (2009), pp. 1720–1731 (cit. on p. 32).

[51] L. Hassan, A. Zemouche, and M. Boutayeb. “Robust Unknown Input Observers For Nonlinear Time-Delay Systems”. *SIAM Journal on Control and Optimization* 51.4 (2013), pp. 2735–2752 (cit. on p. 32).

[52] H. Trinh, T.D. Tran, and T. Fernando. “Disturbance decoupled observers for systems with unknown inputs”. *IEEE Transactions on Automatic Control* 53.10 (2008), pp. 2397–2402 (cit. on p. 32).

[53] G. Phanomchoeng and R. Rajamani. “Real-Time Estimation of Rollover Index for Tripped Rollovers With a Novel Unknown Input Nonlinear Observer”. *IEEE/ASME Transactions on Mechatronics* 19.2 (2014), pp. 743–754 (cit. on p. 32).

[54] M. Benallouch, R. Outbib, M. Boutayeb, and E. Laroche. “Robust Observers for a Class of Nonlinear Systems Using PEM Fuel Cells as a Simulated Case Study”. *IEEE Transactions on Control Systems Technology. DOI: 10.1109/TCST.2017.2658181* (2017) (cit. on p. 32).

[55] B.A. Charandabi and H.J. Marquez. “A novel approach to unknown input filter design for discrete-time linear systems”. *Automatica* 50.2 (2014), pp. 2835–2839 (cit. on p. 32).

[56] M. Hou and P. C. Muller. “Design of observers for linear systems with unknown inputs”. *IEEE Transactions on Automatic Control* 37.6 (1992), pp. 871–875 (cit. on p. 32).

[57] Dirk Söffker, Tie-Jun Yu, and Peter C. Müller. “State estimation of dynamical systems with nonlinearities by using proportional-integral observer”. *International Journal of Systems Science* 26 (1995), pp. 1571–1582 (cit. on p. 32).

[58] Q.H. Nguyen, O. Sadki, H. Rafaralahy, M. Haddad, and A. Zemouche. “Cyberattack Detection by Using a Discrete-Time Model-Based Unknown Input Observer”. *IEEE Control Systems Letters* 8 (2024), pp. 856–861 (cit. on p. 33).

[59] H. Arezki, A. Zemouche, A. Alessandri, and P. Bagnerini. “LMI Design Procedure for Incremental Input/Output-to-State Stability in Nonlinear Systems”. *IEEE Control Systems Letters* 7 (2023), pp. 3403–3408 (cit. on p. 35).

[60] Tom Z. Jiahao, Kong Yao Chee, and M. A. Hsieh. “Online Dynamics Learning for Predictive Control with an Application to Aerial Robots”. *Conference on Robot Learning*. 2022 (cit. on p. 47).

[61] Eugenio Alcalá, Vicenç Puig, Joseba Quevedo, and Ugo Rosolia. “Autonomous racing using Linear Parameter Varying-Model Predictive Control (LPV-MPC)”. *Control Engineering Practice* 95 (2020), p. 104270 (cit. on p. 48).

[62] Masoud Abbaszadeh and Ali Zemouche, eds. *Security and Resilience in Cyber-Physical Systems: Detection, Estimation and Control*. Cham: Springer International Publishing, 2022 (cit. on p. 63).

[63] S. Meng, Q.H. Nguyen, A. Zemouche, F. Meng, and F. Zhang. "Distributed High-Gain Observer for Nonlinear Connected Autonomous Vehicle". *2025 American Control Conference (ACC)*. 2025, pp. 626–631 (cit. on p. 63).

[64] Q. H. Nguyen, O. Sadki, H. Rafaralahy, M. Haddad, and A. Zemouche. "Cyberattack Detection by Using a Discrete-Time Model-Based Unknown Input Observer". *IEEE Control Systems Letters* 8 (2024), pp. 856–861 (cit. on p. 63).

[65] Angelo Barboni, Hamed Rezaee, Francesca Boem, and Thomas Parisini. "Distributed Detection of Covert Attacks for Interconnected Systems" (2019) (cit. on p. 63).

[66] Zihao Li, Yang Zhou, Yunlong Zhang, and Xiaopeng Li. "Enhancing vehicular platoon stability in the presence of communication Cyberattacks: A reliable longitudinal cooperative control strategy". *Transportation Research Part C: Emerging Technologies* 163 (2024), p. 104660 (cit. on p. 63).

[67] Lucile Chaix. *Conception et prototypage d'une carte embarquée pour la détection de cyberattaques et l'estimation d'état dans les véhicules autonomes*. Tech. rep. 2025-086-P0. SEGULA Technologies, 2026 (cit. on pp. 99, 101, 102, 105).

[68] Cohda Wireless. *MK6 V2X OBU/RSU: Technical Granularity and Positioning Accuracy*. Cohda Wireless Pty Ltd. 2025 (cit. on pp. 99, 100).

[69] Commsignia. *ITS-OB4 On-Board Unit Technical Specification and Architecture*. Commsignia Ltd. 2025 (cit. on pp. 99, 100).

[70] Unex Technology. "Integrating Autotalks Craton2 into Modular V2X Systems". *Proceedings of the Intelligent Transportation Systems Congress*. 2024 (cit. on pp. 99, 100).

[71] C-Roads Platform. *C-ITS Working Group 2: Interoperability and Conformance Testing Report*. Tech. rep. European Union, 2023 (cit. on pp. 99, 100).

[72] S. Lien, D. Deng, C. Lin, H. Liang, and C. Chen. "3GPP NR V2X Communications: Standards, Progress, and Perspectives". *IEEE Network* 34.6 (2020), pp. 162–169 (cit. on p. 99).

[73] SAE International. *V2X Communications Message Set Dictionary*. 2024 (cit. on p. 99).

[74] Federal Communications Commission. *Use of the 5.850-5.925 GHz Band for Intelligent Transportation Systems*. Tech. rep. FCC-24-XX. FCC, 2024 (cit. on p. 99).